THE ATMOSPHERES OF THE F SUPERGIANTS

Thesis by

Patrick Stewart Osmer

In Partial Fulfillment of the Requirements

For the Degree of

Doctor of Philosophy

California Institute of Technology

Pasadena, California

1970

(Submitted October 2, 1969)

Acknowledgements

I wish to thank the following people for assistance with this work:

Wallace Sargent, who supervised the project, obtained some of the Palomar spectra, and made valuable suggestions about the scope of the thesis.

Deane Peterson, who made available his computer programs as well as those of R.L. Kurucz and contributed essential advice about the model atmospheres and line transfer problems.

Leonard Searle, who obtained some of the Palomar spectra and offered important comments during the later stages of this work.

In addition I am grateful to Jesse Greenstein for the loan of his infrared spectra and conversations on the project and to George Wallerstein, who loaned his spectra of the G stars. I thank Roger Ulrich for discussions on turbulence and instabilities in stellar atmospheres and Jean Osmer for typing the manuscript and making many of the drawings. Financial support from the National Science Foundation, the State of California, and the Institute is also acknowledged.

Abstract

Coude spectra of 26 supergiants of spectral types F2-G5 were obtained, and spectrophotometric observations of four which occurred in clusters were made. A photoelectric system for measuring the O I 7774 line was established, and the line strength was determined in 59 A0-G3 stars of luminosity classes Ia-V. By calibrating the line strength in 10 F supergiants of known luminosity we find that it indicates the absolute magnitude of F stars brighter than $M_V = -4$ with an accuracy of $\pm 0^m.5$. The curves of growth obtained from the spectra show that the microturbulence determined from the Fe II lines increases with luminosity and is correlated with the oxygen line strength. However, the Fe I microturbulence exhibits a different behavior near spectral type F5, where it is insensitive to luminosity.

The applicability of model atmospheres to the F supergiants was checked by using the spectrophotometric observations. The derived temperatures were reasonable, but the gravities of the Ia stars were a factor of 5 less than expected from stellar interiors calculations. The difference was less for the Ib stars. It was shown that pulsational effects did not account for the discrepancy. Consideration of how the turbulent motions could affect the pressure equilibrium in the atmosphere indicated that the observed velocities were large enough to reduce the gas pressure and cause the observed low gravities. The models also indicated that a decrease in the continuous

absorption combined with the observed microturbulence accounted for the increase in the oxygen line strength with luminosity. Although non-LTE effects may be present in the oxygen line, they do not change significantly with luminosity and do not contribute to the observed increase in strength.

The gradient in radiation pressure beneath the photosphere in F stars with $\log g < 2$ is large enough to cause an inversion in the gas pressure. The zone where this occurs is unstable and could be the cause of mass motions in supergiants. This hypothesis is supported by the fact that the zone appears at the gravity where the oxygen lines become sensitive to luminosity and the turbulence begins to increase. Simple calculations show how the existence of the zone depends on gravity and temperature.

Finally, we demonstrated that a turbulent velocity which increases with height in the atmosphere explains the difference in the behavior of the Fe I and II lines at F5 as well as their similarities at other spectral types. At F5Ib the lines are formed at the same depth, but in the F5Ia stars the increased ionization causes the Fe II lines to be formed at greater heights in the atmosphere than the Fe I lines.

Table of Contents

Table of Contents
(cont.)

I. Introduction

The F type supergiants, some of which are brighter than 10^5 suns, form one of the most luminous known groups of stars. Their high luminosities and moderate effective temperatures (about 6500°) make them important in astronomical research for at least four reasons: (1) They imply that the stars are young and rapidly evolving and have not had time to move very far from their place of origin. Accordingly they are useful tracers of recent star formation in galaxies. (2) The stars can be observed in detail at large distances from the sun, so that they may be studied in distant parts of the galaxy and in the Magellanic Clouds. Therefore we could use them to determine composition differences between galaxies and as a function of radius in our own galaxy. (3) If their luminosity could easily be determined, we would have a distance indicator that is substantially brighter than the cepheid variables. (4) The stars have radii of the order of 200 $R_\odot$ and quite low surface gravities, so that they are useful for the study of low pressure phenomena in stellar atmospheres.

These properties of the F I stars have attracted the interest of many investigators and from their work we can obtain an idea of the basic characteristics of these stars. The photometry by Pesch (1959, 1960a,b) and Mitchell (1960) of F I stars in galactic clusters indicates that their range in absolute magnitude is roughly $-9 < M_V < -4$. Some of the F I stars are cepheids and most of the

others are semi-regular variables with small light and velocity amplitudes (Abt, 1957). The stars are concentrated toward the galactic plane, where they occur in spiral arms.

F I stars are distinguished from lower luminosity stars on classification spectra because they have stronger lines of ionized metals. The hydrogen lines are not as useful luminosity indicators as they are in the A stars, and it is difficult to pick out F I stars on blue sensitive objective prism plates. Merrill (1925, 1934) found in his studies of infrared spectra that the oxygen triplet at 7774A was stronger in early type supergiants than dwarfs. Keenan and Hynek (1950) showed in an extensive study that it was an excellent luminosity criterion for B, A, and F stars, and Parsons (1964) demonstrated that it could be used to pick out supergiants even at objective prism dispersions. Furthermore since it occurs in a clear region of the spectrum he pointed out that narrow band photoelectric techniques should be able to measure the line. Therefore it is now possible to find many new high luminosity F stars.

Struve and Elvey (1934) were the first to show that the unusually large strength of saturated lines in the spectra of A and F high luminosity stars was caused by motions in their atmospheres that occurred on a scale smaller than the one over which the lines were formed. They ascribed the motions to some kind of turbulence and today the velocity derived from the equivalent widths of lines is called microturbulence to distinguish it from larger scale motions (macroturbulence) which affect the line profile but not its strength.

The Doppler part of the line absorption coefficient is assumed to have the form

$$\alpha(v) \propto \exp(-v^2/\Delta v_0^2) \quad \text{where } \Delta v_0 = vV_0/c\,;\ V_0^2 = 2kT/m + \xi^2 \qquad \text{(I-1)}$$

ξ is the microturbulent velocity. A convenient way of determining the microturbulence is to compare the height of the flat part of the observed curve of growth with a theoretical one; Δv_0 is directly proportional to the vertical shift required to make the curves match. If the theoretical curve is appropriate for the stars involved, it will give accurate values of the microturbulence for stars of similar spectral type.

Microturbulent velocities greater than 20 km/sec have been measured in some stars. Most, if not all, of these cases involve stars associated with circumstellar gas streams, so that the velocity does not necessarily mean that the atmospheric turbulence is that high. Abt (1960) obtained a velocity of 16 km/sec for ϕ Cas (F0Ia), which is one of the higher known values for an individual star with no evidence of circumstellar material. In comparison Chaffee (1968) found that for dwarf stars the velocity range is 2 - 4 km/sec. Wright's (1955) summary of the velocity as a function of spectral type and luminosity shows that it increases with luminosity at a given spectral type although among the supergiants it decreases with advancing spectral type. Wright (1946, 1947) had previously found that in α Per (F5Ib) the curves of growth for ionized atoms gave higher microturbulent velocities than did the ones for neutral atoms and that for the neutral atoms the velocity decreased with increasing

excitation potential. He argued that the ionized lines and low excitation lines of a given element were formed at greater heights in the atmosphere than the others; therefore his observations could be explained by the turbulent velocity increasing with height (decreasing density). This idea also accounted for the velocity increase with luminosity since the atmospheric densitites were lower in the high luminosity stars. From a theoretical point of view the velocity could be expected to increase with decreasing density if the flow satisfied the equation of continuity (ρV = const.) or if the motions were of an energy conserving turbulent nature ($\frac{1}{2}\rho V^3$ = const.).

Unno (1959a,b) has used the Goldberg (1958) method, which is insensitive to line transfer problems, to investigate the depth dependence of turbulence in the photosphere and lower chromosphere of the sun. The technique makes use of the fact that at a given height in the atmosphere different lines in a multiplet have the same source function. The Doppler velocity is found by measuring the lines in the multiplet at a particular residual intensity and assuming that the line absorption coefficient is described by a Gaussian. If $\Delta\lambda_1$ and $\Delta\lambda_2$ are the half widths at the specified intensity and gf_1 and gf_2 the respective oscillator strengths, the Doppler width $\Delta\lambda_D$ is obtained from the relation

$$gf_1 \exp(-\Delta\lambda_1^2/\Delta\lambda_D^2) = gf_2 \exp(-\Delta\lambda_2^2/\Delta\lambda_D^2) \quad \text{(I-2)}$$

Unno found that the velocity decreased from 1.5 km/sec at τ_{5000} = 0.6 to 0.7 km/sec at τ_{5000} = 0.2 and then increased outward in the

chromosphere, reaching 6 km/sec at a height of 3000 km. Furthermore the velocity was proportional to $\rho^{-\frac{1}{4}}$ in the chromosphere.

His interpretation of these results gives a good idea of the current understanding of turbulence in stellar atmospheres. He attributes the velocity decrease with increasing height in the photosphere to the decay of convective motions above the region of instability. The chromospheric velocities on the other hand are caused by progressive waves traveling outward; they are proportional to $\rho^{-\frac{1}{4}}$, not $\rho^{-\frac{1}{2}}$, as they would be if they were acoustic waves, because the waves lose energy in being scattered by inhomogeneities in the gas. In addition these waves carry enough energy to balance the radiative losses from the corona. Thus his work is an impressive confirmation of the theory that progressive waves originating in the convection zone are responsible for the heating of the corona.

Besides having turbulent motions two F I stars also exhibit definite evidence of matter being ejected from their atmospheres. ρ Cas, normally an F8Ia star, occasionally throws out enough cool matter to make it look like a K or M star (Payne-Gaposchkin and Mayall, 1946). After one large outburst in 1946 (see Beardsley, 1961) it gradually reverted to its normal spectral type although many strong metallic lines in its spectrum had developed components which were shifted to the blue by 40 km/sec (Bidelman and McKellar, 1957). Its spectrum also showed unusual metallic emission lines which were blue shifted by 25 km/sec (Sargent, 1961). The outflowing material in 89 Her has velocities up to 150 km/sec with respect

to the photosphere, but its nature is different than in ρ Cas, for the absorption components are seen in the Balmer and D lines, not the metallic lines (Sargent and Osmer, 1968). It is not clear whether these stars are peculiar or whether mass loss is a general but sporadic phenomenon in the F supergiants. Rocket ultraviolet observations would be useful in settling this point if Morton's (1967) work on early supergiants is any indication. His spectra show that strong UV resonance lines have components indicating expansion velocities greater than 1000 km/sec in stars with normal visual spectra. We have mentioned ρ Cas and 89 Her for two main reasons: (1) to show that large instabilities can occur in the F I stars and (2) to point out that the line spectra of other stars could be contaminated by unresolved circumstellar material.

The above information about turbulence and luminosity effects in the F I stars raises several questions about their behavior. (1) Does increasing turbulence cause the strengthening of the ionized metal and the oxygen lines? (2) Is the luminosity effect confined to ions which have ionization potentials around 14 eV? (3) Can the oxygen lines, for example, be used to determine supergiant luminosities accurately? (4) Can standard model atmosphere techniques be used to analyze these stars, or do the large motions that occur in their atmospheres alter the parameters significantly? (5) If the models are appropriate, can they be used with a density dependent turbulence to duplicate the observed line strengths of different ions?

We established the following program to investigate these

questions.

(1) Coude spectra of 26 A8-G5 I stars were obtained so that microturbulent velocities from Fe I and Fe II could be determined and the existence of luminosity effects in other lines checked.

(2) Due to the slowness of infrared emulsions we used photoelectric equipment to measure the O I 7774 line strength in a large number of stars to see how closely the line strength is correlated with absolute magnitude and with the behavior of the other lines.

(3) In order to analyze the observations we have computed a grid of low gravity model atmospheres. The applicability of these models is checked using spectrophotometric observations of F I stars in clusters for which the reddening and distance modulus have been found.

(4) Using the models, we have investigated two possible explanations of our line spectra observations: depth dependent turbulence in lines formed according to the hypothesis of LTE or non-LTE effects.

In this paper we have described all the observations in section II. The empirical effects indicated by the data are considered in section III. In section IV the results of the model atmosphere calculations are discussed and in section V the models are used to examine theoretical explanations of the observational effects.

II. The Observational Program

A. Introduction

The fact that most of the F Ia stars are fainter than 5th magnitude prevented a comprehensive high resolution study of their spectra from being done. We believed that more knowledge would be gained about the general properties of F I stars by sacrificing resolution and observing a large number of stars than by observing only a few at greater dispersion. Therefore our observational program centered upon finding the relative behavior of the line spectra with temperature and luminosity.

The observations are divided into three parts: (1) We describe the photographic spectra and results, which we have used to determine turbulent velccities for Fe I and Fe II to see if the effect found by Wright depends on temperature and luminosity. We have also used the spectra for an empirical study of luminosity effects suggested by the lower dispersion classification work. (2) This empirical study was extended to the O I 7774A line using photoelectric techniques, which were much faster than infrared emulsions. Using the scanner we were able to measure the line in a total of 59 stars as well as calibrate its luminosity dependence using stars in clusters. (3) We have also obtained photoelectric scans of the Pesch and Mitchell cluster stars so that we may check the agreement with the continuum fluxes predicted by model atmospheres. Hydrogen line widths were measured photographically for a similar check with

the theory. Since luminosities are known for the cluster stars, we can estimate their masses from stellar evolutionary calculations and see if they are consistent with the gravities found from the model atmospheres.

B. The Spectra

Reliable analyses of stellar line spectra can be done easily only on spectra of fairly high dispersion and in regions of the spectrum where the continuum is well defined. Determinations of element abundances and microturbulence require that the strengths of unsaturated lines be known. In the sun this means that lines of 50 mA equivalent width must be measurable but, for the F I stars, whose velocities are at least twice as large, lines of 100 mA width are still unsaturated. Since the turbulence in these stars is determined from relatively strong lines, we can expect a single plate to give accurate results.

Since Abt (1960) and Searle, Sargent, and Jugaku (1963) have previously measured most of the available F I stars earlier than F5 for turbulence, the present work concentrates on the F5 through G0 stars. The new measures include one of Abt's stars so that possible systematic differences may be elimated. In the F I stars the crowding of the visible spectrum with lines increases markedly with advancing spectral type and at F5 it is difficult to locate the continuum at wavelengths less than 4500A. Therefore lines

beyond 5000A were measured on IIa-D plates for the F5-G5 stars in our program.

The final requirement for an accurate measurement of the turbulence is an element with a rich spectrum of strong and weak lines of different excitation for which good transition probabilities are available. Neutral iron meets these conditions better than any other ion thanks to the work of Corliss and Warner (1964) in determining absolute oscillator strengths for Fe I. Although the Fe II lines are not as numerous and do not have as large a range in equivalent width as the Fe I lines, we measured them to investigate effects caused by differences in the ionization potential.

The 25 program stars listed in table 1 were compiled mostly from Bidelman's (1951, 1957) lists of high luminosity stars. We have included nearly all the known F and G0 Ia stars north of declination -35° and brighter than $m_v = 8.0$. A representative sample of F and G Ib stars meeting these requirements was also chosen and the cluster stars HD 10494, +60° 2532, and α Per were included. Widened coude spectra of them were obtained with the Kitt Peak 84", Mt. Wilson 100", and Palomar 200" telescopes at dispersions of 18, 15, and 14.5 A/mm respectively and calibrated in the usual way. Two plates were taken of some of the brighter stars so that errors in the measurement of turbulence could be estimated. The plates of the G Ib stars were loaned by Wallerstein.

Intensity tracings of all plates were made with the Caltech microphotometer and the equivalent widths of the lines were calculated from measures of their depth and full width at half maximum.

Table 1

Program Stars

Name	HD	α (1900)	δ	m_v	Sp
89 Her	163506	17 51.4	+26 04	5.48	F2Ia
	10494	01 37.3	+61 21	7.5	F5Ia
	17971	02 48.2	+59 59	7.8	F5Ia
	231195	19 16.1	+14 14	8.1	F5Ia
	9973	01 32.4	+60 34	7.1	F5Iab
	195593	20 27.2	+36 36	6.3	F5Iab
α Per	20902	03 17.2	+49 30	1.90	F5Ib
	172052	18 32.9	-23 16	6.79	F5Ib
	180028	19 0918	+05 52	7.24	F6Ib
+60 2532		23 19.8	+61 02	8.31	F7Ib
HR 690	14662	02 16.9	+54 55	6.46	F7Ib
45 Dra	171635	18 30.9	+56 58	4.95	F7Ib
δ CMa	54605	07 04.3	-26 14	1.98	F8Ia
ρ Cas	224014	23 49.4	+56 57	4.1v	F8Ia
	331777	19 59.3	+31 38	8.0	F8Ia
γ Cyg	194093	20 18.6	+39 56	2.32	F8Ib
HR 7542	187203	19 43.7	+10 26	6.38	F8Ib-II
R Pup	62058	07 37.0	-31 25	6.64	GOIa
	6474	01 00.7	+63 15	8.4	GOIa
	18391	02 52.2	+57 16	7.5	GOIa
HR 8752	217476	22 55.9	+56 24	5.48	GOIa
β Aqr	204867	21 26.3	-06 01	2.89	GOIb

Table 1 (cont.)

Name	HD	(1900)		m_v	Sp
β Cam	31910	04 54.5	+60 18	4.22	G0Ib
α Aqr	209750	22 00.6	-00 48	2.93	G2Ib
ψ And	223047	23 41.1	+45 52	4.96	G5Ib

A gaussian profile was assumed so that the equivalent width W = 1.06 x depth x FWHM (A). For 89 Her we used the blue lines measured by Chaffee (1968). For the other stars the Fe I line list consisted of those lines with gf values measured by Corliss and Warner that were judged to be unblended in the solar spectrum from an examination of the revised Rowland atlas (Moore, Minnaert, and Houtgast, 1966). The Fe II lines were taken from the list of Helfer and Wallerstein (1964); their gf values were obtained from a compilation by Cohen (private communication). The measured values of $-\log W/\lambda$ for each star are given in table 2; the errors are estimated to be $\pm 20\%$.

The Wrubel (1949) curve of growth for scattering with $B_0/B_1 = 2/3$ and $\log a = -3.0$, which is commonly used in abundance work, was employed to derive turbulent velocities from the data in table 2. For the Fe I lines the error of a single velocity was determined to be $\pm 10\%$ by comparing the results from two separate spectra of each of four stars. Systematic effects between different observers and telescopes were investigated by comparing the present values with published ones for four stars (table 3). We see that the average error is about 23% and that the present results for 89 Her agree well with the Searle et al. value. Therefore we have used their data and that of Abt (1960) as they stand. Since the velocities derived from Fe II lines are based on only 7 lines their uncertainties are estimated to be 40%.

The above error estimates apply to determinations of the best fit of the observed and theoretical curves of growth. Enough weak

Table 2. Observed Values of -log W/λ

89 Her Fe I Lines, λ < 5000A

λ	Mult	E P	log gf	-log W/λ	λ	Mult	E P	log gf	-log W/λ
4009.71	72	2.22	-0.44	4.29	4202.03	42	1.48	-0.25	3.88
4014.53	802	3.57	0.58	4.27	4203.90	355	2.84	-0.21	4.25
4021.87	278	2.76	0.12	4.27	4210.35	152	2.48	-0.19	4.27
4044.61	359	2.83	-0.17	4.33	4213.65	355	2.84	-0.55	4.44
4045.82	43	1.48	0.68	3.92	4217.55	693	3.43	0.12	4.49
4062.45	359	2.84	0.05	4.38	4219.36	800	3.57	0.79	4.39
4063.60	43	1.56	0.43	3.88	4220.35	482	3.07	-0.56	4.75
4067.98	559	3.21	0.29	4.40	4222.22	152	2.45	-0.35	4.18
4070.77	558	3.24	0.01	4.29	4225.46	693	3.42	0.13	4.01
4071.74	43	1.61	0.40	3.97	4227.43	693	3.33	0.90	4.02
4073.76	558	3.14	-0.14	4.50	4235.94	152	2.42	0.31	4.03
4074.79	524	3.05	-0.14	4.61	4238.82	693	3.40	0.47	4.23
4084.50	698	3.33	0.13	4.50	4250.13	152	2.47	0.25	4.13
4107.49	354	2.83	0.06	4.08	4250.79	42	1.56	-0.28	4.09
4114.45	357	2.83	-0.47	4.54	4260.48	152	2.40	0.63	4.00
4132.06	43	1.61	-0.16	3.88	4266.97	273	2.73	-0.87	4.88
4134.68	357	2.83	0.18	4.09	4267.83	482	3.11	-0.34	4.43
4143.87	43	1.56	-0.07	3.81	4271.76	42	1.48	0.20	3.93
4147.67	42	1.48	-1.47	4.22	4282.41	71	2.18	-0.16	4.13
4153.91	695	3.40	0.33	4.37	4298.04	520	3.05	-0.56	4.81
4157.79	695	3.42	0.17	4.39	4325.77	42	1.61	0.36	3.97
4175.64	354	2.84	0.10	4.28	4352.74	71	2.22	-0.56	4.33
4181.76	354	2.83	0.46	4.13	4383.55	41	1.48	0.51	3.97
4184.90	355	2.83	-0.05	4.30	4388.41	830	3.60	0.02	4.55
4187.04	152	2.45	0.17	4.04	4404.75	41	1.56	0.25	3.89
4187.80	152	2.42	0.13	4.13	4408.42	68	2.20	-0.95	4.38
4191.44	152	2.47	0.06	4.06	4415.13	41	1.61	-0.13	3.84
4196.22	693	3.40	-0.08	4.27	4422.57	350	2.84	-0.22	4.23
4199.10	522	3.05	0.81	4.16	4430.62	68	2.22	-1.02	4.36
4200.93	689	3.40	-0.22	4.55	4446.84	828	3.69	-0.57	4.90

Table 2. Observed Values of -log W/λ (cont.)

89 Her

λ	Mult	E P	log gf	-log W/λ
4447.72	68	2.22	-0.58	4.28
4466.55	350	2.83	0.18	4.19
4469.38	830	3.65	0.19	4.17
4476.02	350	2.84	0.14	4.32
4484.22	828	3.60	0.08	4.62
4525.14	826	3.61	0.03	4.30
4528.62	68	2.18	-0.20	4.10
4611.29	826	3.65	-0.13	4.57
4613.21	554	3.29	-0.88	4.56
4625.05	554	3.24	-0.63	4.83
4654.50	39	1.56	-2.18	4.52
4691.41	409	2.99	-0.59	4.69
4710.29	409	3.02	-0.74	4.90
4736.78	554	3.21	-0.02	4.37

Table 2. Observed Values of -log W/λ (cont.)

Fe I Lines, λ > 5000A

λ	Mult	E P	log gf	HD 10494	HD 17971	HD 231195	HD 9973
5067.16	1092	4.22	-0.49	4.51	4.73	5.00	4.84
5074.75	1094	4.22	0.24	4.41	4.27	4.80	4.39
5083.34	16	0.96	-2.74	4.50	4.42	4.88	4.42
5090.78	1090	4.26	-0.10	4.31	4.53	4.96	4.56
5121.65	1095	4.26	-0.26	4.51	4.94	4.77	4.70
5127.37	16	0.91	-2.91	4.37	4.48	4.63	4.34
5133.70	1092	4.18	0.63	4.20	4.26	4.55	4.32
5150.85	16	0.99	-2.70	4.27	4.30	4.56	4.48
5159.06	1091	4.28	-0.25	4.52	4.73	5.42	4.69
5162.28	1089	4.18	0.50	4.39	4.32	4.64	4.47
5180.07	1166	4.47	-0.37	4.65	4.76	4.66	4.92
5215.19	553	3.26	-0.17	4.42	4.50	4.52	4.36
5217.40	553	3.21	-0.37	4.48	4.56	4.91	4.50
5229.86	553	3.28	-0.19	4.42	4.47	5.10	4.52
5243.78	1089	4.26	-0.43	4.41	4.46	4.63	4.65
5253.47	553	3.28	-0.80	4.69	4.85	5.10	4.80
5293.96	1031	4.14	-0.89	4.64	4.50	4.65	4.58
5302.31	553	3.28	-0.04	4.27	4.29	4.69	4.35
5321.11	1165	4.43	-0.47	5.04	4.91	5.15	5.06
5324.19	553	3.21	0.47	4.18	4.20	4.34	4.20
5339.94	553	3.26	-0.11	4.33	4.19	4.37	4.27
5367.48	1146	4.41	0.65	4.34	4.29	4.53	4.31
5371.49	15	0.96	-1.60	4.08	4.05	4.40	4.11
5373.71	1166	4.47	-0.13	4.73	4.94	5.21	4.88
5383.38	1146	4.31	0.89	4.25	4.19	4.52	4.34
5389.49	1145	4.41	0.05	4.53	4.72	4.86	4.62
5393.18	553	3.24	-0.10	4.37	4.31	4.90	4.48
5397.14	15	0.91	-1.88	4.12	4.10	4.27	4.13
5405.78	15	0.99	-1.75	4.13	4.10	4.46	4.17
5410.92	1165	4.47	0.68	4.25	4.26	4.57	4.32
5415.21	1165	4.39	0.89	4.23	4.20	4.44	4.34

Table 2. Observed Values of -log W/λ (cont.)

λ	HD 195593	α Per	HD 172052	HD 180028	+60° 2532	HR 690
5067.16	4.67	4.70	4.57	4.37	4.61	4.60
5074.75	4.25	4.57	4.39	4.26	4.10	4.40
5083.34	4.34	4.53	4.08	4.17	4.24	4.16
5090.78	4.38	4.52	4.24	4.31	4.53	4.59
5121.65	4.27	4.84	4.44	4.62	4.57	4.52
5127.37	4.31	4.46	4.51	4.24	4.15	4.21
5133.70	4.13	4.43	4.22	4.14	4.24	4.27
5150.85	4.28	4.42	4.13	4.00	4.25	4.46
5159.06	4.38	4.82	4.27	4.36	4.37	4.64
5162.28	4.28	4.53	4.16	4.05	4.10	4.26
5180.07	4.56	4.82	4.38	4.55	4.42	4.49
5215.19	4.07	4.35	4.17	4.08	4.08	4.19
5217.40	4.38	4.62	4.25	4.39	4.26	4.33
5229.86	4.43	4.52	4.29	4.31	4.32	4.39
5243.78	4.35	4.74	4.26	4.49	4.42	4.65
5253.47	4.61	4.68	4.46	4.49	4.52	4.73
5293.96	4.53	4.79	4.70	4.57	4.54	4.61
5302.31	4.25	4.50	4.27	4.23	4.14	4.13
5321.11	4.80	4.90	4.66	4.59	4.74	4.89
5324.19	4.20	4.33	4.17	4.11	4.18	4.22
5339.94	4.23	4.30	4.22	4.26	4.26	4.37
5367.48	4.33	4.43	4.31	4.23	4.26	4.40
5371.49	4.08	4.18	4.15	4.08	4.12	4.13
5373.71	4.63	4.80	4.91	4.70	4.63	4.69
5383.38	4.26	4.39	4.28	4.27	4.34	4.31
5389.49	4.66	4.56	4.55	4.56	4.58	4.81
5393.18	4.29	4.38	4.45	4.25	4.25	4.33
5397.14	4.09	4.07	4.15	4.00	4.15	4.10
5405.78	4.08	4.19	4.15	4.09	4.13	4.16
5410.92	4.24	4.30	4.28	4.16	4.33	4.47
5415.21	4.29	4.32	4.29	4.18	4.22	4.42

Table 2. Observed Values of -log W/λ (cont.)

λ	45 Dra	δ CMa	ρ Cas	HD 331777	γ Cyg	HR 7542	R Pup
5067.16	4.77	4.51	4.73	--	4.58	4.45	4.60
5074.75	4.31	4.14	4.31	--	4.30	4.21	3.94
5083.34	4.37	4.10	4.34	--	4.30	4.18	3.94
5090.78	4.63	4.38	4.46	--	4.68	4.21	4.27
5121.65	4.68	--	4.50	--	--	4.43	4.42
5127.37	4.40	4.07	4.06	3.91	4.27	4.20	4.00
5133.70	4.35	4.15	4.34	4.06	4.24	4.16	4.20
5150.85	4.35	4.13	4.28	4.08	4.35	4.15	4.09
5159.06	4.67	4.38	4.53	4.46	4.57	4.36	4.26
5162.28	4.35	4.21	4.33	4.09	4.31	4.16	4.11
5180.07	4.66	4.51	4.52	4.52	4.53	4.54	4.58
5215.19	4.41	4.15	4.45	4.18	4.32	4.26	4.22
5217.40	4.47	4.07	4.45	4.19	4.40	4.25	4.19
5229.86	4.43	4.27	4.60	4.16	4.41	4.31	4.26
5243.78	4.64	4.29	4.50	4.21	4.43	4.42	4.42
5253.47	4.70	4.34	4.73	--	4.77	4.49	4.60
5293.96	4.94	4.54	4.38	4.24	4.69	4.59	4.30
5302.31	4.37	4.12	4.29	4.08	4.21	4.14	4.08
5321.11	5.08	5.10	--	--	4.78	4.42	4.86
5324.19	4.30	4.04	4.23	3.95	4.18	4.14	4.07
5339.94	4.33	3.88	4.14	4.19	4.18	4.23	4.11
5367.48	4.35	4.07	4.22	4.20	4.31	4.21	4.18
5371.49	4.07	3.88	3.79	3.73	4.04	4.00	3.80
5373.71	4.85	4.45	4.66	4.76	4.59	4.55	4.51
5383.38	4.34	4.10	4.24	4.09	4.24	4.22	4.11
5389.49	4.58	4.50	4.53	4.59	4.40	4.34	4.41
5393.18	4.32	4.17	4.28	4.23	4.27	4.26	4.19
5397.14	4.05	3.78	3.81	3.75	4.03	3.90	3.73
5405.78	4.14	3.91	--	3.84	4.05	3.95	3.82
5410.92	4.27	4.05	4.15	4.13	4.30	4.12	4.09
5415.21	4.27	4.09	4.21	4.05	4.16	4.22	4.18

Table 2. Observed Values of -log W/λ (cont.)

λ	HD 6474	HD 18391	HR 8752	β Aqr	β Cam	α Aqr	ψ And
5067.16	--	4.41	4.33	4.29	4.54	--	--
5074.75	--	4.09	3.97	4.41	4.30	4.08	4.20
5083.34	--	3.93	3.79	4.16	4.19	3.99	4.07
5090.78	4.48	4.30	4.24	4.40	4.51	4.09	4.21
5121.65	--	4.32	4.25	4.36	4.52	4.44	4.16
5127.37	3.98	3.92	3.72	4.18	4.32	3.94	3.90
5133.70	3.95	4.08	4.00	4.20	4.35	4.10	4.18
5150.85	3.99	4.22	3.77	4.16	4.44	4.14	4.12
5159.06	4.31	4.32	4.37	4.19	4.53	4.20	4.32
5162.28	3.99	4.23	3.91	4.05	4.34	4.09	4.11
5180.07	4.39	4.41	4.22	4.23	4.52	4.37	4.32
5215.19	4.03	4.04	--	4.01	4.29	4.13	4.29
5217.40	4.06	--	--	4.21	4.12	4.28	4.20
5229.86	4.18	4.18	4.36	4.18	4.29	4.12	4.11
5243.78	4.26	4.32	4.39	4.39	4.43	4.43	4.31
5253.47	4.28	4.48	--	4.17	4.39	4.33	4.12
5293.96	4.17	4.01	--	4.78	4.68	4.81	--
5302.31	4.01	3.93	3.89	4.06	4.21	4.28	4.06
5321.11	--	4.73	--	4.46	4.56	4.77	4.30
5324.19	3.88	3.92	3.78	4.12	4.16	4.23	4.07
5339.94	3.85	3.82	--	4.18	4.18	4.22	4.02
5367.48	4.00	4.04	3.93	4.24	4.20	4.34	4.16
5371.49	3.74	3.70	3.68	4.00	4.01	4.10	3.90
5373.71	4.46	4.62	4.37	4.46	4.38	4.47	4.29
5383.38	4.07	3.99	3.85	4.17	4.18	4.33	4.21
5389.49	4.30	4.26	4.16	4.42	4.34	4.47	4.12
5393.18	4.08	4.04	4.00	4.20	4.18	4.26	4.13
5397.14	3.67	3.63	3.60	3.98	3.96	4.12	3.86
5405.78	3.78	3.73	3.62	3.99	3.96	4.13	3.93
5410.92	4.09	4.02	4.09	4.15	4.13	4.23	4.10
5415.21	3.97	4.04	3.93	4.22	4.12	4.36	4.21

Table 2. Observed Values of -log W/λ (cont.)

λ	Mult	E P	log gf	HD 10494	HD 17971	HD 231195	HD 9973
5429.71	15	0.96	-1.78	4.13	4.11	4.43	4.15
5434.53	15	1.01	-1.97	4.20	4.22	4.73	4.28
5445.05	1163	4.39	0.37	4.45	4.35	4.63	4.51
5461.56	1145	4.44	-0.97	5.21	5.46	5.53	5.19
5473.91	1062	4.15	-0.21	4.54	4.54	4.86	4.52
5497.53	15	1.01	-2.49	4.37	4.25	4.54	4.30
5501.48	15	0.96	-2.66	4.25	4.29	4.44	4.46
5506.79	15	0.99	-2.44	4.42	4.36	4.55	4.39
5525.55	1062	4.23	-0.52	4.48	4.43	4.48	4.62
5554.90	1183	4.55	0.00	4.70	4.76	4.84	4.76
5560.20	1164	4.43	-0.50	4.87	4.89	4.78	4.98
5569.63	686	3.42	0.07	4.47	4.35	4.41	4.47
5576.10	686	3.43	-0.31	4.55	4.47	4.64	4.60
5586.77	686	3.37	0.34	4.22	4.21	4.34	4.33
5618.64	1107	4.21	-0.38	5.20	5.11	4.88	5.27
5619.61	1161	4.39	-0.75	5.14	5.14	5.01	4.90
5620.50	1061	4.15	-0.79	5.03	4.84	4.82	5.10
5635.83	1088	4.26	-0.61	5.07	5.10	5.01	5.52
5638.27	1087	4.22	-0.16	4.75	4.75	5.11	4.79
5679.03	1183	4.65	-0.02	4.84	4.96	--	4.97
5717.84	1107	4.28	-0.20	5.01	5.01	4.91	4.84
5741.86	1086	4.26	-0.62	4.94	--	4.88	--
5806.73	1180	4.61	-0.20	4.76	4.89	5.02	4.98
5856.10	1128	4.29	-0.56	5.10	5.28	5.14	5.38
5859.60	1181	4.55	0.04	4.84	4.72	5.13	4.79
5862.37	1180	4.55	0.18	4.61	4.77	5.07	4.70
5905.68	1181	4.65	-0.10	4.97	4.78	--	5.00
5956.70	14	0.86	-4.06	--	4.89	--	--
5983.69	1175	4.55	-0.10	4.78	4.94	--	--
6024.07	1178	4.55	0.45	--	4.63	--	--

Table 2. Observed Values of -log W/λ (cont.)

λ	HD 195593	α Per	HD 172052	HD 180028	+60° 2532	HR 690
5429.71	4.13	4.19	4.15	4.01	4.09	4.24
5434.53	4.24	4.26	4.16	4.16	4.17	4.30
5445.05	4.41	4.43	4.35	4.25	4.38	4.59
5461.56	5.13	4.83	4.70	--	5.02	5.13
5473.91	4.34	4.41	4.34	4.60	4.42	4.50
5497.53	4.26	4.24	4.26	4.20	4.26	4.41
5501.48	4.43	4.19	4.28	4.21	4.28	4.42
5506.79	4.28	4.29	4.36	4.23	4.29	4.31
5525.55	4.47	4.50	4.51	4.42	4.43	4.73
5554.90	4.59	4.66	4.65	4.59	4.54	4.83
5560.20	4.75	4.68	4.90	4.81	4.75	5.06
5569.63	4.36	4.38	4.37	4.25	4.34	4.44
5576.10	4.40	4.37	4.47	4.46	4.40	4.55
5586.77	4.22	4.18	4.25	4.14	4.25	4.32
5618.64	4.94	5.08	4.88	4.62	4.67	4.85
5619.61	4.74	5.06	4.83	4.84	4.79	5.03
5620.50	4.76	4.98	4.55	4.81	4.58	5.04
5635.83	4.93	5.02	4.80	4.80	4.88	5.43
5638.27	4.54	4.74	4.44	4.60	4.60	4.76
5679.03	4.78	4.90	4.77	--	4.65	5.13
5717.84	4.74	4.92	4.88	4.56	4.63	4.99
5741.86	--	5.06	4.86	4.79	4.88	5.20
5806.73	4.98	4.90	4.72	4.82	4.81	4.87
5856.10	4.95	5.09	5.18	4.95	5.08	5.25
5859.60	4.73	4.72	4.67	4.58	4.63	4.74
5862.37	4.58	4.57	4.70	4.42	4.59	4.64
5905.68	4.91	4.94	4.92	4.68	4.73	4.75
5956.70	4.65	--	4.48	4.45	4.79	4.89
5983.69	4.81	4.47	4.72	4.60	4.85	4.45
6024.07	--	4.34	--	4.45	4.55	4.50

Table 2. Observed Values of -log W/λ (cont.)

λ	45 Dra	δ CMa	ρ Cas	HD 331777	γ Cyg	HR 7542	R Pup
5429.71	4.14	3.91	3.85	3.86	4.00	4.05	3.85
5434.53	4.13	3.96	4.06	3.94	4.10	4.12	3.92
5445.05	4.39	4.28	4.13	4.27	4.32	4.27	4.21
5461.56	--	5.21	4.94	--	5.05	4.85	4.95
5473.91	4.45	4.08	3.96	4.12	4.11	4.23	4.07
5497.53	4.20	3.97	3.98	4.03	4.10	4.14	3.94
5501.48	4.26	3.93	3.86	4.02	4.11	4.15	3.93
5506.79	4.24	4.04	4.08	4.04	4.07	4.19	4.12
5525.55	4.53	4.25	4.10	4.15	4.26	4.39	4.43
5554.90	4.64	4.55	4.55	4.55	4.38	4.62	4.59
5560.20	4.80	4.88	4.70	4.72	4.56	5.06	4.94
5569.63	4.32	4.17	4.17	4.21	4.16	4.30	4.31
5576.10	4.42	4.34	4.28	4.31	4.26	4.36	4.40
5586.77	4.28	4.00	4.07	4.02	4.09	4.18	4.08
5618.64	4.94	4.81	4.69	4.68	4.72	4.93	5.19
5619.61	4.95	5.16	--	--	4.81	--	--
5620.50	4.91	4.76	4.48	4.68	4.70	4.88	4.59
5635.83	5.14	5.07	4.72	4.88	4.92	4.83	5.18
5638.27	4.64	4.50	4.26	4.52	4.54	4.46	4.73
5679.03	4.84	4.77	4.61	--	4.78	4.75	4.80
5717.84	5.02	4.55	4.67	4.67	4.54	4.57	4.50
5741.86	4.83	4.85	4.49	--	4.81	4.76	4.75
5806.73	4.80	4.67	4.52	--	4.42	4.75	4.40
5856.10	--	5.25	4.93	5.24	4.89	5.17	5.24
5859.60	4.76	4.60	4.54	4.85	4.53	4.64	4.69
5862.37	4.75	4.57	4.41	4.60	4.28	4.59	4.55
5905.68	--	4.85	--	4.76	4.80	4.80	--
5956.70	--	--	4.47	--	4.55	4.75	--
5983.69	--	--	4.36	4.75	4.51	--	--
6024.07	--	--	4.27	4.44	4.41	--	--

Table 2. Observed Values of -log W/λ (cont.)

λ	HD 6474	HD 18391	HR 8752	β Aqr	β Cam	α Aqr	ψ And
5429.71	3.76	3.80	3.69	4.03	3.95	4.13	3.97
5434.53	3.81	3.84	3.59	4.12	4.16	4.25	4.08
5445.05	4.08	4.13	4.00	4.27	4.24	4.25	4.28
5461.56	--	--	--	5.15	4.71	4.66	4.26
5473.91	3.97	3.93	3.75	4.35	4.13	4.42	4.25
5497.53	3.89	3.83	3.72	4.21	4.07	4.27	4.15
5501.48	3.85	3.80	3.74	4.06	4.08	4.24	4.12
5506.79	3.89	3.79	3.73	4.21	4.07	4.23	4.14
5525.55	4.25	4.19	3.87	4.33	4.21	4.61	4.31
5554.90	4.33	4.38	4.23	4.45	4.30	4.47	4.42
5560.20	4.56	4.55	4.43	4.64	4.31	4.70	4.49
5569.63	4.13	4.02	3.93	4.26	4.12	4.28	4.18
5576.10	4.15	4.14	4.05	4.33	4.15	4.34	4.23
5586.77	4.01	3.84	3.72	4.21	4.02	4.22	4.17
5618.64	4.59	4.53	--	4.90	4.48	4.81	4.59
5619.61	--	--	--	4.67	4.55	4.57	4.33
5620.50	4.57	4.31	4.26	4.54	4.45	4.65	4.48
5635.83	4.71	4.95	--	4.85	4.51	4.61	4.49
5638.27	4.41	4.40	4.13	4.50	4.20	4.43	4.31
5679.03	4.41	4.53	4.39	4.61	4.59	4.41	4.37
5717.84	4.49	4.32	4.24	5.16	4.39	4.88	4.77
5741.86	4.62	4.55	--	4.72	4.65	4.52	4.41
5806.73	4.69	4.70	3.99	4.59	4.56	4.43	4.44
5856.10	4.94	--	--	--	4.83	4.97	4.82
5859.60	4.47	--	4.42	4.59	4.56	4.38	4.43
5862.37	4.39	--	4.41	4.50	4.35	4.33	4.41
5905.68	4.76	--	--	4.74	4.58	4.54	4.59
5956.70	4.55	--	--	4.49	--	--	4.20
5983.69	4.51	--	--	4.67	--	4.39	4.46
6024.07	4.42	--	--	--	--	--	--

Table 2. Observed Values of -log W/λ (cont.)

Fe II Lines, λ> 5000A

λ	Mult	E P	log gf	89 Her	HD 10494	HD 17971	HD 231195
5197.57	49	3.22	-2.54	4.04	3.83	3.93	3.95
5234.62	49	3.21	-2.37	4.04	3.91	3.91	3.92
5256.89	41	2.88	-3.28	4.53	4.48	4.36	4.32
5325.56	49	3.21	-3.27	4.36	4.15	4.15	4.17
5414.09	48	3.21	-3.29	4.49	4.27	4.22	4.42
5425.27	49	3.19	-3.29	4.66	4.11	4.07	4.27
5991.38	46	3.14	-3.49	4.34	4.17	4.28	4.38
6084.11	46	3.19	-3.82	4.49	--	--	--

λ	HD 9973	HD 195593	α Per	HD 172052	HD 180028	+60 2532
5197.57	4.07	4.06	4.22	4.02	4.00	3.99
5234.62	3.99	3.97	4.15	3.96	3.91	4.00
5256.89	4.46	4.18	4.58	4.53	4.43	4.43
5325.56	4.31	4.30	4.34	4.28	4.25	4.20
5414.09	4.29	4.36	4.46	4.25	4.32	4.36
5425.27	4.23	4.28	4.35	4.35	4.26	4.28
5991.38	--	4.43	4.38	4.47	4.42	4.47
6084.11	--	--	4.55	--	--	--

λ	HR 690	45 Dra	δ CMa	ρ Cas	HD 331777	γ Cyg	HR 7542
5197.57	4.05	4.09	3.85	3.84	3.64	4.00	4.03
5234.62	4.10	4.09	3.75	3.77	3.59	4.00	3.98
5256.89	4.40	4.56	4.24	4.31	4.14	4.55	4.54
5325.56	4.30	4.29	4.04	4.15	3.94	4.18	4.25
5414.09	4.52	4.40	4.12	3.99	4.11	4.26	4.29
5425.27	4.40	4.15	3.94	4.09	3.93	4.15	4.29
5991.38	4.41	--	--	4.22	4.13	4.16	--
6084.11	4.45	--	--	4.26	--	4.25	--

Table 2. Observed Values of -log W/λ (cont.)

λ	R Pup	HD 6474	HD 18391	HR 8752	β Aqr	β Cam	α Aqr	ψ And
5197.57	3.73	3.75	3.84	3.55	4.01	4.10	4.13	4.04
5234.62	3.71	3.72	3.70	3.52	3.96	4.00	4.02	4.10
5256.89	4.22	4.17	4.25	4.06	4.41	4.51	4.64	4.46
5325.56	4.08	3.98	3.98	3.88	4.21	4.29	4.32	4.37
5414.09	3.99	4.03	3.99	4.10	4.41	4.33	4.61	4.35
5425.27	3.94	3.97	3.90	4.03	4.33	4.21	4.55	4.26
5991.38	--	4.19	--	3.98	4.59	--	4.27	4.37
6084.11	--	--	--	4.06	--	--	--	--

Table 3. Comparison of Fe I V_t with Published Values

Star	V_t	Reference
89 Her	8.5 km/sec	Present work
	9.1 km/sec	Searle et al. (1963)
α Per	5.2 km/sec	Present work
	5 km/sec	Parsons (1967)
	5.4 km/sec	Abt, Osmer, and Kraft (1966)
δ CMa	9.8 km/sec	Present work
	12 km/sec	Bell and Rodgers (1965)
β Aqr	6.2 km/sec	Present work
	4 km/sec	Parsons (1967)
	5.4 km/sec	Danziger (1965)

Fe I lines were measured to reduce possible zero point errors in the derived velocity to $\Delta \log V = \pm 0.15$. However, all the Fe II lines are on the flat part of the curve of growth and the zero point errors in the Fe II velocities could be twice as large as for Fe I. Therefore the Fe II microturbulent velocities indicate only the relative behavior between stars with an accuracy of 40%.

We have listed in table 4 the values of the microturbulence derived from the Fe I lines and from the Fe II lines for 25 stars in the spectral range F0-G5; figures 1 and 2 display the results graphically. We see immediately that the Fe II results are systematically greater than the Fe I values and that the discrepancy changes with spectral type for the Ia stars. At F2 Fe I and Fe II give nearly the same velocity while at F5 the Fe II velocity is twice that of the Fe I value. In the later stars the difference decreases. We can summarize the raw data as follows:

(1) In the Ia stars the Fe II microturbulence ranges from 9 to 21 km/sec. The Fe I microturbulence decreases from 15 km/sec at F0 to 6 km/sec at F5 and rises above 10 km/sec at G0. Correlations with luminosity will be discussed in the next section; the main feature here is the different behavior of the Fe I and Fe II velocities.

(2) The Fe I velocity in the F5-G5 Ib stars is in the 5-7 km/sec range. The Fe II values are only slightly higher. The F3 Ib star in our list has an Fe I velocity of 12 km/sec, but Abt (1960) has shown that this star is more luminous than the Ib stars of

Table 4. Measured Values of V_t from Fe I and Fe II

Star	Sp.	Fe I V_t (km/sec)	Fe II V_t (km/sec)
89 Her	F2Ia	8.5	8.9
HD 10494	F5Ia	6.2	12.0
HD 17971	F5Ia	6.6	11.7
HD 231195	F5Ia	4.3	12.0
HD 9973	F5Iab	4.8	8.5
HD 195593	F5Iab	5.4	8.5
α Per	F5Ib	5.2	6.3
HD 172052	F5Ib	4.9	8.1
HD 180028	F6Ib	5.9	9.5
+60° 2532	F7Ib	6.5	8.5
HR 690	F7Ib	5.4	7.2
45 Dra	F7Ib	5.2	7.2
δ CMa	F8Ia	9.8	14.5
ρ Cas	F8Ia	7.2	13.2
HD 331777	F8Ia	11.7	18.2
γ Cyg	F8Ib	7.2	9.1
HR 7542	F8Ib	6.0	8.7
R Pup	G0Ia	8.7	16.6
HD 6474	G0Ia	11.0	15.0
HD 18391	G0Ia	9.6	15.0
HR 8752	G0Ia	12.6	20.9
β Aqr	G0Ib	6.2	9.5
β Cam	G0Ib	6.9	8.3
α Aqr	G2Ib	6.0	8.0
ψ And	G5Ib	6.2	7.2

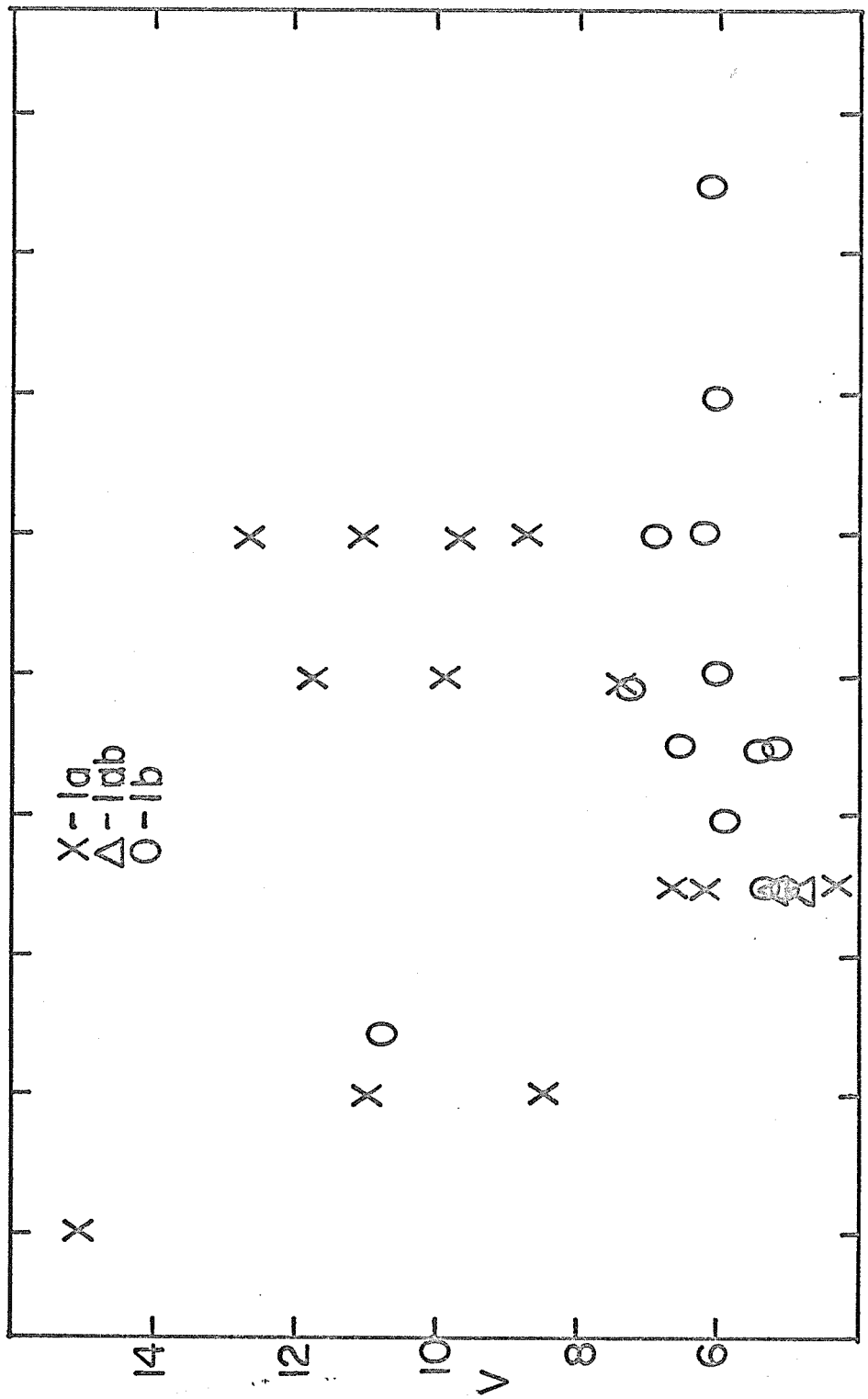

Fig. 1. The Fe I microturbulent velocity, V, as a function of spectral type and luminosity class. Except for 89 Her (F2Ia) the values for the stars earlier than F5 are taken from Searle et al. (1963) and Abt (1960).

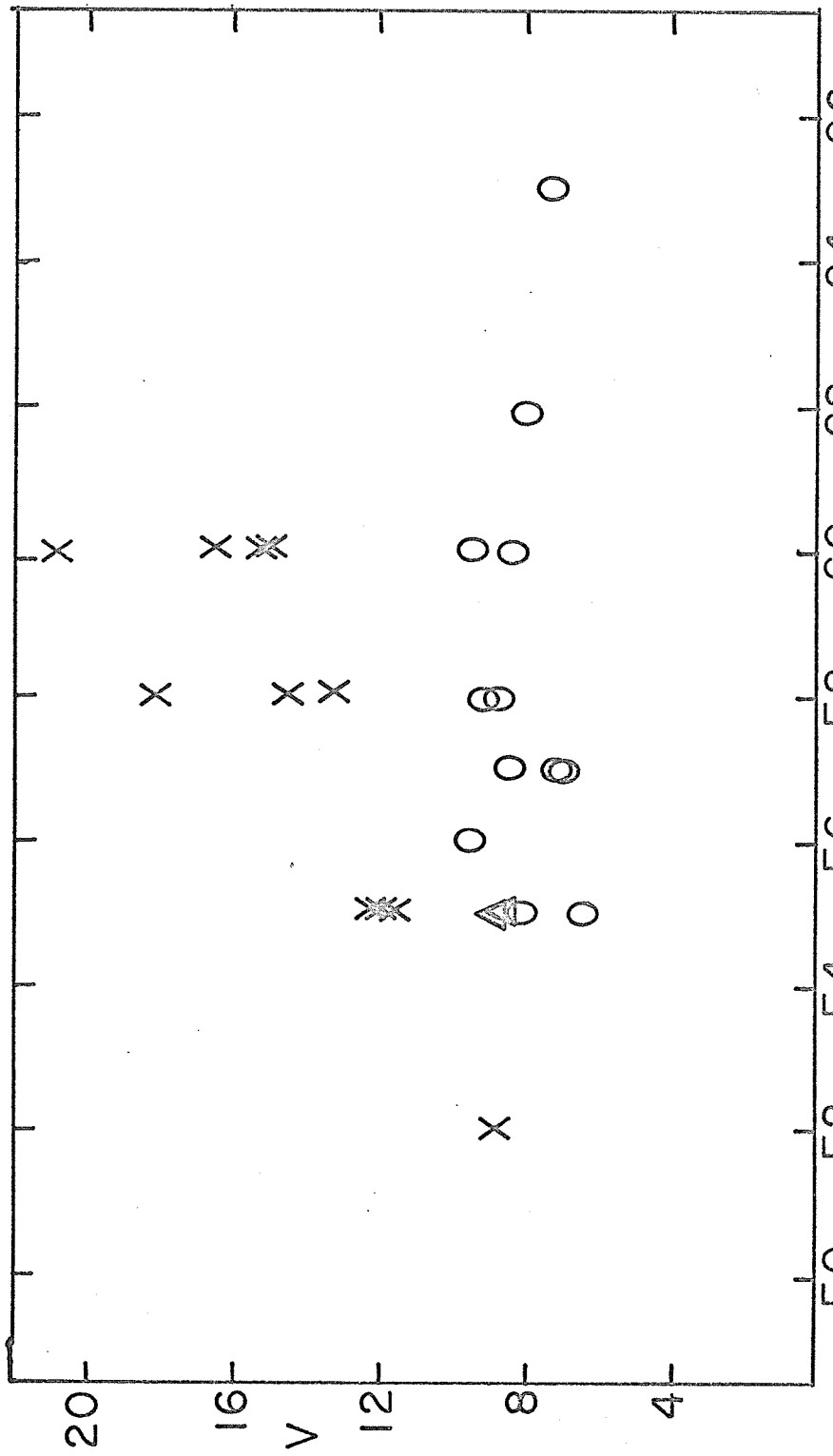

Fig. 2. The Fe II microturbulent velocity, V, as a function of spectral type and luminosity class. The symbols have the same meaning as in fig. 1.

later spectral type.

Because the same theoretical curve of growth was used for all stars, our results would be altered if the mechanism of line formation changed with luminosity or spectral type. For example if the lines were formed by pure absorption in the Ib stars and by scattering in the Ia stars, we would have underestimated the Ib results by 40%. The turbulent velocity V and the central depth of saturated lines R_c are related by R_c V = const. approximately. R_c = 1 for scattering and for the F I stars the models indicate that R_c = 0.7 for absorption. Thus a line deepening effect could simulate an increase in the turbulent velocity, but would not account for the observed range of velocities by itself.

In an attempt to investigate this possibility we have compiled in table 5 the central intensities r (where r = 1 - R_c) for a strong line of Fe I and Fe II. Because rotation and macroturbulence both raise the central intensity we should consider the minimum value within a group of stars as being representative for that group. Taking the stars earlier than F8 we see that the lines in +60° 2532, which has a low turbulent velocity, are as deep as any of the others. For the F8-G5 stars there is a greater tendency for the ones with higher turbulence to have deeper lines although the Fe I line in ψ And is an exception. Obviously the lines should be measured at higher resolution in order for the results to be conclusive; our material indicates that line deepening causes only a small part of the velocity increase at most.

Table 5. Line center residual intensities for Fe I 5371 and Fe II 5234. The respective microturbulent velocities (V_t) are given for comparison.

Star	5371	Fe I V_t (km/sec)	5235	Fe II V_t (km/sec)
HD 10494	0.41	6.2	0.28	12.0
HD 17971	0.46	6.6	0.33	11.7
HD 231195	0.72	4.3	0.46	12.0
HD 9973	0.45	4.8	0.35	8.5
HD 195593	0.35	5.4	0.32	8.5
α Per	0.66	5.2	0.63	6.3
HD 172052	0.39	4.9	0.32	8.1
HD 180028	0.50	5.9	0.44	9.5
+60° 2532	0.24	6.5	0.30	8.5
HR 690	0.50	5.4	0.49	7.2
45 Dra	0.52	5.2	0.43	7.2
ρ Cas	0.52	7.2	0.26	13.2
HD 331777	0.27	11.7	0.09	18.2
γ Cyg	0.45	7.2	0.44	9.1
HR 7542	0.47	6.0	0.49	8.7
R Pup	0.31	8.7	0.11	16.6
HD 6474	0.20	11.0	0.26	15.0
HD 18391	0.28	9.6	0.24	15.0
HR 8752	0.24	12.6	0.00	20.9
β Aqr	0.36	6.2	0.47	9.5
β Cam	0.51	6.9	0.55	8.3
α Aqr	0.30	6.0	0.31	8.0
ψ And	0.06	6.2	0.51	7.2

Table 6. Photographic equivalent widths of luminosity sensitive lines.

Line	Mult	E P	α Per	ρ Cas	ε Aur
O I 7774	1	9.11	1.44A	2.74A	3.08A
O I 8446	4	9.48	0.68	1.15	1.52
Mg II 7877	8	9.95	0.18	0.37	0.30
Mg II 7896	8	9.96	0.30	0.53	0.51

For the O I 6158 data photoelectric measures of O I 7774 are given for comparison.

Line	Mult	E P	α Per	+60° 2532	HD 10494	HD 231195	HD 331777
6156	10	10.69	0.10A	0.04A	0.17A	0.08A	0.15A
6157	10	10.69	0.13	0.06	0.18	0.16	0.14
6158	10	10.69	0.16	0.10	0.22	0.16	0.18
7774	1	9.11	0.95	0.59	1.77	2.17	2.12

Line	log gf (Wiese, Smith, and Glennon
O I 7774	0.66 1966)
O I 6156	-0.70
O I 6157	-0.48
O I 6158	-0.33

In addition to the spectral coverage in the blue and green we obtained Palomar I-N plates of ε Aur and α Per which covered the region from Hα to 8600A at 14.5 A/mm. In addition Greenstein made available similar plates of ρ Cas taken with the same equipment. Measures of this material showed that the Mg II 7877 and 7896 lines and the O I 8446 line increased in strength with luminosity in roughly the same way as the O I 7774 line. Keenan and Hynek's values for the 8446 line confirmed this idea and their figure 4 also suggested that the infrared nitrogen lines showed the same effect. Finally the O I 6158 triplet was measured on the IIa-D plates because it arises from the upper level of the 7774 line. If non-LTE effects were important in oxygen, the 6158 line might behave differently than the 7774 line. However our measures indicate that it increases in strength with luminosity also. All the data for these line strengths are given in table 6.

C. Photoelectric Measures of the O I 7774 Line

The work of Keenan and Hynek and of Parsons (1964) indicated that the 7774 line was such a good luminosity indicator that we believed it was important to establish a photoelectric system for measuring it. Current photomultipliers are sufficiently sensitive in the infrared that it is practical to observe much fainter stars than are accessible photographically. The F I stars are the coolest group in which the line is strong and are the brightest in the infrared at a given bolo-

metric luminosity. Thus they can be observed at greater distances than B and A supergiants. If the line strength is well correlated with luminosity, the F I stars could become very useful distance indicators.

Table 6 shows that the equivalent width of the line is as high as 3A so that it should be measurable with a narrow band filter or a low resolution scanner. For our observations we used the Mt. Wilson Cassegrain scanner and an S-1 photomultiplier. The S-1 was chosen because it has a flat response at 7800A and is as sensitive as any available tube at this wavelength. The scanner is intended for measuring continuum fluxes, not spectral lines, and we decided that a bandpass of 20A was the minimum that could be used safely. Due to the optical design and seeing fluctuations narrower values cannot be defined with enough precicion. With a 20A exit slit a line of 2A equivalent width will reduce the measured flux to 90% of the neighboring continuum. The scanner is operated with pulse counting electronics so we could estimate the measuring errors from the observed counts. The error $=\sqrt{N}$ where N is the number of counts. For N = 10,000 the standard deviation of N is 100 or 1%. Since we are measuring a difference of two observations, the standard deviation of the difference is $\sqrt{2N}$ for small differences.

The technique used to determine the line strength was to make observations at 7754, 7774, 7794, repeat at 7774, and then measure the sky using the same integration time for each measure.

Accordingly

$$W = \frac{N(7754) + N(7794) - N(7774) - N(7774)}{N(7754) + N(7794) - 2 * N\,(sky)} * 20A \qquad (II\text{-}1)$$

is the equivalent width of the line in A. The integration time was adjusted so that roughly 10,000 counts were accumulated at 7754 or 7794; therefore the standard deviation in W was 0.2A, for the sky counts were much less than the star counts. With the scanner on the 60" telescope this accuracy could be achieved in 100 sec. for an unreddened 7th magnitude F star. Two complete measures of such a star took about 15 minutes.

As the scanner is a single channel instrument, only nights of top photometric quality could be used for this program; all the measures given here were made on nights when the counts repeated to 1%. In order to check for time variations in the line strength, observations were made at one month intervals from August to November, 1967, and June through August, November, and December, 1968. No convincing evidence of variability was found; instead we determined that the error of a single determination was closer to 0.30A than the theoretical 0.20A. A double channel instrument would be much more useful for answering the question of variability. Table 7 contains the mean line strength for 60 stars, the estimated standard deviation of the mean, and the number of measures from which the mean was found. The data are plotted as a function of spectral type and luminosity class in figure 3.

Inspection of figure 3 shows clearly that the line strength

Table 7. Photoelectric measures of the O I 7774 triplet.

Star	Sp.	W	dev	n
HR 5291	A0III	0.72	0.08	5
HD 21389	A0Ia	1.79	0.02	6
HD 39970	A0Ia	1.58	0.14	2
HD 3940	A1Ia	2.13	0.28	2
HD 12953	A1Ia	1.84	0.09	4
HD 14433	A1Ia	2.12	0.03	4
HD 14489	A2Ia	1.91	0.15	1
HD 207260	A2Ia	2.09	0.02	2
HR 5532	A3III	0.78	0.07	6
HD 13476	A3Iab	2.27	0.06	4
HD 213470	A3Ia	1.85	0.19	2
HD 223385	A3Ia^{+}	2.47	0.15	1
HD 17378	A5Ia	2.21	0.14	4
HR 5433	A7IV-V	0.65	0.20	1
HR 5329	A7IV	0.66	0.13	5
HR 5127	A7III	0.44	0.02	2
HR 5435	A7III	0.84	0.06	6
HR 6144	A7Ib	1.76	0.14	6
ε Aur	A8Ia	2.51	0.05	7
HR 6095	A9III	0.81	0.11	3
HR 4775	F0IV	0.29	0.03	2
HR 5129	gF0	0.73	0.10	4
HR 5017	F0II-IIIp	0.36	0.03	2
α Lep	F0Ib	1.70	0.25	1
φ Cas	F0Ia	2.26	0.06	16
HR 6699	gF1	0.80	0.08	6
HR 6707	F2II	0.82	0.04	3
89 Her	F2Ia	1.54	0.07	22
HR 5487	F3IV	0.60	0.23	2
HR 6965	cF3	1.02	0.04	4

Table 7 (cont.)

Star	Sp.	W	dev	n
HD 161796	F3Ib	1.65	0.08	18
HR 4753	F5IV	0.62	0.08	2
HR 6724	F5II	0.87	0.01	3
α Per	F5Ib	0.95	0.04	23
HD 172052	F5Ib	0.89	0.10	7
HD 9973	F5Iab	1.23	0.06	5
HD 195593	F5Iab	1.13	0.05	10
HD 10494	F5Ia	1.77	0.11	9
HD 17971	F5Ia	1.79	0.15	2
HD 231195	F5Ia	2.17	0.07	16
HR 5317	F6IV	0.29	0.16	3
HD 180028	F6Ib	0.62	0.09	12
HR 5185	F7V	0.18	0.08	6
HR 5338	F7IV	0.30	0.34	2
45 Dra	F7Ib	0.72	0.08	14
HR 690	F7Ib	0.86	0.30	1
+60° 2532	F7Ib	0.59	0.14	10
HR 5304	F8IV	0.50	0.23	3
HR 7542	F8Ib-II	0.48	0.10	5
γ Cyg	F8Ib	1.18	0.03	20
ρ Cas	F8Ia	2.30	0.06	18
δ CMa	F8Ia	1.43	0.18	4
HD 331777	F8Ia	2.12	0.11	12
HD 25056	F9Ib	0.69	0.12	3
β Cam	G0Ib	0.43	0.16	2
HR 8752	G0Ia	1.57	0.06	16
HD 18391	G0Ia	1.52	0.06	3
HD 6474	G0Ia	1.59	0.07	9
Sun	G2V	0.19	(taken from Rowland Atlas)	
ξ Pup	G3Ib	0.03	0.06	6

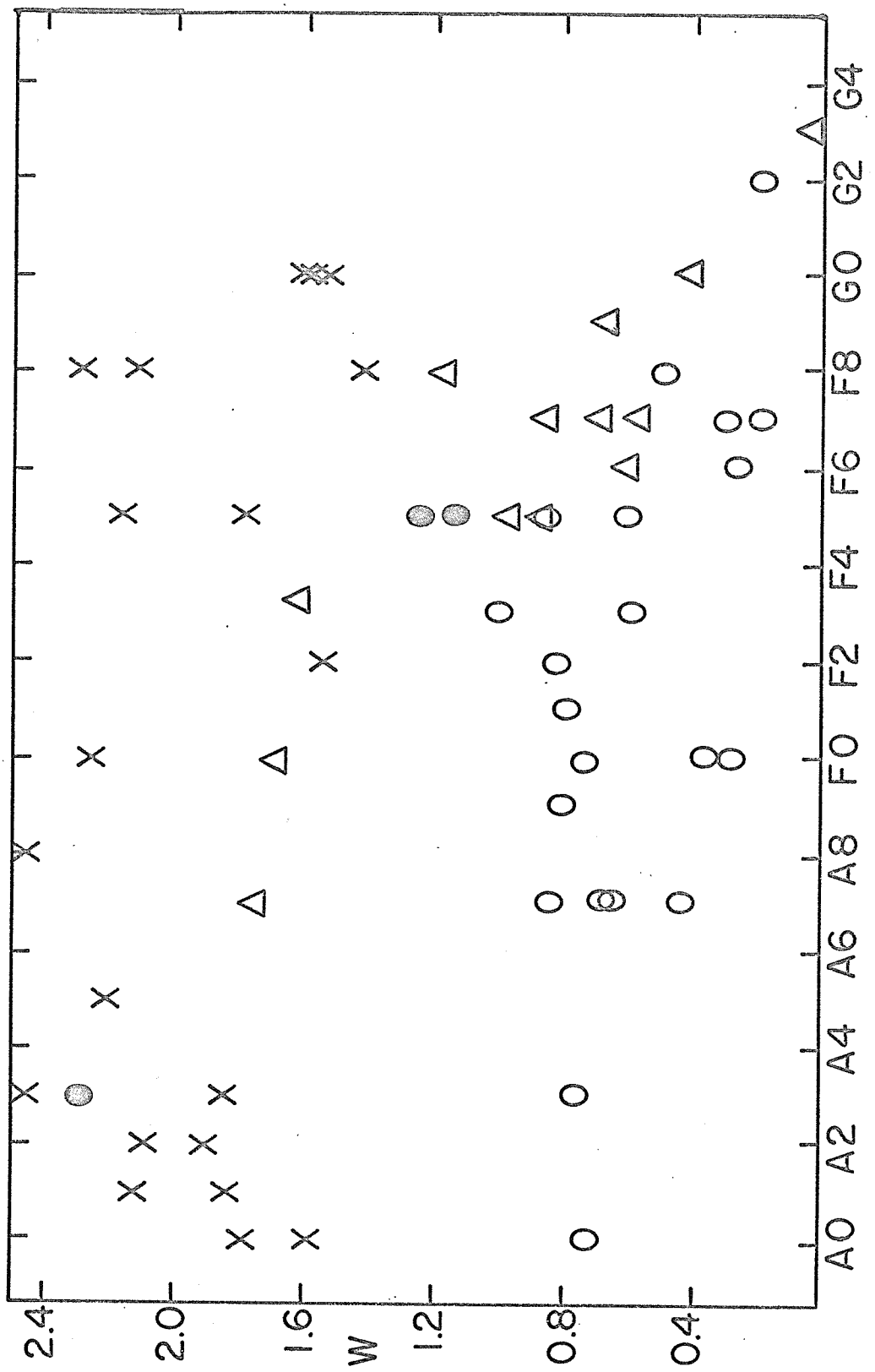

Fig. 3. The oxygen line strength, W (in Å), as a function of spectral type and luminosity class. X = Ia, ⊛ = Iab, Δ = Ib, O = II-V.

increases with luminosity class at all spectral types and that it distinguishes the Ia stars from the other classes. The Ib's have values intermediate between the Ia's and II - V's though the difference between the Ib's and lower luminosity stars decreases for types F5 and later. The line strength increases from A0 to A8 and then decreases almost to zero in the middle G stars. Thus our photoelectric measures verify the behavior noted by Keenan and Hynek and by Parsons (1964).

In order to see how our photometric system compares with photographic measures, we compared our results with the photographic ones listed above and with Keenan and Hynek's values, which were obtained from 48 A/mm spectra. Table 8 lists the widths found by the different techniques. We see that the Palomar widths average 30% greater than the scanner values while the values of Keenan and Hynek are 5% greater than the scanner ones. As a check on the scanner zero point, it was used to measure the oxygen deficient A star γ Equ; the result was $W = 0.01 \pm 0.20$. The system zero point is correct.

It is not surprising that the scanner values are lower than the Palomar ones. The scanner side channels are not corrected for any line blocking, so that the scanner continuum is lower than the one which would be drawn on the microphotometer tracing. This effect reduces the equivalent width measured by the scanner. Since calibration errors can cause 20% differences (Wright, 1966) in photographic equivalent widths measured with different spectographs, we

Table 8. Comparison of independent measures of the O I 7774 line

Star	Scanner	K and H	Palomar
α Per	0.97A	1.15A	1.44A
ρ Cas	2.30		2.74
ε Aur	2.51	2.34	3.08
δ CMa	1.43	1.88	
γ Cyg	1.18	0.93	

believe that our 30% difference based on three measures is not excessive and that the scanner measures define an acceptable system of equivalent widths.

D. Spectrophotometry and Balmer Line Widths of the Cluster Stars

In order to interpret the line strengths described above, models of the atmospheric structure are required. To match a given star with the appropriate model, we need observations which will determine the basic parameters of a stellar atmosphere, the effective temperature and the surface gravity. Three observable quantities which are sensitive to the temperature and gravity are: (1) the Balmer discontinuity, (2) the slope of the Paschen continuum, and (3) the width of the Balmer line wings. One of these, the Paschen continuum, is affected by interstellar reddening. Although the three quantities overdetermine the problem, they can be used in pairs to check the consistency between theory and observation.

There are four F I stars occurring in galactic clusters for which luminosities and reddening have been determined. Pesch (1959, 1960 a,b) observed φ Cas (F0Ia), HD 10494 (F5Ia), and BD +60° 2532 (F7Ib); Mitchell (1960) observed α Per (F5Ib). The Mt. Wilson Cassegrain scanner was used on the 60" telescope to determine the continuum fluxes of the cluster stars in the blue and the near infrared. The data were reduced on the Oke (1964) system

Table 9. Photometry of the cluster stars.

The estimated blanketing corrections, Δm_v, are scaled from Parsons (1967) values. The others were measured directly from Mt. Wilson and Palomar coude spectra.

Star:	φ Cas		α Per		HD 10494		+60° 2532	
λ	m_v	Δm_v	m_v	Δm_v	m_v	Δm_v	m_v	Δm_v
3390	7.80	-0.18 (est.)	4.00	-0.36 (est.)	11.05	-0.36 (est.)	11.52	-0.36 (est.)
3448	7.67	"	4.05	"	11.05	"	11.53	"
3509	7.62	"	3.97	"	11.03	"	11.40	"
3571	7.54	"	3.91	"	10.85	"	11.27	"
4032	5.73	-0.22	2.44	-0.52	8.81	-0.41	9.72	-0.46
4167	5.67	-0.24	2.22	-0.29	8.69	-0.40	9.57	-0.49
4255	5.61	-0.23	2.24	-0.19	8.57	-0.28	9.46	-0.44
7100	4.56	-0.00 (est.)	1.54	-0.03 (est.)	6.46	-0.03 (est.)	7.42	-0.03 (est.)
7530	4.51	"	1.54	"	6.34	"	7.34	"
7850	4.46	"	1.51	"	6.20	"	7.22	"
8080	4.43	"	1.48	"	6.14	"	7.18	"

and converted to magnitudes m_ν. m_ν is a magnitude per unit frequency interval. The average error in m_ν is $\pm 0^m.05$, based on observations from different nights. Table 9 contains the mean value of m_ν at each wavelength for the four stars.

We obtained line blocking corrections for the blue wavelengths beyond 4000A from Mt. Wilson and Palomar coude spectra; they are listed in table 9 also. Since the Pesch stars were very faint at wavelengths less than 3700A, we took Parsons' (1967) corrections for α Per and assumed they could be used for HD 10494 and +60° 2532. The ultraviolet corrections for φ Cas were estimated from the line blocking in the blue to be half as large. The Balmer jump measures could have uncertainties of $\pm 0^m.10$ because of errors in these values. Parsons' infrared corrections were around $0^m.03$, and we have applied them to all stars but φ Cas, which is early enough for the correction to be negligible. From these data we have found the deblanketed $m_\nu(4110) - m_\nu(7550)$ color index and corrected the values for reddening using the standard Whitford (1958) extinction curve: the color excess $E(4110-7550) = 2.3\ E(B-V)$. Table 10 contains the deblanketed and unreddened color indices along with the Balmer jumps.

The half width of $H\gamma$ at a depth of 0.2 is a convenient way of characterizing the Balmer line widths, for it is less sensitive to measuring errors than the equivalent width of the whole line. The Balmer lines have broad wings which contribute significantly to the equivalent width; these wings are quite dependent on the placement

Table 10. Cluster star data.

Color indices, half widths of Hγ at a depth of 0.2, and Balmer jumps.

Star	m(4110)-m(7550)	Hγ	B.J.
φ Cas	-0.19	3.55A	$1^m.55$
α Per	+0.24	5.25	1.36
HD 10494	+0.10	3.48	1.75
+60° 2532	+0.31	2.45	1.00

of the continuum. We measured the widths of Hγ on the same plates used for the blanketing corrections and have listed their values in table 10.

III. Observed Luminosity and Temperature Effects in the F I Stars

A. Introduction

This section uses the data just described for an empirical investigation of the luminosity and temperature dependence of the spectral lines we have observed in the F I stars. First we examine the relation between the O I 7774 line strength and absolute magnitude and show that it accurately indicates the absolute magnitude of F stars brighter than $M_V = -4$. Using this technique we can trace the variation of the Fe I and Fe II microturbulent velocities with spectral type and absolute magnitude. Finally we discuss the behavior of all the lines and suggest why the Fe I lines are different than the rest.

B. The Correlation of Absolute Magnitude and the Strength of O I 7774

Absolute magnitudes are available for 10 of the F stars and 11 of the A stars in table 6. Pesch (1959, 1960 a,b) observed three galactic clusters containing F I stars and derived absolute magnitudes for them by obtaining the reddening from photometry of the main sequence stars and fitting the corrected main sequence to the standard zero age one. Mitchell (1960) found the absolute

magnitude of α Per by using the same technique. Four of the other F and G0 I stars and all of the A stars are members of associations, and their luminosities were obtained photometrically. Pesch estimated that the errors in absolute magnitudes found from this procedure were $\pm$ $0^m.5$ and we believe this value applies to all of the above stars. Searle et al. derived luminosities for 89 Her and HD 161796 by comparing spectroscopic determinations of the temperature and electron pressure with those of the cluster stars φ Cas and α Per. We have assigned a lower weight to their values since the combination of spectroscopic and photometric uncertainties raises their errors to $\pm$ $1^m.0$. Table 11 contains the absolute magnitudes and oxygen line strengths of the 21 stars.

We will consider the F stars first. They cover a 4 magnitude range in luminosity and the line strengths for seven of them are based on 9 to 22 individual measures. The error in the equivalent width is estimated to be $\pm$ 0.1A for these stars and $\pm$ 0.2A for the other three, δ CMa, HD 17971, and HD 18391, which were measured four times or less. The plot of absolute magnitude versus oxygen line strength (fig. 4) shows that the two quantities are well correlated. We can draw a straight line through the data for which the average deviation is $0^m.5$, the same as the estimated error in M_V. Therefore we conclude that the relation between M_V and W is linear within our measuring error and that the oxygen line strength can be used to determine the absolute magnitudes of F stars brighter than $M_V = -4$ with an accuracy of $\pm$ $0^m.5$.

Table 11. The oxygen line strength in stars of known absolute magnitude

Star	Sp	M_V	W(OI)	Ref.
φ Cas	F0Ia	-8.8	2.26	Pesch (1959)
89 Her	F2Ia	-7.1	1.54	Searle et al. (1963)
HD 161796	F3Ib	-6.4	1.65	Searle et al. (1963)
HD 10494	F5Ia	-7.5	1.77	Pesch (1960a)
HD 17971	F5Ia	-6.4	1.79	Wildey (1964)
α Per	F5Ib	-4.6	0.95	Mitchell (1960)
+60° 2532	F7Ib	-4.8	0.59	Pesch (1960b)
ρ Cas	F8Ia	-8.4	2.30	Sargent (1961)
δ CMa	F8Ia	-7.3	1.43	Feinstein (1967)
HD 18391	G0Ia	-6.7	1.52	Wildey (1964)
HD 21389	A0Ia	-6.9	1.79	Hiltner (1956)
HD 39970	A0Ia	-6.2	1.58	Hardie, Seyfert, and Gulledge (1960)
HD 3940	A1Ia	-6.8	2.13	Hiltner (1956)
HD 12953	A1Ia	-8.0	1.84	Wildey (1964)
HD 14433	A1Ia	-7.4	2.12	Ibid.
HD 14489	A2Ia	-7.4	1.91	Ibid.
HD 207260	A2Ia	-6.3	2.09	Hiltner (1956)
HD 13476	A3Iab	-6.8	2.27	Wildey (1964)
HD 213470	A3Ia	-7.5	1.85	Hiltner (1956)
HD 223385	A3Ia$^+$	-8.3	2.47	Hiltner (1956)
HD 17378	A5Ia	-7.7	2.21	Wildey (1964)

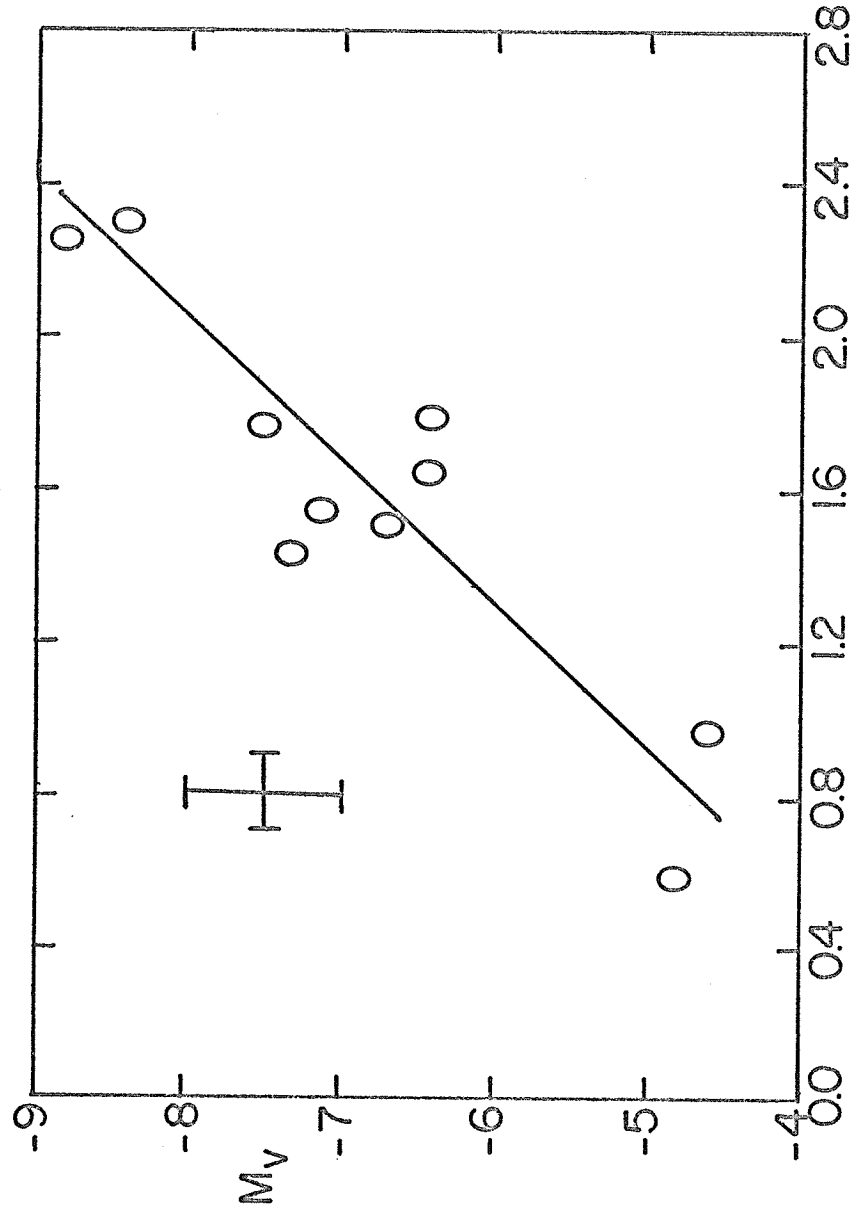

Fig. 4. The absolute magnitude (M_V) - oxygen line strength (W) relation for the F I stars. The cross indicates the estimated errors for the well determined values.

At visual wavelengths stars like φ Cas and ρ Cas are among the most luminous stars known. If the relation shown in figure 4 is true for all F I stars, they can be used as distance indicators which are substantially brighter than the classical cepheids. Since we have observed nearly all the F I stars accessible in the northern hemisphere, further studies will have to be done at southern latitudes. The Magellanic Cloud supergiants are very important here, for they provide an opportunity to see if the relation holds for stars in another galaxy, and if so, whether it is the same as in our own.

After the above data were taken, we attempted to see how the oxygen lines correlated with luminosity for the A I stars using a list of stars taken from Rosendhal's (1968) compilation of A supergiants in associations. Bad weather at the end of the 1968 observing season limited the average number of measures per star to three, so that the observational error for the A stars is roughly twice as great as for the well determined F stars in figure 4. We have plotted the results for both groups of stars in figure 5. It shows that the oxygen line in the A I stars could have the same kind of luminosity dependence as in the F's although the line is stronger in the A stars. More observations of these A I stars and of less luminous ones are needed in order to draw any conclusions about the linearity and tightness of the M_V - W relation for the A supergiants. We should note that since the A stars have a larger bolometric correction than the F's, it is

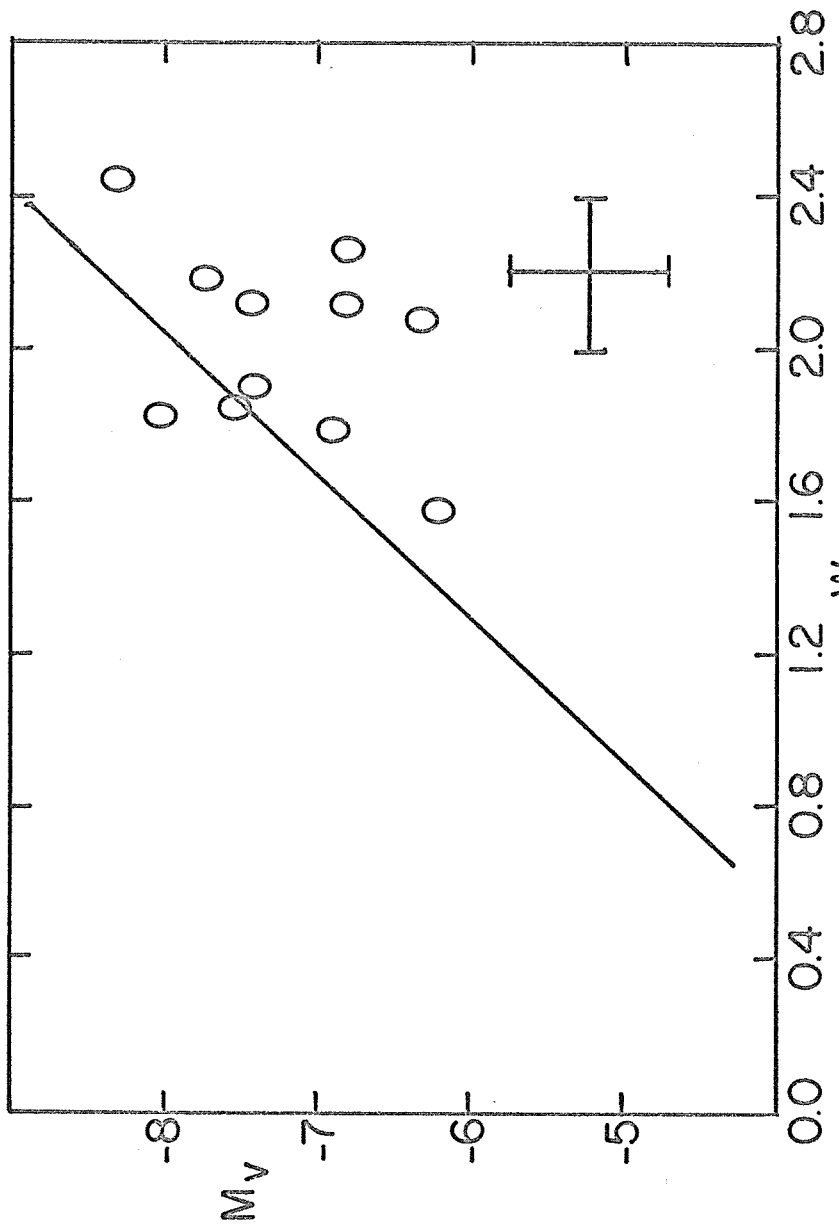

Fig. 5. The absolute magnitude (M_V) - oxygen line strength (W) relation for the A I stars in associations. The straight line indicates the results for the F stars in fig. 4.

quite possible that the M_{bol} - W relation for the two types could be the same.

We conclude that the equivalent width of the 7774 triplet is an excellent indicator of luminosity for the F supergiants. Accurate measures of its width may determine a star's luminosity with an error of 0.5 magnitude. Low resolution photoelectric techniques are quite satisfactory for measuring the line strength. The applicability of the new high transmission interference filters with bandpasses similar to those used for measuring Hβ should be tested. They could deliver more light to the photocell than a scanner with many internal reflections and therefore allow fainter stars to be observed. The main disadvantage at present of using the oxygen line to determine luminosity is the slowness of the near infrared detectors currently available. If their sensitivity could be made comparable with blue tubes, it would be possible to measure line strengths in M31 supergiants.

C. The Relationship of the O I Line and the Fe I and Fe II Turbulent Velocities

The O I 7774 line is strong enough to be on the flat part of the curve of growth for the F I stars and its strength is sensitive to the microturbulent velocity. This fact suggests that a microturbulent velocity increasing with luminosity could explain the observed relation between absolute magnitude and the oxygen line

strength. This section discusses the correlations of the Fe I and II turbulent velocities with luminosity (i.e., with the oxygen line strength).

First we consider the Fe I lines. Figure 6 displays the strength of the oxygen lines as a function of turbulent velocity for all the stars in which both were measured. We see that in general the stars with stronger lines have higher turbulence, but there is so much scatter we doubt that there is a real correlation. The problem is more pronounced at F5, where we have 7 stars of roughly the same temperature, than at earlier and later spectral types. The average value of the line strength for the F5 Ia stars is nearly twice that of the Ib's, yet the average velocity is 5.7 km/sec for the Ia's and 5.1 for the others. In HD 231195 (F5Ia) the velocity is 4.3 km/sec and the line strength = 2.17A while in HD 172052 (F5Ib) the values are 4.9 km/sec and 0.9A. Therefore at F5 there is no correlation between the oxygen line strength and the Fe I microturbulence.

When we consider the Fe II velocities, the situation is much different. Figure 7 shows the oxygen line strength as a function of the Fe II microturbulence. Not only is the scatter less than in figure 6 but it is caused by the large strengths of the Fe II lines in the G0 Ia stars, which mark the low temperature cutoff of the oxygen lines. In contrast to Fe I, the Fe II lines do show a significant increase with luminosity at F5. It is of interest that HR 8752 (G0 Ia), which has the strongest Fe II lines of the

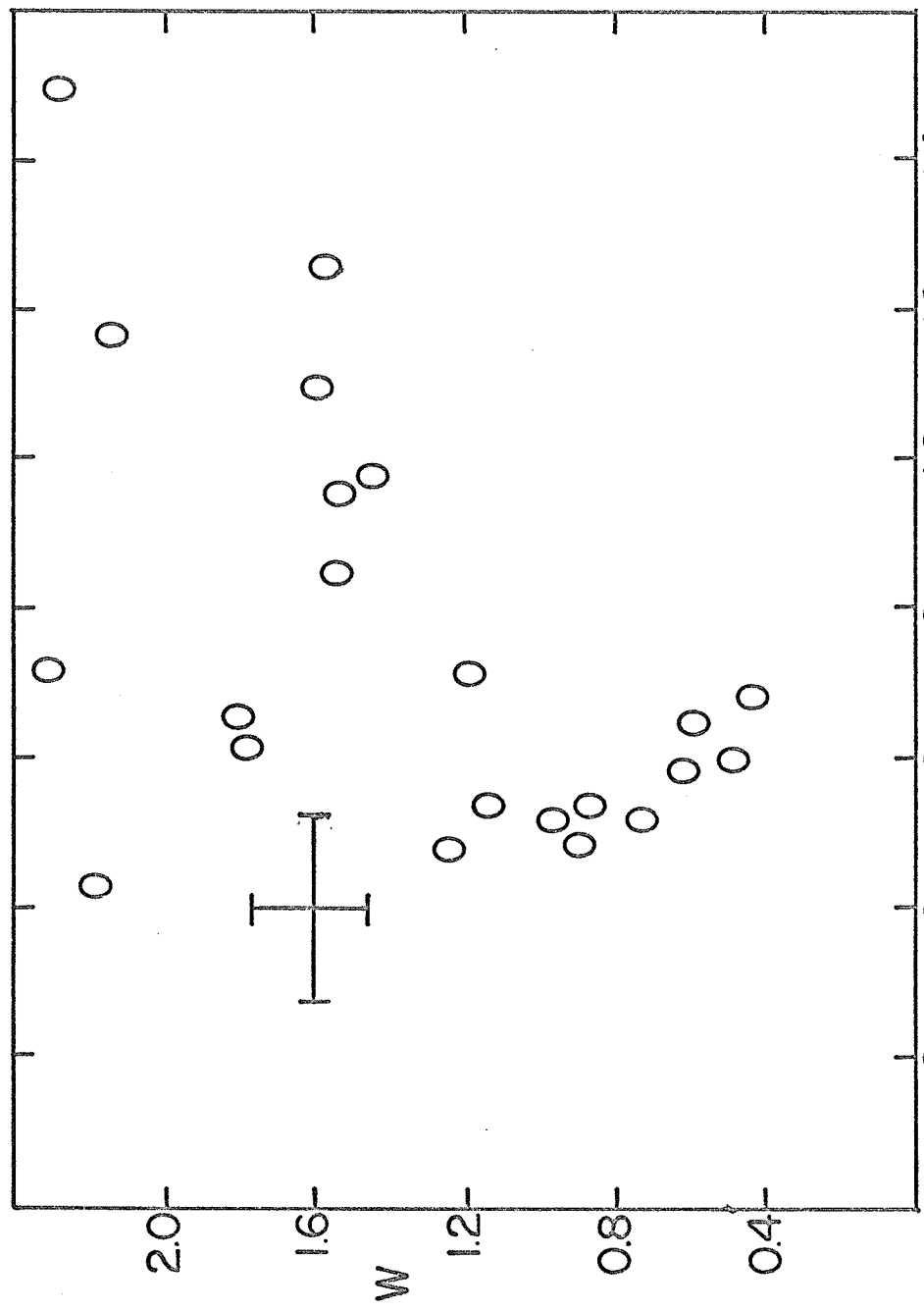

Figure 6. The oxygen line strength, W (in A), vs. the Fe I turbulent velocity, V_t (in km/sec). The cross indicates the estimated errors.

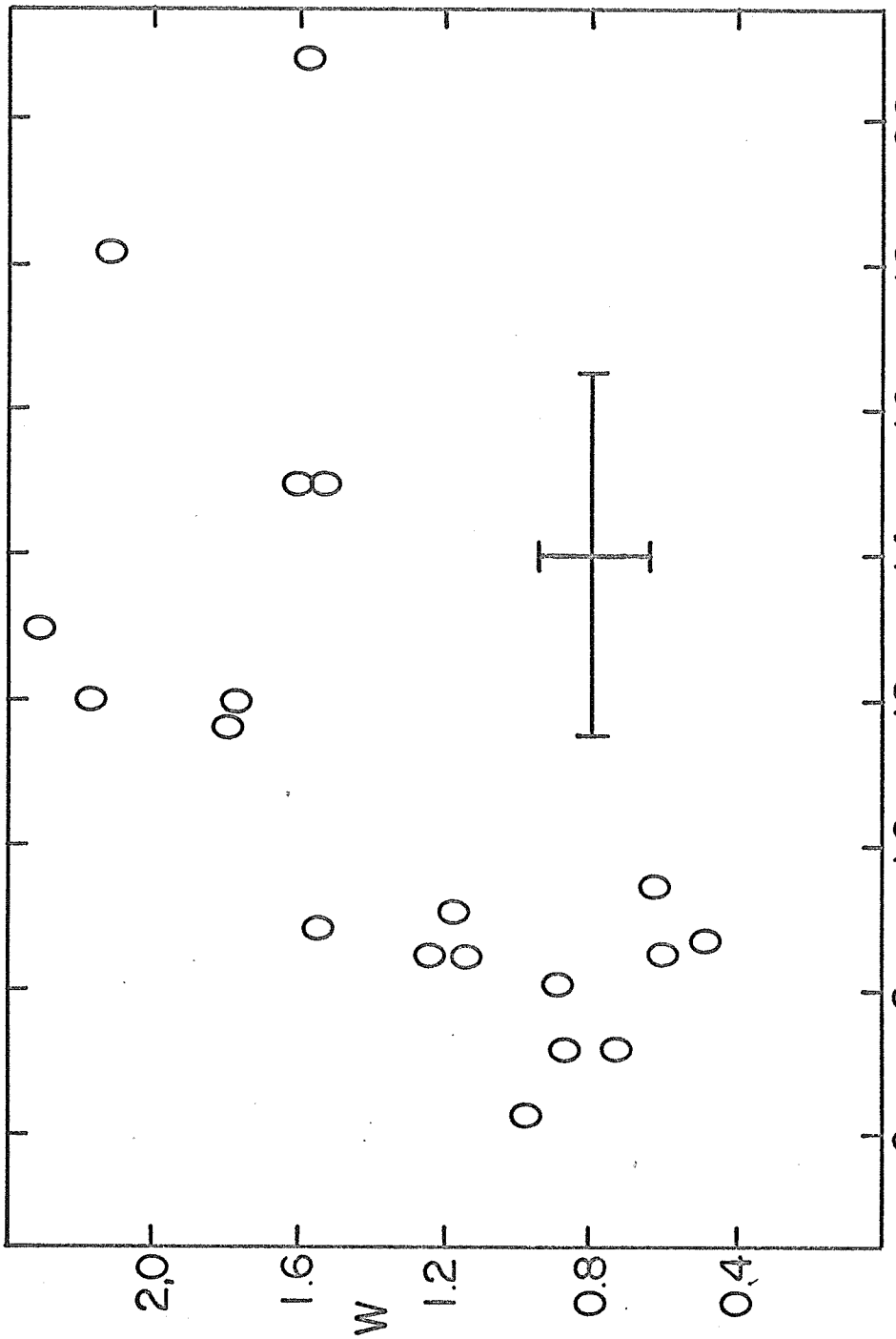

Fig. 7. The oxygen line strength, W (in A), vs. the Fe II turbulent velocity, V_t (in km/sec).

stars measured, shows evidence of a high excitation circumstellar shell (Sargent, 1965). It is possible that the Fe II absorption lines are enhanced by the shell. With the exception of this star the oxygen line strengths and the Fe II velocities are well correlated. Thus our data show: (1) that the O I, Fe II, and Mg II lines increase in strength with luminosity and (2) that the Fe I lines have a significantly different behavior with temperature and luminosity than the others. The curve of growth analysis suggests that an increase in the microturbulent velosity is the primary reason for the line strengthening. However the lack of weak Fe II lines allows us to conclude only that the saturated Fe II lines vary in the same way as the O I lines. We will show in section V that a decrease in the continuous opacity contributes to the line strengthening but that an increase in the microturbulence with luminosity accounts for most of the effect.

D. Implications of the Spectral Line Measures

In this section we compare the MK luminosity classifications of the F stars with the absolute magnitudes determined from the oxygen line measures to see what luminosities the MK types imply. We then summarize the observational picture of the F I stars.

Now that we have shown that the 7774 line is a good indicator of absolute magnitude, we can use the data to determine what range of absolute magnitudes are included in the Ia and Ib classifications.

Figure 3 indicates that for the F0 through G0 stars:

(1) $M_V = -9$ is an upper limit for the luminosity of the Ia stars; all the ones in our sample are in the range $-6.5 > M_V > -9$. There is little tendency for stars of one spectral type to be more luminous than ones of another.

(2) The one F0Ib and the one F3Ib star in our list have absolute magnitudes near -7 and are as bright as the less luminous Ia stars. The F5-G5 Ib stars fall in the range $-4 > M_V > -6$.

(3) The two F5Iab stars have $M_V = -6$.

Thus we see that for the Ia stars $M_V = -7.7 \pm 1.2$ and for the F5-G0 Ib's $M_V = -5 \pm 1$; the F0-F3 Ib stars can be outside the latter range by 1 magnitude. The use of the oxygen lines has increased the accuracy of luminosity classification by at least a factor of two for the F supergiants.

Next we summarize the luminosity and temperature dependence of the line strengths in the F I stars:

(1) Our observations do not show any variation with spectral type of the oxygen line strength for the stars of known luminosity. φ Cas (F0Ia) and ρ Cas (F8Ia) have nearly equal oxygen lines and luminosities although their effective temperatures differ by approximately 1000°.

(2) Our data are consistent with the idea that the lines of O I, Mg II, and Fe II have the same behavior. The Fe II curves of growth indicate that the luminosity effect for these lines is correlated with an increase in the microturbulence.

(3) The strong Fe I lines increase only slightly with luminosity at F5; at other spectral types they are luminosity dependent and their turbulent velocities vary in approximately the same way as the Fe II lines.

(4) Measures of the Fe I and II line depths show that line deepening effects do not account for the increase in turbulent velocity with luminosity; although the velocity scale could be incorrect, the relative values reflect actual changes in the turbulence.

We believe that the difference in ionization potential between Fe I and Fe II accounts for their behavior. In the F I stars nearly all the iron is singly ionized; 1% or less is neutral in the outer atmosphere. The ratio $N(\text{Fe I})/N(\text{Fe II}) \sim N(\text{Fe I})/N(\text{Fe})$ drops off sharply toward the surface because of the decreasing electron pressure (the temperature is nearly constant in the region of line formation). This implies (1) that the Fe I lines could be formed at greater depths than the Fe II lines and (2) that relative depths of formation in different stars will depend on the ionization equilibrium. The data support the hypothesis that strong lines of any ion A_i of an element A for which the ratio $N(A_i)/N(A)$ is relatively constant in the outer atmosphere will behave like O I and Fe II. It will be shown in section V that this idea does account for the differences in the Fe I and Fe II lines.

IV. Computation of Model Atmospheres for the F I Stars and Comparison with Observations

A. Background

The physical conditions in the atmospheres of the supergiants must be known in order to test the idea that ionization differences account for the observations described previously. The curve of growth technique, which assumes that the ratio of line to continuous absorption is constant in the atmosphere, is not adequate for comparing the relative behavior of Fe I and Fe II, and we need to use a model which allows variations of the physical parameters with depth.

Great progress has been made in recent years in the theory of main sequence stellar atmospheres. The development of large computers and efficient numerical techniques combined with better knowledge of the sources of opacity enable hydrostatic and radiative equilibuium LTE models to be calculated routinely. Another purpose for computing supergiant atmospheres besides using them for the spectral lines is to see how well the modern theory applies to low gravity stars. Aller states (1963, p.251) that giants and supergiants often show effective gravities $\sim 10^{-2}\ GM/R^2$ and that the assumption of hydrostatic equilibrium is not valid for such stars.

In this section we describe a grid of supergiant atmospheres

that we have calculated for the F I stars using a program developed at the Smithsonian observatory. We then compare the models with the observations of the cluster stars and show that although the gravities do come out to be less than expected, the models are suitable for analyzing the relative behavior of the lines.

B. The Model Atmosphere and Hydrogen Line Programs

The Smithsonian model atmospheres program was developed originally by Strom (see Strom and Avrett, 1965). It has been rewritten by Kurucz, who incorporated numerical techniques which are described in his recent article (1969), and we have used his version of the program to calculate models for the F I stars. Since the wings of the Balmer lines are sensitive to the effective temperatures and gravities of the stars, we have also computed hydrogen line profiles from the models with a program written by Peterson (Strom and Peterson, 1968), which employs the Edmonds, Schluter, and Wells broadening theory.

The model atmospheres are computed by solving the equation of transfer and the equation of hydrostatic equilibrium subject to the conditions that (1) the total flux is conserved at all depths, and (2) there is no incident radiation at the surface of the atmosphere. Plane parallel geometry is assumed. The major advance of modern techniques over earlier models is that flux constancy is enforced to

high accuracy. The program takes an initial temperature-depth relation and iterates it until the desired convergence is achieved at all points. It includes the following ions and processes as opacity sources: neutral hydrogen, H_2^+, H^-, Si I, Mg I, He I, He II, electron scattering, and Rayleigh scattering. In order to save time each source is calculated only in the temperature range where it makes an appreciable contribution to the total opacity. The program also has provisions for including turbulent pressure, convective flux, and deviations from LTE models; we have investigated the effects of these processes on the standard models.

C. The Models

We have computed a grid of radiative LTE models for the temperature and gravity ranges $6000° < T_e < 7500°$ and $0.1 < \log g < 1.5$. The calculation of the models with $\log g < 1$ is difficult because the acceleration caused by the radiation pressure in the deeper layers exceeds the surface gravity. The characteristics of the resulting gas pressure inversion zone change rapidly with temperature and gravity and the pressure terms in the calculation tend to diverge if the initial model parameters are not carefully chosen. As the program usually obtains a starting model by scaling a previously calculated one, small steps in temperature and gravity (as low as 75° and 0.1 in log g) are needed in order for the models to converge. However this technique was not successful for the

6000° models and the iteration technique for the electron pressure had to be changed slightly in order to calculate them. The procedure uses an initial guess for the electron pressure to calculate the ionization equilibrium, from which a new value of the electron pressure is found. Then some combination which empirically is found to have good convergence properties is used for the next attempt. In the original program

$$P_e(2) = P_e(\text{initial})^{0.31}\, P_e(\text{new})^{0.69} \qquad \text{(IV-1)}$$

but for the 6000° models the process would converge rapidly enough only for the form

$$P_e(2) = P_e(\text{initial})^{0.7}\, P_e(\text{new})^{0.3} \qquad \text{(IV-2)}$$

In this manner we were able to calculate models with log g as low as 0.1 for temperatures of 6750° or less. At 7000° we could not obtain convergence below log g = 0.3, and the program would have to be modified further to reduce this limit. We did not go to lower gravities since the program stars fell within the above limits.

Table 12 contains two models which represent the conditions found in the F supergiant stars. The variation of their physical parameters with optical depth is shown in figures 8 and 9. It is seen that the absorption coefficient reaches a maximum near an optical depth of 10 and then decreases at greater depths due to the ionization of hydrogen. The gas pressure and density inversions occur before the absorption coefficient reaches a maximum and are associated with its steep increase. The beginning of this increase is not indicated well in the figures because of the linear

TEFF 6500. LOG G 0.100 NORMAL ITERATION 2

FRACTIONAL ABUNDANCES HYDROGEN 0.900 HELIUM 0.100

AL -5.70 C -3.50 CA -5.80 CO -7.30 CR -6.60 FE -5.10 K -7.10 MG -4.50 MN -6.90 NA -5.80 NI -6.10 SI -4.50 TI -7.20

	TAU 5000.	TEMP	PRESSURE	ELECTRON NUMBER DENSITY	ABSORPTION COEFFICIENT	HEIGHT (KM)	GRADIENTS ADIAB	RADIAT	ION FRACTIONS H 1	HE 1	HE 2	PER CENT FLUX ERROR	DERIV
1	0.0	5171.7	0.152E-04	0.851E 07 0.278E-16	0.204E 00	0.648E 08	0.44E-01	-0.71E-03	0.144	1.000	0.000	-0.142	-0.000
2	0.100E-04	5164.4	0.304E-04	0.171E 08 0.556E-16	0.204E 00	0.508E 08	0.65E-01	0.15E-01	0.260	1.000	0.000	-0.142	0.000
3	0.147E-04	5181.2	0.547E-04	0.284E 08 0.104E-15	0.181E 00	0.475E 08	0.58E-01	0.22E-02	0.345	1.000	0.000	-0.142	-0.000
4	0.215E-04	5173.5	0.806E-04	0.384E 08 0.162E-15	0.158E 00	0.445E 08	0.56E-01	-0.31E-02	0.428	1.000	0.000	-0.142	-0.000
5	0.316E-04	5165.2	0.131E-03	0.546E 08 0.279E-15	0.130E 00	0.412E 08	0.54E-01	-0.48E-03	0.529	1.000	0.000	-0.142	-0.000
6	0.464E-04	5170.5	0.247E-03	0.861E 08 0.564E-15	0.102E 00	0.380E 08	0.52E-01	0.86E-03	0.631	1.000	0.000	-0.142	-0.000
7	0.681E-04	5171.1	0.496E-03	0.136E 09 0.121E-14	0.750E-01	0.350E 08	0.52E-01	0.20E-03	0.729	1.000	0.000	-0.142	-0.000
8	0.100E-03	5172.0	0.104E-02	0.215E 09 0.269E-14	0.536E-01	0.323E 08	0.53E-01	0.13E-03	0.809	1.000	0.000	-0.142	-0.000
9	0.147E-03	5172.2	0.223E-02	0.334E 09 0.607E-14	0.371E-01	0.297E 08	0.56E-01	0.21E-03	0.868	1.000	0.000	-0.142	-0.000
10	0.215E-03	5173.7	0.488E-02	0.517E 09 0.137E-13	0.255E-01	0.273E 08	0.61E-01	0.39E-03	0.910	1.000	0.000	-0.142	-0.001
11	0.316E-03	5175.3	0.107E-01	0.791E 09 0.307E-13	0.176E-01	0.250E 08	0.69E-01	0.60E-03	0.938	1.000	0.000	-0.142	-0.001
12	0.464E-03	5178.5	0.231E-01	0.120E 10 0.675E-13	0.123E-01	0.228E 08	0.80E-01	0.75E-03	0.958	1.000	0.000	-0.142	-0.002
13	0.681E-03	5181.3	0.494E-01	0.179E 10 0.146E-12	0.865E-02	0.207E 08	0.94E-01	0.10E-02	0.971	1.000	0.000	-0.142	-0.003
14	0.100E-02	5186.6	0.104E 00	0.267E 10 0.309E-12	0.625E-02	0.187E 08	0.11E 00	0.16E-02	0.980	1.000	0.000	-0.142	-0.005
15	0.147E-02	5193.1	0.213E 00	0.395E 10 0.636E-12	0.467E-02	0.168E 08	0.13E 00	0.17E-02	0.986	1.000	0.000	-0.142	-0.008
16	0.215E-02	5199.3	0.425E 00	0.572E 10 0.127E-11	0.357E-02	0.149E 08	0.16E 00	0.26E-02	0.990	1.000	0.000	-0.141	-0.014
17	0.316E-02	5211.5	0.824E 00	0.828E 10 0.247E-11	0.287E-02	0.132E 08	0.18E 00	0.43E-02	0.992	1.000	0.000	-0.142	-0.021
18	0.464E-02	5227.7	0.153E 01	0.119E 11 0.457E-11	0.244E-02	0.115E 08	0.20E 00	0.52E-02	0.994	1.000	0.000	-0.142	-0.038
19	0.681E-02	5244.0	0.272E 01	0.167E 11 0.810E-11	0.218E-02	0.100E 08	0.23E 00	0.71E-02	0.995	1.000	0.000	-0.142	-0.061
20	0.100E-01	5269.0	0.460E 01	0.234E 11 0.137E-10	0.208E-02	0.860E 07	0.24E 00	0.91E-02	0.996	1.000	0.000	-0.142	-0.101
21	0.147E-01	5292.1	0.742E 01	0.320E 11 0.220E-10	0.208E-02	0.732E 07	0.26E 00	0.12E-01	0.997	1.000	0.000	-0.143	-0.173
22	0.215E-01	5327.5	0.114E 02	0.439E 11 0.337E-10	0.220E-02	0.616E 07	0.27E 00	0.18E-01	0.997	1.000	0.000	-0.143	-0.235
23	0.316E-01	5369.0	0.169E 02	0.601E 11 0.492E-10	0.245E-02	0.510E 07	0.28E 00	0.25E-01	0.997	1.000	0.000	-0.146	-0.335
24	0.464E-01	5424.6	0.239E 02	0.831E 11 0.690E-10	0.284E-02	0.416E 07	0.28E 00	0.36E-01	0.997	1.000	0.000	-0.150	-0.443
25	0.681E-01	5497.0	0.325E 02	0.118E 12 0.926E-10	0.347E-02	0.330E 07	0.28E 00	0.52E-01	0.997	1.000	0.000	-0.158	-0.572
26	0.100E 00	5591.2	0.425E 02	0.172E 12 0.119E-09	0.446E-02	0.254E 07	0.27E 00	0.77E-01	0.997	1.000	0.000	-0.171	-0.691
27	0.147E 00	5713.6	0.537E 02	0.261E 12 0.147E-09	0.606E-02	0.187E 07	0.25E 00	0.10E 00	0.996	1.000	0.000	-0.199	-0.861
28	0.215E 00	5834.6	0.655E 02	0.385E 12 0.176E-09	0.820E-02	0.127E 07	0.24E 00	0.17E 00	0.995	1.000	0.000	-0.244	-0.875
29	0.316E 00	6097.7	0.771E 02	0.745E 12 0.197E-09	0.146E-01	0.772E 06	0.20E 00	0.36E 00	0.991	1.000	0.000	-0.136	-1.414
30	0.464E 00	6397.0	0.855E 02	0.144E 13 0.207E-09	0.277E-01	0.417E 06	0.16E 00	0.62E 00	0.984	1.000	0.000	0.409	-1.757
31	0.681E 00	6772.2	0.912E 02	0.292E 13 0.205E-09	0.605E-01	0.162E 06	0.12E 00	0.14E 01	0.966	1.000	0.000	0.367	-0.713
32	0.100E 01	7259.3	0.937E 02	0.630E 13 0.189E-09	0.163E 00	0.0	0.89E-01	0.77E 01	0.920	1.000	0.000	-0.014	0.413
33	0.147E 01	7864.4	0.932E 02	0.131E 14 0.158E-09	0.497E 00	-0.916E 05	0.72E-01	-0.46E 01	0.800	1.000	0.000	-0.237	1.254
34	0.215E 01	8548.5	0.906E 02	0.222E 14 0.118E-09	0.129E 01	-0.149E 06	0.71E-01	-0.21E 01	0.546	1.000	0.000	-0.075	0.929
35	0.316E 01	9279.1	0.861E 02	0.274E 14 0.864E-10	0.202E 01	-0.206E 06	0.89E-01	-0.13E 01	0.235	1.000	0.000	0.109	0.602
36	0.464E 01	10060.1	0.799E 02	0.263E 14 0.678E-10	0.191E 01	-0.302E 06	0.16E 00	-0.89E 00	0.065	1.000	0.000	0.245	1.090
37	0.681E 01	10873.1	0.719E 02	0.225E 14 0.551E-10	0.147E 01	-0.518E 06	0.24E 00	-0.62E 00	0.016	0.998	0.002	-0.186	-0.453
38	0.100E 02	11720.9	0.623E 02	0.182E 14 0.440E-10	0.108E 01	-0.104E 07	0.26E 00	-0.45E 00	0.004	0.982	0.013	-0.007	-0.032
39	0.147E 02	12636.5	0.514E 02	0.140E 14 0.334E-10	0.804E 00	-0.239E 07	0.23E 00	-0.34E 00	0.001	0.867	0.133	-0.497	-0.294
40	0.215E 02	13651.7	0.396E 02	0.103E 14 0.233E-10	0.629E 00	-0.596E 07	0.22E 00	-0.26E 00	0.000	0.441	0.559	-0.728	-0.314
												-1.808	0.009

Table 12. The adopted model for HD 10494 (F5Ia)

TEFF 6500. LOG G 1.500 NORMAL ITERATION 2

FRACTIONAL ABUNDANCES HYDROGEN 0.900 HELIUM 0.100

AL -5.70 C -3.50 CA -5.80 CO -7.30 CR -6.60 FE -5.10 K -7.10 MG -4.50 MN -6.90 NA -5.80 NI -6.10 SI -4.50 TI -7.20

	TAU 5000.	TEMP	PRESSURE	ELECTRON NUMBER	DENSITY	ABSORPTION COEFFICIENT	HEIGHT (KM)	GRADIENTS ADIAB	RADIAT	ION FRACTIONS H 1	HE 1	HE 2	PER CENT FLUX ERROR	DERIV
1	0.0	5340.7	0.585E-02	0.631E 09	0.158E-13	0.269E-01	0.142E 07	0.44E-01	-0.72E-03	0.819	1.000	0.000	0.079	0.007
2	0.100E-04	5333.0	0.117E-01	0.126E 10	0.317E-13	0.270E-01	0.125E 07	0.53E-01	0.49E-02	0.904	1.000	0.000	0.079	0.009
3	0.147E-04	5337.9	0.211E-01	0.176E 10	0.584E-13	0.206E-01	0.120E 07	0.59E-01	-0.22E-03	0.928	1.000	0.000	0.079	0.023
4	0.215E-04	5332.1	0.312E-01	0.213E 10	0.873E-13	0.168E-01	0.115E 07	0.64E-01	-0.24E-02	0.941	1.000	0.000	0.079	0.036
5	0.316E-04	5325.2	0.497E-01	0.268E 10	0.141E-12	0.132E-01	0.109E 07	0.72E-01	-0.14E-02	0.955	1.000	0.000	0.079	0.050
6	0.464E-04	5323.4	0.907E-01	0.363E 10	0.260E-12	0.985E-02	0.102E 07	0.84E-01	-0.12E-02	0.966	1.000	0.000	0.079	0.080
7	0.681E-04	5317.0	0.173E 00	0.500E 10	0.501E-12	0.723E-02	0.949E 06	0.10E 00	-0.19E-02	0.976	1.000	0.000	0.079	0.130
8	0.100E-03	5309.8	0.338E 00	0.694E 10	0.987E-12	0.530E-02	0.876E 06	0.12E 00	-0.23E-02	0.983	1.000	0.000	0.079	0.208
9	0.147E-03	5300.7	0.667E 00	0.961E 10	0.196E-11	0.394E-02	0.803E 06	0.15E 00	-0.24E-02	0.989	1.000	0.000	0.079	0.312
10	0.215E-03	5292.7	0.131E 01	0.132E 11	0.385E-11	0.303E-02	0.731E 06	0.18E 00	-0.23E-02	0.992	1.000	0.000	0.079	0.449
11	0.316E-03	5284.5	0.249E 01	0.179E 11	0.737E-11	0.246E-02	0.662E 06	0.21E 00	-0.22E-02	0.994	1.000	0.000	0.079	0.635
12	0.464E-03	5278.1	0.456E 01	0.239E 11	0.135E-10	0.213E-02	0.598E 06	0.24E 00	-0.16E-02	0.996	1.000	0.000	0.079	0.726
13	0.681E-03	5274.5	0.791E 01	0.314E 11	0.235E-10	0.199E-02	0.540E 06	0.27E 00	-0.12E-02	0.997	1.000	0.000	0.079	0.890
14	0.100E-02	5271.5	0.130E 02	0.403E 11	0.388E-10	0.197E-02	0.487E 06	0.29E 00	-0.30E-03	0.998	1.000	0.000	0.079	0.948
15	0.147E-02	5273.0	0.204E 02	0.510E 11	0.608E-10	0.204E-02	0.440E 06	0.30E 00	0.54E-03	0.998	1.000	0.000	0.080	1.005
16	0.215E-02	5274.0	0.307E 02	0.632E 11	0.914E-10	0.218E-02	0.397E 06	0.32E 00	0.13E-02	0.999	1.000	0.000	0.080	1.079
17	0.316E-02	5278.3	0.447E 02	0.775E 11	0.133E-09	0.239E-02	0.357E 06	0.33E 00	0.32E-02	0.999	1.000	0.000	0.082	1.111
18	0.464E-02	5286.1	0.632E 02	0.949E 11	0.188E-09	0.267E-02	0.321E 06	0.34E 00	0.46E-02	0.999	1.000	0.000	0.083	1.086
19	0.681E-02	5294.5	0.874E 02	0.115E 12	0.259E-09	0.300E-02	0.286E 06	0.35E 00	0.71E-02	0.999	1.000	0.000	0.085	1.091
20	0.100E-01	5309.8	0.119E 03	0.141E 12	0.351E-09	0.345E-02	0.254E 06	0.35E 00	0.11E-01	0.999	1.000	0.000	0.089	1.085
21	0.147E-01	5328.6	0.158E 03	0.172E 12	0.467E-09	0.400E-02	0.223E 06	0.35E 00	0.15E-01	0.999	1.000	0.000	0.094	1.098
22	0.215E-01	5356.3	0.208E 03	0.214E 12	0.611E-09	0.471E-02	0.194E 06	0.36E 00	0.23E-01	0.999	1.000	0.000	0.102	1.097
23	0.316E-01	5393.7	0.270E 03	0.270E 12	0.786E-09	0.566E-02	0.166E 06	0.36E 00	0.32E-01	0.999	1.000	0.000	0.113	1.080
24	0.464E-01	5444.0	0.344E 03	0.349E 12	0.993E-09	0.694E-02	0.140E 06	0.36E 00	0.46E-01	0.999	1.000	0.000	0.129	1.072
25	0.681E-01	5511.8	0.432E 03	0.466E 12	0.123E-08	0.876E-02	0.115E 06	0.36E 00	0.65E-01	0.999	1.000	0.000	0.152	1.019
26	0.100E 00	5600.0	0.532E 03	0.645E 12	0.149E-08	0.114E-01	0.915E 05	0.35E 00	0.89E-01	0.999	1.000	0.000	0.183	1.094
27	0.147E 00	5711.2	0.644E 03	0.928E 12	0.177E-08	0.154E-01	0.700E 05	0.34E 00	0.11E 00	0.999	1.000	0.000	0.240	0.843
28	0.215E 00	5836.2	0.764E 03	0.135E 13	0.205E-08	0.210E-01	0.502E 05	0.33E 00	0.19E 00	0.999	1.000	0.000	0.533	2.749
29	0.316E 00	6074.3	0.885E 03	0.245E 13	0.228E-08	0.343E-01	0.328E 05	0.30E 00	0.34E 00	0.998	1.000	0.000	1.184	2.909
30	0.464E 00	6351.3	0.987E 03	0.457E 13	0.243E-08	0.587E-01	0.190E 05	0.27E 00	0.50E 00	0.996	1.000	0.000	1.253	0.510
31	0.681E 00	6692.0	0.107E 04	0.894E 13	0.250E-08	0.108E 00	0.808E 04	0.22E 00	0.83E 00	0.992	1.000	0.000	0.972	0.007
32	0.100E 01	7142.4	0.114E 04	0.195E 14	0.246E-08	0.234E 00	0.0	0.16E 00	0.16E 01	0.981	1.000	0.000	0.633	-0.706
33	0.147E 01	7723.8	0.117E 04	0.449E 14	0.229E-08	0.619E 00	-0.516E 04	0.11E 00	0.37E 01	0.953	1.000	0.000	0.140	-1.120
34	0.215E 01	8418.9	0.119E 04	0.100E 15	0.201E-08	0.188E 01	-0.805E 04	0.85E-01	0.11E 02	0.880	1.000	0.000	-0.433	-0.744
35	0.316E 01	9176.9	0.120E 04	0.189E 15	0.164E-08	0.528E 01	-0.968E 04	0.75E-01	0.66E 02	0.722	1.000	0.000	-0.570	0.306
36	0.464E 01	9956.8	0.119E 04	0.281E 15	0.128E-08	0.109E 02	-0.109E 05	0.77E-01	-0.44E 02	0.470	1.000	0.000	-0.516	0.516
37	0.681E 01	10737.1	0.119E 04	0.330E 15	0.103E-08	0.147E 02	-0.123E 05	0.92E-01	-0.25E 02	0.227	1.000	0.000	-0.556	-0.079
38	0.100E 02	11519.6	0.119E 04	0.336E 15	0.892E-09	0.145E 02	-0.146E 05	0.13E 00	-0.27E 02	0.091	0.999	0.001	-0.827	0.062
39	0.147E 02	12307.4	0.119E 04	0.325E 15	0.811E-09	0.125E 02	-0.187E 05	0.20E 00	0.17E 04	0.035	0.997	0.003	-0.081	0.161
40	0.215E 02	13117.1	0.119E 04	0.309E 15	0.755E-09	0.105E 02	-0.264E 05	0.25E 00	0.10E 02	0.014	0.983	0.017	2.895	0.690

Table 12 (cont.). The adopted model for α Per (F5Ib)

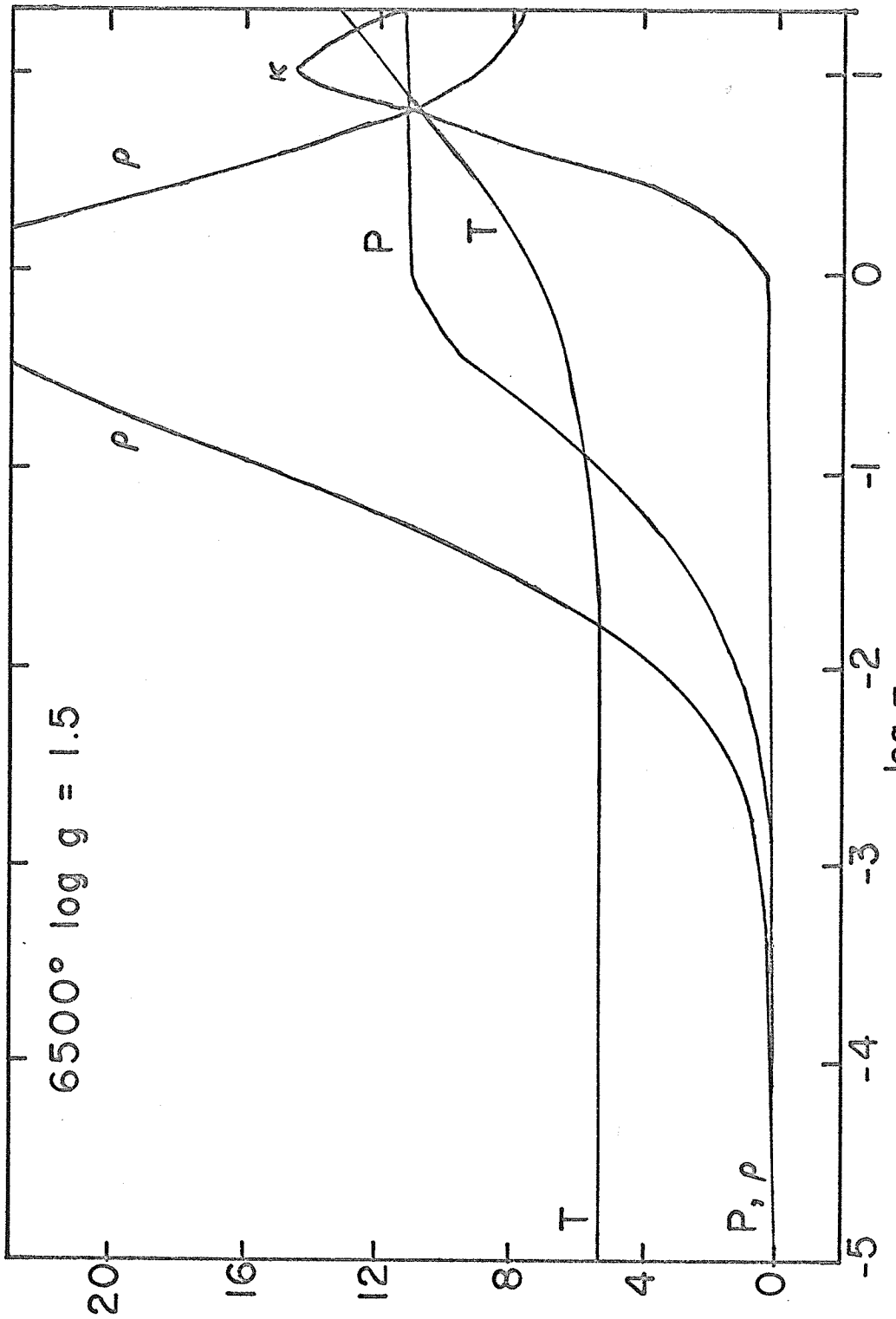

Fig. 8. The variation of the physical parameters with optical depth in the 6500° log g = 1.5 model. The scale ranges are $5200 < T < 13{,}200°$, $0 < P < 1.2 \times 10^{3}$, $0 < \rho < 2.5 \times 10^{-9}$, and $0 < k < 15$.

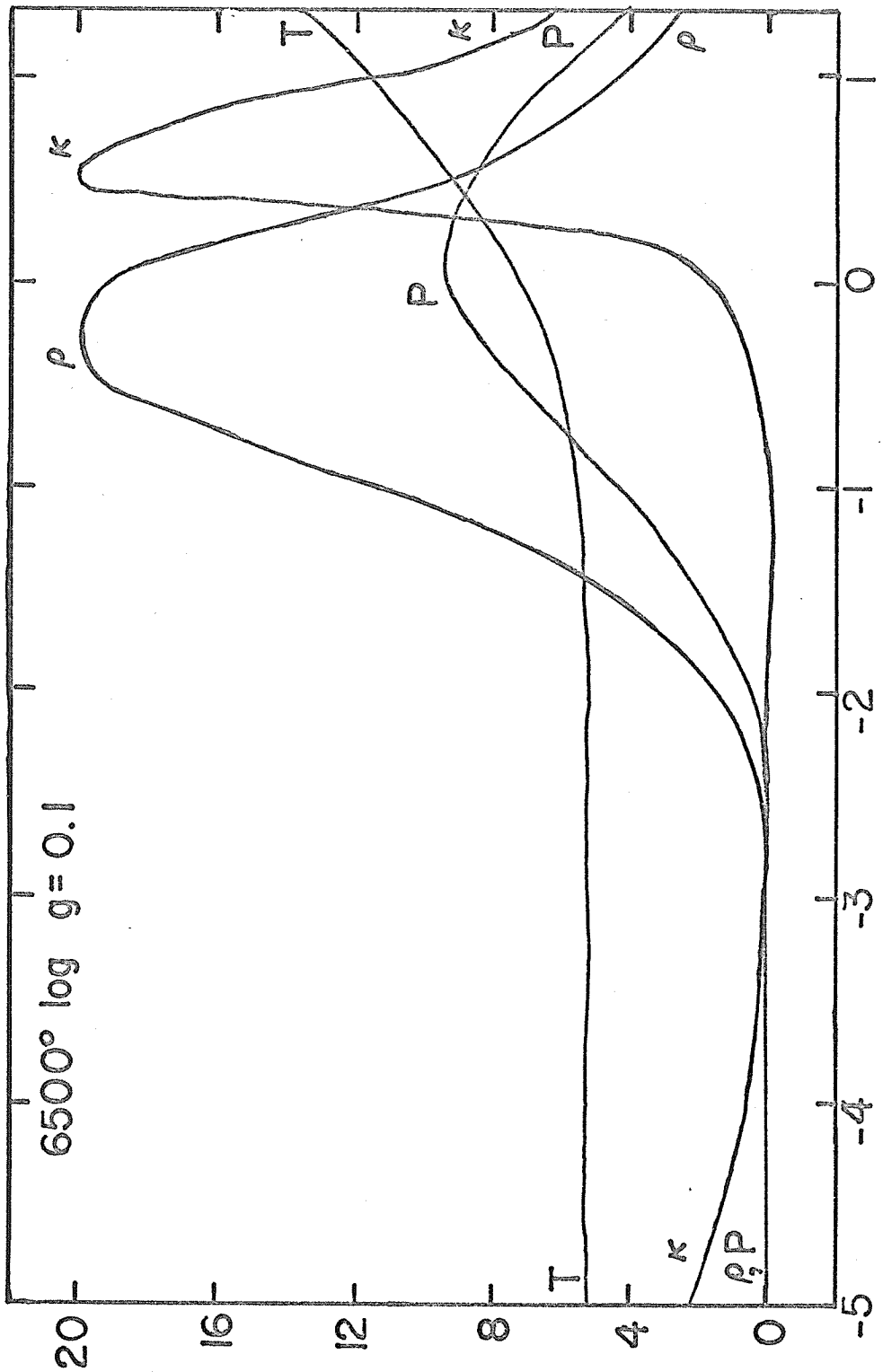

Fig. 9. The variation of the physical parameters with optical depth in the 6500° log g = 0.1 model. The scale ranges are $5200 < T < 13,600°$, $0 < P < 51.5$, $0 < \rho < 2.1 \times 10^{-10}$, and $0 < k < 20$.

scale, but inspection of table 12 shows that it starts near $\tau = 0.1$. Consideration of the hydrostatic equilibrium equation

$$dP/d\tau = g/k \qquad \text{(IV-3)}$$

indicates that an increase in the absorption coefficient k causes a drop in the pressure gradient. At the same time the temperature gradient must increase to maintain constant flux. Since

$$\rho \propto P/T \qquad \text{(IV-4)}$$

it is not surprising that a density inversion occurs. In fact Mihalas' (1965) models indicate that a similar inversion exists on the main sequence at 7000° although it is weaker.

An inversion in the gas pressure occurs only when the acceleration due to radiation pressure, g_{rad}, exceeds the surface gravity. We see from figure 8 that this condition is barely met for log g = 1.5 and evidently the gas pressure inversion will not exist in F stars with log g > 2. The dependence on temperature and gravity of some characteristics of the zone are shown in figure 10. The maximum value of g_{rad}/g in a model and the density ratio $\rho(\tau = 2.15)/\rho(\tau = 21.5)$ increases with decreasing gravity and with decreasing temperature while the upper boundary of the region where $g_{rad} > g$ moves outward with decreasing gravity and increasing temperature. However none of these parameters are parallel to the line of constant luminosity drawn in figure 10.

The existence of the gas pressure inversion and its dependence on gravity can be understood in the following way. From the hydrostatic equation g_{rad} is defined as

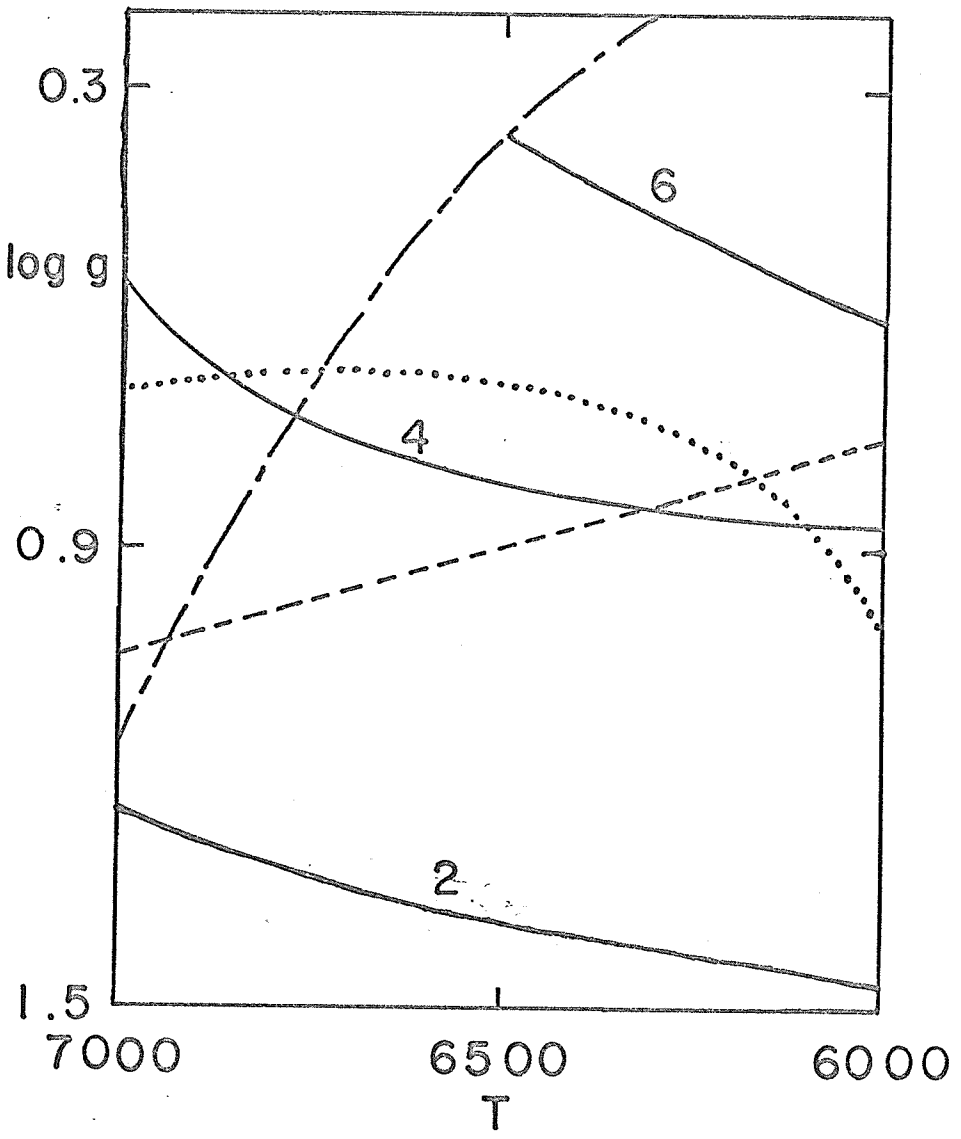

Fig. 10. Characteristics of the gas pressure inversion zone as a fucntion of temperature and gravity. The solid lines denote the maximum value of g_{rad}/g in a given model. The dotted line is for the density ratio $(\tau = 2.15)/(\tau = 21.5) = 3$, and the dot-dashed line indicates where the upper boundary of the zone occurs at $\tau = 2$. The dashed line indicates the locus of constant luminosity.

$$g_{rad} = k\ dP_{rad}/d\tau \quad (k \text{ in } cm^2/gm) \qquad \text{(IV-5)}$$

In equilibrium

$$P_{rad} = a\ T^4/3 \qquad \text{(IV-6)}$$

so that

$$g_{rad} = \frac{4}{3}\ k\ a\ T^3\ dT/d\tau \qquad \text{(IV-7)}$$

If we assume that the temperature distribution is that of a gray atmosphere,

$$T^4(\tau) = \frac{3}{4}\ T_e{}^4\ (\tau + 2/3) \qquad \text{(IV-8)}$$

then

$$g_{rad} = k\ a\ T_e{}^4/4 \qquad \text{(IV-9)}$$

At a given effective temperature g_{rad} reaches a maximum value where k does. In the F stars this occurs in the hydrogen ionization zone where the continuous opacity is due primarily to neutral hydrogen. Table 12 indicates that the hydrogen is 75% ionized at the opacity maximum, so that as an approximation we may consider it to be mostly ionized. At slightly greater depths this is certainly true.

In this case

$$P_e \sim \tfrac{1}{2} P_g \qquad \text{(IV-10)}$$

$$K = N_H f(T) \sim P_e\, g(T) \qquad \text{(IV-11)}$$

Using the hydrostatic equation again we have

$$dP_e/d\tau \propto g/P_e\, g(T) \qquad \text{(IV-12)}$$

and at a given optical depth and temperature

$$P_e \propto \sqrt{g}\ ;\ K \propto \sqrt{g} \qquad \text{(IV-13)}$$

Therefore

$$g_{rad} \propto \sqrt{g} \qquad \text{(IV-14)}$$

and

$$g_{rad}/g \propto 1/\sqrt{g} \qquad \text{(IV-15)}$$

If we use the value of k_{max} from one of the models in table 12 we find that at $T_e = 6500°$ the maximum value of g_{rad}/g is given by

$$g_{rad}/g = q/\sqrt{g} \qquad \text{(IV-16)}$$

which indicates that the inversion zone occurs in stars with log g < 1.9. This value and the $1/\sqrt{g}$ dependence are in good agreement with the results found from the models (figure 10).

We can also estimate how the value of g at which $g_{rad}/g = 1$ depends on temperature. According to the Saha equation

$$\frac{N(H\,II)}{N(H\,I)} P_e = \text{const.}\ T^{5/2}\ 10^{-\varepsilon\theta} \qquad \text{(IV-17)}$$

As long as the main contribution to the mean opacity comes from neutral hydrogen in the second level

$$K \propto P_e\ 10^{3.40\theta}\ T^{-5/2} \qquad \text{(IV-18)}$$

Using the hydrostatic equation as was done before, we find

$$P_e \propto \sqrt{g}\ T^{5/4}\ 10^{-3.40\theta/2} \qquad \text{(IV-19)}$$

and therefore

$$g_{rad} \propto kT^4 \propto T^{2.75}\ 10^{1.7\theta}\ \sqrt{g} \qquad \text{(IV-20)}$$

The calibration from the 6500° model yields

$$g_{rad}/g = \frac{q}{\sqrt{g}} \left(\frac{T}{6500}\right)^{2.75} 10^{1.7(\theta - 0.795)} \qquad \text{(IV-21)}$$

At 10,000° $g_{rad}/g = 1$ occurs at log g = 2 while at 20,000° it occurs at log g = 2.85. Both values are roughly a factor of 10 greater than Mihalas (1965) found from his models; our treatment of the opacity does not predict its variation with temperature as well

as its dependence on gravity. Mihalas' work indicates that the gravity at which $g_{rad}/g = 1$ is 10^2 at 20,000° and $10^{3.5}$ at 50,000°. The drop in opacity at higher temperatures is enough to keep $g_{rad}/g < 1$ in all but the hottest main sequence stars.

We have discussed the behavior of g_{rad} because of its possible connection with turbulence in the F I stars. Underhill (1949) has pointed out that the zone in which $g_{rad}/g > 1$ is unstable and could produce violent activity in the atmosphere. Mihalas (1965, 1969) has used his models to find the values of T_e and g for which the zone first appears in hot stars and discussed the phenomena which could be connected with it. We will consider its relation to the F I stars in section V, where it will be shown that it first occurs at the gravity where the oxygen lines become sensitive to luminosity.

In figure 11 we show the computed dependence of the Hγ width and the continuum slope on the gravity and effective temperature. The values given for Hγ are its half width at a depth of 0.2 while the continuum slope is a color index $m_\nu(4110A) - m_\nu(7550A)$. $m_\nu(\lambda)$ signifies a magnitude per unit frequency interval at the given wavelength. Similarly figure 12 gives the Balmer jump (in the same magnitude system) and Hγ dependence. We see that the Hγ - Balmer jump curves intersect at large angles and will be useful for temperature and gravity determinations outside the $T_e > 7000°$ $\log g < 0.6$ region while the Hγ - color index curves will be good outside the $T_e < 6500°$ $\log g > 1.0$ range.

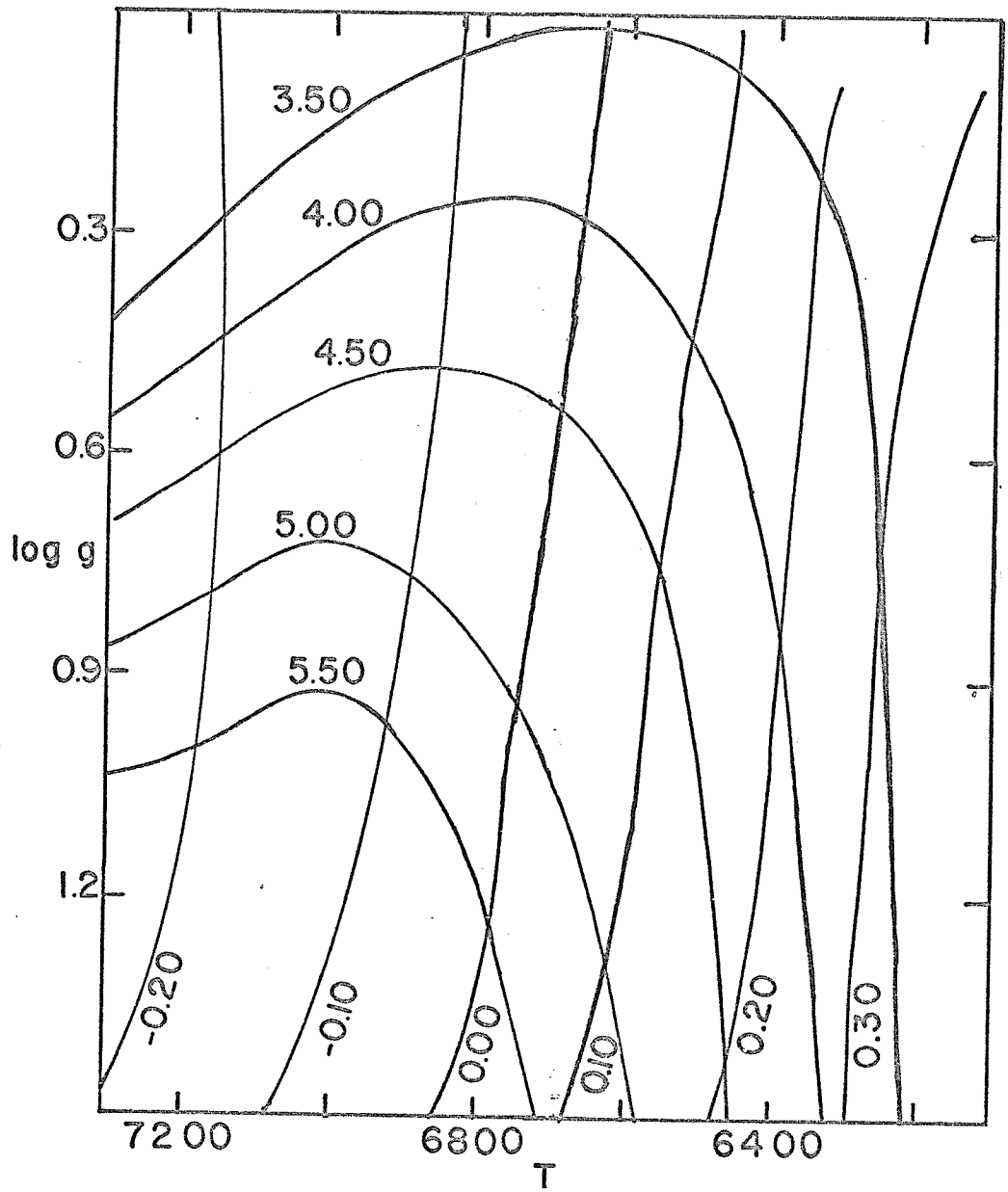

Fig. 11. The Hγ-color index grid. The vertical lines with numbers from -0.20 to +0.30 denote the color index. The others, marked 3.50 to 5.50, are for the Hγ widths.

Star	C.I.	Hγ
φ Cas	-0.19	3.55A
α Per	+0.24	5.25
HD 10494	+0.10	3.48
+60° 2532	+0.31	2.45

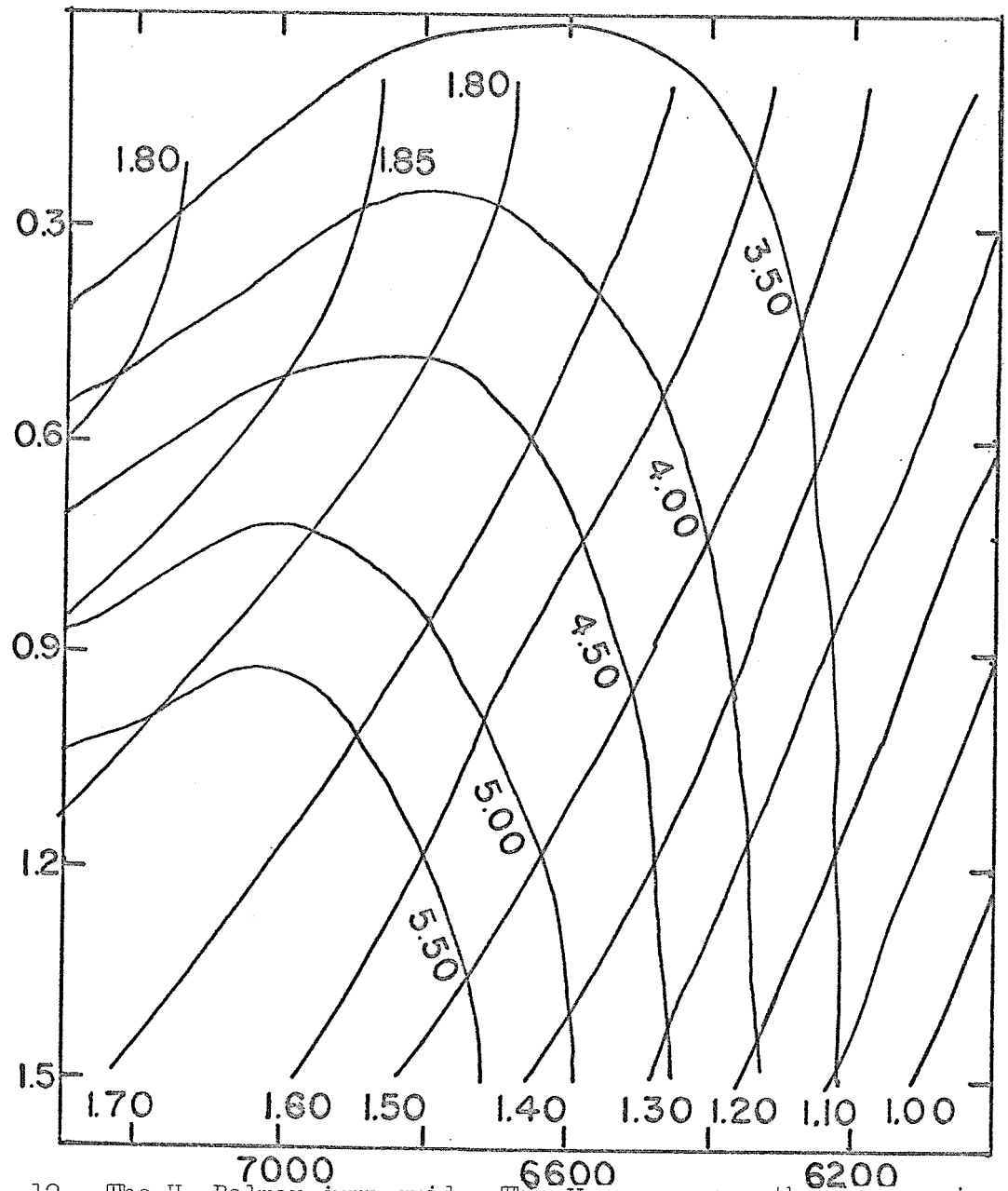

Fig. 12. The Hγ-Balmer jump grid. The Hγ curves are the same as in fig. 11. The Balmer jump curves range from $1^{m}.00$ to $1^{m}.80$.

Star	B.J.	Hγ
φ Cas	1.55	3.55A
α Per	1.36	5.25
HD 10494	1.75	3.48
+60° 2532	1.00	2.45

The variation in the relative importance of different opacity sources explains the behavior of the Balmer jump and Hγ width. The Balmer jump reaches a maximum value in the 7000° - 7500° range and decreases at lower temperatures due to the increasing importance of H^- as a continuous opacity source. Similarly the dominance of H^- in the higher gravity and lower temperature areas of our grid makes the Hγ width insensitive to gravity. The Stark broadening in the line and the H^- opacity are both proportional to the electron pressure and thus the ratio of line to continuous absorption does not depend on the pressure. At low gravities the opacity due to neutral hydrogen becomes important and the hydrogen line widths begin to exhibit a gravity dependence analogous to that of the A stars. Table 13 summarizes the opacity at different depths for the 6500° log g = 0.1 and 1.5 models and lists the opacity sources at each point in order of importance.

In addition we have compiled values at $\tau_{5000} = 0.1$ of the electron number density N_e and the continuous absorption coefficient k as a function of temperature and gravity in table 14. Figure 13 shows that N_e is nearly proportional to $\sqrt{g}$ as would be expected from an argument analogous to that used above for greater depths. The continuous opacity increases more slowly than N_e because H^- is not the only source of opacity. These quantities are useful for analyzing supergiant spectra with the technique developed by Searle et al, which employs the Hγ width, the ionization of iron, and the strength of the Fe II lines in the determination of temperature

Table 13. Continuous Opacities

$T_e = 6500°$ log g = 0.1

τ_{5000}	k (cm^2/gm)	Source
0.01	2.08×10^{-3}	Electron scattering, H^-, H
0.10	4.46×10^{-3}	H^-, electron scattering, H
1.00	1.63×10^{-1}	$H^- \sim$ H, electron scattering

$T_e = 6500°$ log g = 1.5

0.01	3.45×10^{-3}	H^-, electron scattering, H
0.10	1.14×10^{-2}	H^-, H, electron scattering
1.00	2.34×10^{-1}	H^-, H, electron scattering

Table 14

Electron number density (cm^{-3}) at $\tau = 0.10$

	log g		
	0.3	0.9	1.5
6000°	1.00×10^{11}	1.74×10^{11}	3.02×10^{11}
6500°	2.15×10^{11}	4.01×10^{11}	6.45×10^{11}
7000°	3.71×10^{11}	7.56×10^{11}	1.33×10^{11}
7500°		1.20×10^{12}	2.27×10^{12}

Absorption coefficient (cm^2/gm) at $\tau = 0.10$

	log g		
	0.3	0.9	1.5
6000°	2.70×10^{-3}	4.15×10^{-3}	6.71×10^{-3}
6500°	5.01×10^{-3}	7.65×10^{-3}	1.14×10^{-2}
7000°	1.00×10^{-2}	1.40×10^{-2}	2.05×10^{-2}
7500°		2.90×10^{-2}	3.74×10^{-2}

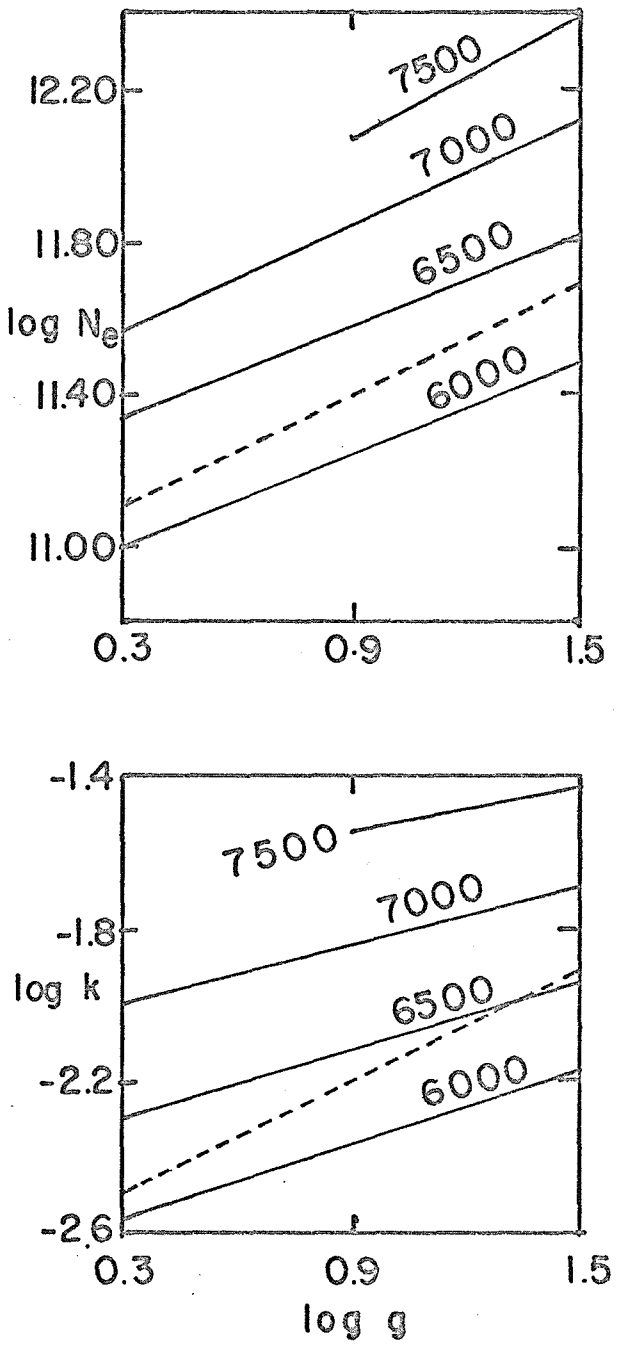

Fig. 13. The variation in the electron density, N_e, and the continuous opacity, k, with temperature and gravity at $\tau = 0.1$.

and electron pressure in the atmosphere.

The neglect of convection should have no effect on the outer layers of the atmosphere. Parsons (1969a) has shown that the convective flux becomes significant only for $\tau > 5$ in a 6000° log g = 1.8 model. For higher temperatures and lower gravities it is less important. The omission of line blanketing is a more serious deficiency; nonetheless we obtain nearly the same temperature and gravity for α Per that Parsons does from his blanketed models. In addition we will show in section V that the computed line strengths are insensitive to changes that would be caused by line blanketing.

We also computed models that allow for deviations in the level populations of H and H^- to investigate how non-LTE effects could change the hydrogen line wings and continuum fluxes. An eight level model of the hydrogen atom was used in which the upper two levels were assumed to be in LTE. At the depths where the line wings and continuum are formed the assumption of detailed balancing in the bound-bound radiative transitions is a good approximation and these transitions are not included in the statistical equilibrium equations. The calculations do include the radiative and collisional ionization rates as well as the bound-bound collisional transitions. We found that at temperatures near 6500° the differences between the LTE and non-LTE models were negligible. Table 15 gives the Hγ width and color index for the two cases. At $\tau_{5000} = 0.1$ the populations of all levels were within 4% of their equilibrium

Table 15. Investigation of non-LTE and turbulence effects at $T_e = 6750°$ log g = 0.3

Model	V (km/sec)	$H\gamma$	m_v(4110-7550)
LTE	0	4.10A	-0.06
NLTE	0	4.04	-0.06
LTE	7	3.70	-0.08

Table 16. Temperatures and gravities for the cluster stars

	Observed			Calculated	
Star	T_e	log g	M_V	$m/m_\odot$	log g
φ Cas	7150 ± 200	0.3 ± 0.2	-8.8	27	0.8
α Per	6500 ± 200	1.6 ± 0.2	-4.6	7	1.8
HD 10494	6500 ± 200	0.1 ± 0.2	-7.5	17	1.0
+60° 2532	6100 ± 200	1.2 ± 0.2	-4.8	8	1.6

values and at $\tau_{5000} = 1$ the deviations are less than 1%. Evidently the radiative bound-free rates are not large enough in 6500° stars to cause significant departures from equilibrium.

An effect that could be important in the atmospheres of F supergiants is the change in the pressure equilibrium caused by convective or turbulent motions. We have investigated the effect that these motions have on the models by assuming that the turbulent pressure has the form $P_t = \frac{1}{2} \rho V_t^2$. The hydrostatic equation takes the form

$$dP_g/d\tau = (g - g_{rad} - g_x)/\kappa \qquad \text{(IV-22)}$$

$$g_{rad} = \kappa \, dP_{rad}/d\tau \; ; \; g_x = \kappa \, dP_x/d\tau \qquad \text{(IV-23)}$$

and models with arbitrary velocities can be calculated. If a velocity which is constant with depth is used, table 15 shows that a 7 km/sec velocity (roughly the sound speed) reduces the gas and electron pressure enough to narrow the Balmer lines by 10%. This reduction simulates a change in log g of about 0.2 for the lower values of log g in our grid. If we try a density dependence for V such as $\rho^{-1/3}$, we find that for the velocity to be reasonable in the region of line formation (i.e. less than 20 km/sec at $\tau_{5000} = 0.01$), it is so small at $\tau = 1$ that it does not change the hydrogen line wings. If a $\rho^{-\frac{1}{2}}$ dependence is used, P_t is constant in the atmosphere and also does not change the hydrogen lines for a reasonable velocity in the outer atmosphere. The microturbulent pressure was not used in the models because we were not certain how it should be treated. Thus our calculations are only a first step toward

accurate supergiant atmospheres.

D. Comparison with Observations

The four cluster stars for which observations are described in section II offer two tests of the models. (1) Their consistency can be checked from seperate determinations of T_e and log g made from the Hγ-color index values and from the Hγ-Balmer jump data. (2) From the photometric luminosities of the stars we can estimate their masses by using the mass-luminosity relation computed from stellar interiors theory. Since the luminosity L, stellar radius R, and effective temperature T_e, are related by

$$L = 4\pi R^2 \sigma T_e^4 \qquad \text{(IV-24)}$$

R can be found from L and the T_e indicated by the data in (1). Thus the expected gravity

$$g = GM/R^2 \qquad \text{(IV-25)}$$

can be computed and compared with the g in (1). We now discuss the results of this procedure.

Using the Hγ and color index data (table 10) with figure 11 we see that for φ Cas T_e = 7150° and log g = 0.3 while for HD 10494 T_e = 6450° and log g = 0.1. However the α Per and +60 2532 values are not consistent, probably because of errors in the data and because Hγ and the color index are not good indicators for $T_e < 6500°$ and log g > 1.0. We can estimate temperatures for the two stars by assuming log g > 1.0 for both. The Hγ widths imply

T_e = 6650° for α Per and 5900° for +60° 2532 while the color indices imply T_e = 6400° for α Per and 6300° for +60° 2532. If we use the Balmer jump data and Hγ widths, we obtain T_e = 6650° and log g = 1.6 for α Per and T_e = 5900° log g = 1.2 for +60° 2532. The Hγ and Balmer jump values for HD 10494 give T_e = 6550° and log g = 0.1, in good agreement with the other method. However the Balmer jump for φ Cas is $0^m.25$ lower than what is expected for a 7150° log g = 0.3 star and indicates a temperature of 6300° or about 8000°, both of which are excluded by its spectral type. Here, too, the discrepancy occurs in a region where the curves intersect at low angles.

Since +60° 2532 is located in a region of non-uniform reddening and has an estimated error of $\pm$ $0^m.10$ in E(B-V) ($\pm$ $0^m.23$ in E(4110-7550)), most of the 400° difference in temperature implied by the color index and Hγ width could be caused by the observational error. In fact for +60° 2532, HD 10494, and α Per nearly all the discrepancy in T_e could be caused by such errors. We conclude that for these stars the different methods define temperatures which are consistent within $\pm$ 150°. The range in log g allowed by the observations is about $\pm$ 0.2.

The problem with φ Cas is more serious and indicates that the computed temperature-depth relation is not correct. Such an error does not affect the relative values of Hγ and the color index very much because both are formed near optical depth unity. However the continuum on the short wavelength side of a large Balmer jump is formed much closer to the surface than the one on the long

wavelength side and the jump reflects errors in the T-τ relation. Thus within the observational errors our data indicate that the models and observations are consistent for the stars with $T_e < 6600°$, but the Balmer jump of the 7100° star is smaller than expected. We conclude that the models will predict relative differences in the atmospheric parameters correctly for the cooler range but may err in predicting fluxes for the hot stars by 25%. Observations of more early F stars are needed to see if the problem with φ Cas is typical or not.

Parsons (private communication) obtained $T_e = 6400°$ and $\log g = 1.7$ for α Per from his blanketed models and photometry by Bahner, which is close to the average temperature we find. We estimate that our errors are $\pm$ 200° in T_e and $\pm$ 0.2 in log g. The adopted values for the four stars are listed in table 16.

Next we compare the g's derived from the observations with the ones calculated from the evolutionary models of Iben (1966) for a 9 $M_\odot$ star and Stothers (1966) for a 30 $M_\odot$ star. We derive a mass-luminosity relation of the form

$$\log M/M_\odot = 0.25 - 0.132\, M_{bol} \qquad \text{(IV-26)}$$

from their calculations for stars with $T_e \sim 6500°$. The masses given in table 16 are found from this relation and the absolute magnitudes of Pesch and Mitchell. Parsons' (private communication) models indicate that the bolometric correction is $0^m.0$ for the F5 I stars and we estimated it to be $0^m.1$ for φ Cas from his results. We obtain the stellar radii from the luminosities and effective

temperatures indicated by the models; thus we can calculate the surface gravity $g = GM/R^2$ (table 16).

A comparison of the gravities found from the observations with the ones predicted by the evolutionary models shows that the latter are greater by 0.3 in the log on the average for the Ib stars and 0.7 greater for the Ia stars. The accidental errors in log g are probably not large enough to account for this systematic effect, so that Aller's statement about supergiants exhibiting lower gravity than expected is correct. However the difference is less than a factor of 5, not 100.

For the Ia stars the discrepancy is caused by the hydrogen lines having half widths of 3.5A at a depth of 0.2 instead of the predicted 4.5A. This means that the electron pressure in their atmospheres is lower than expected. We can use the difference in widths to estimate the corresponding change in electron pressure; then we will consider what processes could cause this change. If we assume the continuous opacity is due to hydrogen, the ratio of line to continuous absorption is

$$l_\nu / k_\nu \propto P_e \, \Delta\lambda^{-5/2} \qquad \text{(IV-27)}$$

At a given depth in the line l_ν/k_ν will be constant so the reduction in width means that the electron pressure decreased by a factor of 2. The problem is to understand how this reduction can occur in the region where the hydrogen line wings are formed. First we will show that the accelerations which are needed to produce the observed radial velocity variations in supergiants are too small to affect

the hydrogen lines. Then we will use the results of part C, in which effects of microturbulent pressure on the atmosphere were considered, to demonstrate that observed turbulent velocities are large enough to reduce the electron pressure by a factor of two.

If we assume that the semi-regular velocity variations of supergiants can be characterized by the formula

$$V_{radial} = A \cos(2\pi t/P) \text{ km/sec} \qquad \text{(IV-28)}$$

then the acceleration which produces them is

$$g_{puls} \leq A\, 2\pi/P \qquad \text{(IV-29)}$$

Abt's (1957) work indicates that an upper limit for A is 10km/sec while Bohm-Vitense (1956) found a period of 70 days for 89 Her. Using these values we find that

$$g_{puls} < 1 \text{ cm/sec}^2 \qquad \text{(IV-30)}$$

This value is roughly 10% of the expected gravity in an F Ia star. Since the electron pressure varies as the square root of the gravity, it would be changed by 5% or less because of the pulsations and their effect on the atmosphere can be neglected.

It was shown in part C how the inclusion of a turbulent pressure term in the hydrostatic equation can affect the atmosphere. A constant velocity of 7 km/sec in the 6750° log g = 0.3 model reduced the width of $H\gamma$ from 4.1A to 3.7 and simulated a decrease in the gravity by a factor of 1.6. This result can be used with a simple treatment of turbulence effects to estimate what velocity is needed to account for the observed $H\gamma$ widths.

The radiation pressure effects are small in the outer

atmosphere so that for constant velocity

$$dP_g/dT + dP_t/dT = g/K \qquad \text{(IV-31)}$$

$$dP_t/dT = \tfrac{1}{2} V^2 \, d\rho/dT \qquad \text{(IV-32)}$$

If we consider the outer atmosphere to be isothermal,

$$d\rho/dT \propto dP_g/dT \qquad \text{(IV-33)}$$

and therefore

$$dP_g/dT = (g/K)/(1 + \text{const.}\, V^2) \qquad \text{(IV-34)}$$

It has already been shown (fig. 13) that

$$P_e \propto \sqrt{g} \qquad \text{(IV-35)}$$

so the electron pressure and turbulence are related by

$$P_e \propto \sqrt{g/(1 + \text{const.}\, V^2)} \qquad \text{(IV-36)}$$

Using the results for the 7 km/sec velocity to evaluate the constant we find that a velocity of 16 km/sec will reduce the electron pressure by a factor of 2 and account for the 1A narrowing of Hγ.

Although the present work shows that microturbulent velocities of this order exist in the F Ia stars, they were derived from strong lines and do not indicate the velocity field in the region where the hydrogen line wings are formed. In fact the results of the next section indicate that the microturbulent velocities would be very small in this region because they decrease with increasing density. However there is evidence that large scale motions with the proper velocity could exist in this region. Sargent (1961) analyzed the profiles of weak lines, which are formed at the same depth as the hydrogen line wings, in ρ Cas and found macroturbulent velocities of 19 km/sec for the ionized atoms and 15 km/sec for

the neutral atoms. Thus, it is plausible that the observed atmospheric motions in the Ia stars do account for the reduced electron pressure.

The models and observations evidently do not yield accurate absolute values of g. They do predict the electron pressure within a factor of two approximately and by reducing the gravity we can choose a model which matches the observations accurately. Therefore the adopted models are suitable for analyzing the relative behavior of the line spectra and in the next section we use them to interpret the oxygen and iron lines.

V. Analysis of the Iron and Oxygen Lines in the F I Stars

A. Summary of the Data and Statement of the Problem

The data presented in the previous sections have indicated that the F I stars have the following important characteristics:

1. The equivalent width of the O I 7774 triplet increases linearly with absolute magnitude for the range $-4 > M_V > -9$. Other lines of O I, Fe II, and Mg II also increase in strength with luminosity and support the idea that strong lines of any ion for which the ionization fraction is constant in the outer atmosphere will exhibit the luminosity effect.

2. The Fe II curves of growth and line profiles indicate that an increase in the microturbulent velocity with luminosity is one cause of the luminosity effect.

3. The Fe I lines behave quite differently than the Fe II lines at F5, where the Fe I lines show almost no luminosity effect. The decrease of the N(Fe I)/N(Fe II) ratio toward the surface in the atmosphere and its sensitivity to temperature and electron pressure are probably related to this behavior.

In this section we use the model atmospheres to show that an increase in the microturbulence and a decrease in the continuous opacity produce the luminosity effect and that a density dependent turbulence can explain the behavior of the Fe I and Fe II lines. We then show that it is unlikely non-LTE effects could account for

the phenomena although they are important in determining the abundance scale and the magnitude of the turbulent velocities.

B. Discussion of the Oxygen and Iron Line Strengths

The ratio of the O I 7774 strength in HD 10494 and α Per is 1.9 while the ratio of Fe II turbulent velocities is 2. Since the models in table 12 are appropriate for the two stars, we can use them and the following simple treatment to show that the line strengths and velocities are mutually consistent. For lines on the flat part of the curve of growth the equivalent width varies approximately as

$$W/\Delta\lambda_D \propto (\lambda_v/k_v)^{0.3} \qquad \text{(V-1)}$$

The value of the exponent depends on the curve used. Our value was derived empirically from calculations with the models. For a given line the width, turbulent velocity, and number of atoms producing the line are related by

$$W \propto V^{0.7} (N/k)^{0.3} \qquad \text{(V-2)}$$

Using the values of the temperature and continuous opacity at $\tau = 0.01$ in table 12 we find that the continuous opacity is less in the log g = 0.1 model and N/k is larger by a factor of 1.45 in HD 10494 than it is in α Per. Since V is twice as large, the above formula predicts that the oxygen line strengths should have a ratio of 1.83, in good agreement with the observations.

If more luminous stars than we have in our sample exist, we would expect the oxygen line strength to level off. The continuous opacity will stop decreasing as H^- becomes less important, and at very low pressures the onset of electron scattering will make the opacity increase. However since φ Cas and ρ Cas are only 1 magnitude fainter than the most luminous stars known, this effect cannot be observed at present.

Next we consider the behavior of the iron lines in terms of the models. The LTE model atmosphere approach to absorption line strength explicitly calculates the line absorption coefficient at each point in the atmosphere and includes all the variations in physical parameters with depth which affect the emergent line profile. We have used another one of the Smithsonian programs written by R.L. Kurucz to investigate the line strengths which the adopted models predict for the F I stars. The program was modified slightly to produce equivalent widths for arbitrary abundances so that the temperature and gravity effects on the absorption lines could be found for the case of constant abundance. The line absorption coefficient calculated in the program can include either a constant microturbulence or one that has an arbitrary density dependence. The program also computes mean and line center depths of formation for the lines. In a typical saturated line unit optical depth at the line center occurs at $\tau_{5000} = 5 \times 10^{-3}$ while if we average over the whole line by weighting each point according to its contribution to the equivalent

width, optical depth unity is reached at $\tau_{5000} = 0.2$.

We chose one saturated Fe I line and two saturated Fe II lines which were close to the observed mean curve of growth for each ion to represent the luminosity effects described above. Table 17 contains the line strengths in four stars: 89 Her (F2Ia), α Per (F5Ib), HD 10494 (F5Ia), and δ CMa (F8Ia). Fe I 4202 was substituted for 5371 in 89 Her because ionization effects made the latter too weak to be saturated. These four stars include all the peculiarities mentioned in part A; in addition, we have determined temperatures and gravities for the two F5 stars and can estimate them for the other two.

Table 17 shows that the Fe II lines, which had the same strength as the Fe I line in α Per are 60% stronger than the Fe I line in HD 10494. In δ CMa the Fe II lines are approximately 20% stronger. The problem is to duplicate this behavior using the models.

Preliminary runs with the program showed that an overabundance of a factor of 10 with respect to the sun was needed to match the observed Fe II line strengths if we used the curve of growth turbulent velocities. As the oxygen line widths required a similar overabundance, we adopted the ratio $N(Fe)/N(H) = 10^{-4.10}$ for the calculations. The question of the abundances and size of the turbulent velocities will be discussed in part C; it is not important here since we are concerned with the relative behavior of the Fe I and Fe II lines.

Using the adopted abundance ratio and the 6500° log g = 1.5

Table 17. Observed and calculated strengths of Fe I and II lines in the test stars

HD 10494 (F5Ia)

T_e = 6500° log g = 0.1

		log W (A)		
Line	Obs.	$3.5 \times 10^{-5} \rho^{-\frac{1}{2}}$	$9 \times 10^{-3} \rho^{-\frac{1}{4}}$	$1.4 \times 10^{-10} \rho^{-1}$
Fe I 5371	2.64	2.64	2.46	2.69
Fe II 5197	2.89	2.78	2.54	2.54
Fe II 5234	2.81	2.84	2.60	2.60

α Per (F5Ib)

T_e = 6500° log g = 1.5

Line	Obs.	$6.5 \times 10^{-5} \rho^{-\frac{1}{2}}$	$9 \times 10^{-3} \rho^{-\frac{1}{4}}$	$1.4 \times 10^{-10} \rho^{-1}$
Fe I 5371	2.54	2.55	2.44	2.44
Fe II 5197	2.50	2.50	2.30	2.34
Fe II 5234	2.57	2.56	2.36	2.42

89 Her (F2Ia)

T_e = 6750° log g = 0.3

Line	Obs.	$2.0 \times 10^{-5} \rho^{-\frac{1}{2}}$
Fe I 4202	2.74	2.74
Fe II 5197	2.67	2.61
Fe II 5234	2.67	2.68

δ CMa (F8Ia)

T_e = 6000° log g = 0.1

Line	Obs.	$6.5 \times 10^{-5} \rho^{-\frac{1}{2}}$
Fe I 5371	2.84	2.85
Fe II 5197	2.87	2.86
Fe II 5234	2.97	2.92

model for α Per, we found that the observed and computed Fe I and II line strengths agreed well when a constant velocity of 6 km/sec was used for the microturbulence. A 7 km/sec velocity and the 6500° log g = 0.1 model produced similar agreement for the Fe I line in HD 10494, but the observed Fe II line strengths required a 12 km/sec velocity. The mean depths of formation for the Fe I and II lines were nearly the same in the log g = 1.5 model, while the Fe II lines were formed closer to the surface in the log g = 0.1 model. This information led us to believe that a turbulent velocity increasing with height in the atmosphere could explain the relative strengthening of the Fe II lines in the Ia star.

The change in the relative depths of formation of the Fe I and II lines with gravity can be understood in the following way. For a particular line the ratio of continuous to line aborption, k_ν/l_ν, is a measure of where the line is formed on the continuum optical depth scale. Strong lines are formed at smaller depths (greater heights) than weak lines. First we will assume that the same turbulent velocity applies to both Fe I and Fe II and show how k_ν/l_ν varies with gravity for each ion. In the atmospheres of F supergiants virtually all the iron is singly ionized, so that the number of Fe II ions per gram of material does not depend on the temperature or pressure. At a given temperature the number of Fe I atoms is proportional to the electron pressure, which varies as the square root of the gravity. For the Fe II lines

$$k_\nu/l_\nu \propto k_\nu \qquad \text{(V-3)}$$

while for Fe I

$$k_\nu / l_\nu \propto k_\nu / \sqrt{\gamma} \qquad \text{(V-4)}$$

Thus, the relative depth of formation varies as

$$\tau(\text{Fe I}) / \tau(\text{Fe II}) \propto 1/\sqrt{\gamma} \qquad \text{(V-5)}$$

and the Fe I lines move inward with respect to the Fe II lines as the gravity is decreased. The calculations with the models have already shown that the use of the same turbulent velocity for Fe I and II matches the observed line strengths in the F5Ib star (log g = 1.5). In the F5 Ia star (log g = 0.1) the Fe II lines required a larger turbulent velocity than was needed for the Fe I lines. Thus we see that a turbulent velocity increasing with height in the atmosphere can exist in both stars and not be noticed in the Ib star because the Fe I and II lines are formed at the same depth.

Consideration of the ionization equilibrium also indicates why the difference in the Fe I and II velocities decreases in the Ia stars of later spectral type. The ratio N(Fe I)/N(Fe II) increases in the cooler stars and reduces the difference in the depths of formation. The Fe I and Fe II lines become less sensitive to changes in the turbulent velocity with height as the temperature of the star decreases.

By the same argument the stratification effects should be greater at spectral type F2Ia than at F5Ia, and yet the same turbulent velocity was derived from the Fe I and II lines. Again the observations are explained by the lines being formed in the same region. We recall that the weakness of the Fe I lines beyond 5000A made it

necessary to measure lines in the blue, which are strong enough to be formed in the same place as the Fe II lines we measured near 5200A. Therefore we conclude that the stratification effects in our data were larger at F5Ia than other spectral types because of the particular Fe I and II lines that were used to determine turbulent velocities.

Now we will show that calculations using the models and a depth dependent turbulence reproduce satisfactorily the line strengths in the four test stars. First we have to decide what the form of the velocity is likely to be. If the motions in the atmosphere are caused by acoustic waves in a gas at constant temperature, the velocity varies with density as

$$V_t \propto \rho^{-1/2} \tag{V-6}$$

If the motions are produced by energy conserving turbulence,

$$V_t \propto \rho^{-1/3} \tag{V-7}$$

Finally, Unno's (1959b) observations of the solar chromosphere indicate that

$$V_t \propto \rho^{-1/4} \tag{V-8}$$

In view of these possibilities we tried three forms which bracket this range to get an idea of how the results depend on the type of motion. They are $\rho^{-\frac{1}{4}}$, $\rho^{-\frac{1}{2}}$, ρ^{-1}. The criterion for deciding which form is acceptable is that it should yield the observed Fe I/Fe II line ratio in the two F5 stars. These stars are chosen since they are cluster members and their atmospheric parameters have been found observationally.

The results given in table 17 show that the $\rho^{-\frac{1}{2}}$ law matches the ratio better than the other forms. The $\rho^{-\frac{1}{4}}$ dependence predicts a ratio that is too low by a factor of 1.25 in both stars. The ρ^{-1} law gives a ratio that is 8% larger than observed in the Ia star while it is too low by 15% in the Ib star. For $\rho^{-\frac{1}{2}}$ the predicted value is too small by 5% in the Ib star and by 10% in the Ia. From these calculations we estimate that the exponent in the density dependence (defined as ρ^{x}) will give agreement within 10% if it is in the range $-\frac{3}{4} < x < -\frac{1}{2}$. Table 17 also indicates that the $\rho^{-\frac{1}{2}}$ law duplicates the Fe I and Fe II lines in 89 Her (F2Ia) and δ CMa (F8Ia) within 10%. Therefore this form accounts for the observed behavior of the iron lines in the F supergiants.

The effects on the theoretical curve of growth of a density dependent turbulence are shown in figures 14 and 15. We computed curves for the Fe I 5371 line and the Fe II 5234 line in the stars where the former was measured (all but 89 Her). For each case the value of A in

$$V_t = A \rho^{-1/2} \qquad \text{(V-9)}$$

was adjusted so that the computed line strengths agreed with the observations for an abundance $N(Fe)/N(H) = 10^{-4.10}$. In figure 14 the Fe I and Fe II curves are identical in the neighborhood of the observed line strengths for the 6500° log g = 1.5 model (F5Ib). The curves for log g = 0.1 (F5Ia) are separated from each other over the entire range and make the stratification effects of the turbulence quite obvious. Comparing the gravity effects on the two ions,

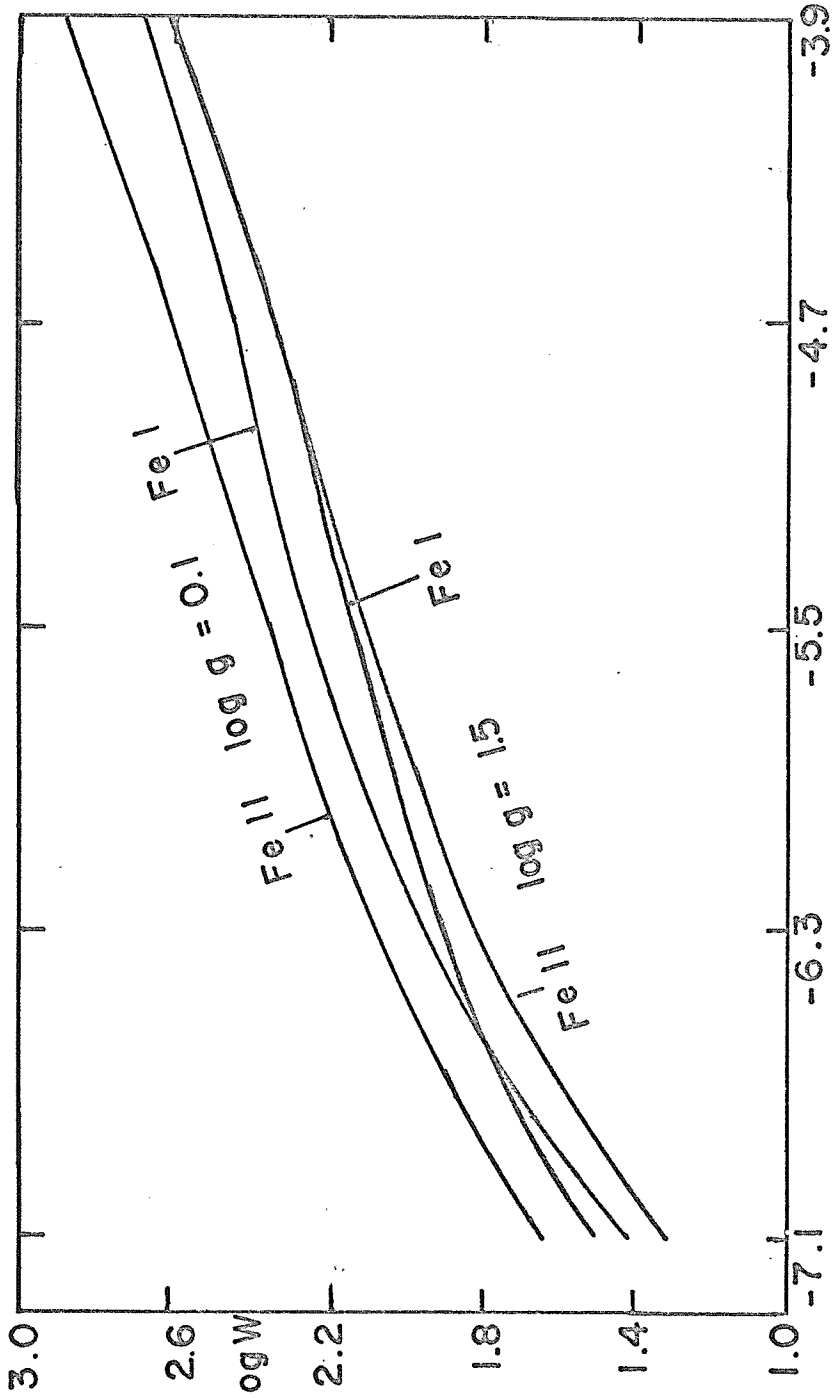

Fig. 14. Theoretical curves of growth for Fe I 5371 and Fe II 5234 at 6500° with $V \propto \rho^{-\frac{1}{2}}$.

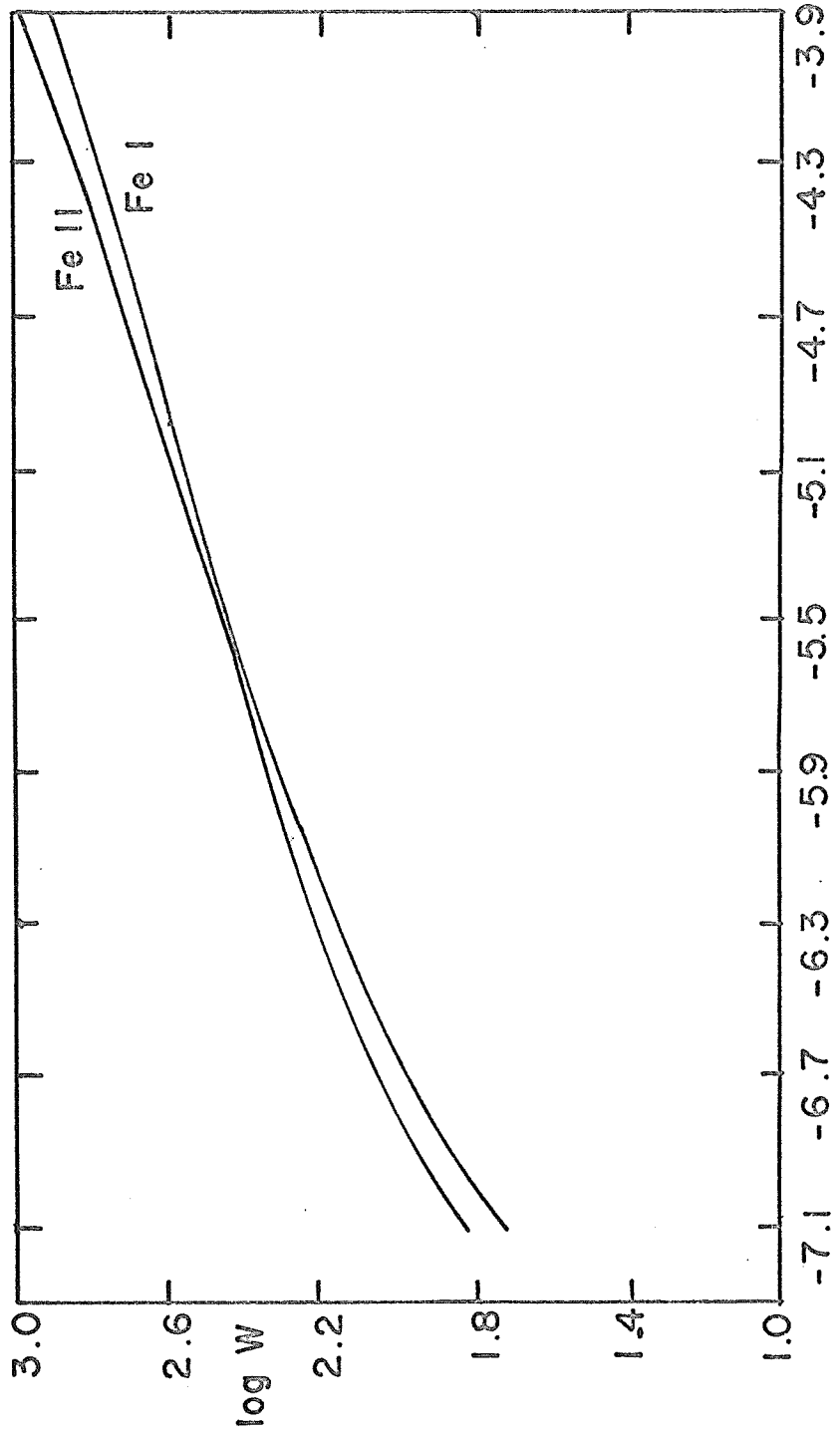

Fig. 15. Theoretical curves of growth for Fe I 5371 and Fe II 5234 at 6000° log g = 0.1 with $V \propto \rho^{-\frac{1}{2}}$.

we see that at the upper end of the curves the Fe II moved up roughly three times as much as the Fe I curve in going from log g = 1.5 to log g = 0.1. This shows why the Fe I lines are observed to be insensitive to gravity at F5. The curves computed with the 6000° log g = 0.1 model (F8Ia) indicate how the difference in the behavior of the two ions decreases in the cooler stars. At the upper end of the curves the distance between them is one fourth as large as it is in the 6500° log = 0.1 model, and the curves cross each other near the middle of the horizontal scale. Thus it is clear that the difference between the Fe I and II lines is larger at F5Ia than at other spectral types.

If the motions in the outer atmosphere of the F I stars originate in the zone where $g_{rad}/g > 1$, as Underhill (1949) and Mihalas (1969) have suggested, then the velocities should depend on the strength of the driving mechanism as well as the density of the gas in the region of line formation. It is possible that the constant of proportionality A in

$$V = A \rho^{x} \qquad \text{(V-10)}$$

will reflect the behavior of the inversion zone. We see from table 17 that if $x = -\frac{1}{2}$, A must vary with both temperature and luminosity in order to match the strengths of the iron lines. In the 6500° models (F5) it decreases from 6.5×10^{-5} at log g = 1.5 to 3.5×10^{-5} at log g = 0.1. In the Ia stars it decreases with increasing temperature. It is 6.5×10^{-5} at 6000° and 2.0×10^{-5} at 6750°. This variation in A is not correlated with the characteristics of

the inversion zone which were discussed in section IV, and we do not understand its physical meaning.

The one empirical relation that was found between the variation of the line strengths and the inversion zone involves the value of the gravity where the zone first appears. We showed in in section IV that g_{rad}/g is greater than unity in the F5 stars with log $g < 1.9$. At the same time the measures of the oxygen line strength in the F stars indicate that it is sensitive to luminosity only in the Ib and Ia stars. The line does not begin to increase in strength with luminosity until class Ib is reached, and the observations show that log g for an F5Ib star is roughly 1.5. Thus the onset of the gas pressure inversion zone and the luminosity effect in the spectral lines occur at approximately the same gravity at spectral type F5. This suggests, but does not prove, that the two phenomena are connected with each other.

In order to investigate how possible errors in the structure of the model atmosphere could affect the calculated line strengths we varied the temperature - optical depth relation to simulate the effect of line blanketing. Line strengths were recomputed with the adjusted models and compared with the original results. Parsons' (1969a)work indicates that the surface temperature in a blanketed model which is appropriate for the line absorption in an F star is 100° to 150° lower than in the corresponding unblanketed case and is higher by the same amount near optical depth unity. We arbitrarily dropped the boundary temperature by 300° in the 6500° models and

varied the distribution so that it had approximately the same relation to the unblanketed temperatures as Parsons' relation did. Figure 16 shows the original and adjusted T-τ curves. New values of the physical parameters were computed with the adjusted temperatures and were used to predict the Fe I and II line strengths with the $\rho^{-\frac{1}{2}}$ form for the turbulence. Table 18 compares the results from the original and adjusted models. It shows that the Fe I line in the log g = 0.1 model increased in strength by 7% while the Fe II lines did not change. In the log g = 1.5 model the lines of both ions increased: Fe I by 7%, Fe II by 5%. The Fe I/Fe II line ratio increased by 7% in the log g = 0.1 case and by 2% in the log g = 1.5 case. This change is not large enough to affect the results found from the unblanketed models about the turbulence increasing with height in the atmosphere. The computed line strengths are insensitive to effects caused by line blanketing in the atmosphere.

Thus our analysis of the oxygen and iron lines in the F supergiants indicates: (1) An increase in the microturbulence with luminosity is the major reason for the luminosity effect shown by the O I and Fe II lines. A drop in the continuous opacity also contributes to the line strengthening but is a secondary effect because the lines are saturated. (2) A microturbulent velocity increasing with height in the atmosphere accounts for the observed differences in the behavior of the Fe I and Fe II line strengths with spectral type and luminosity.

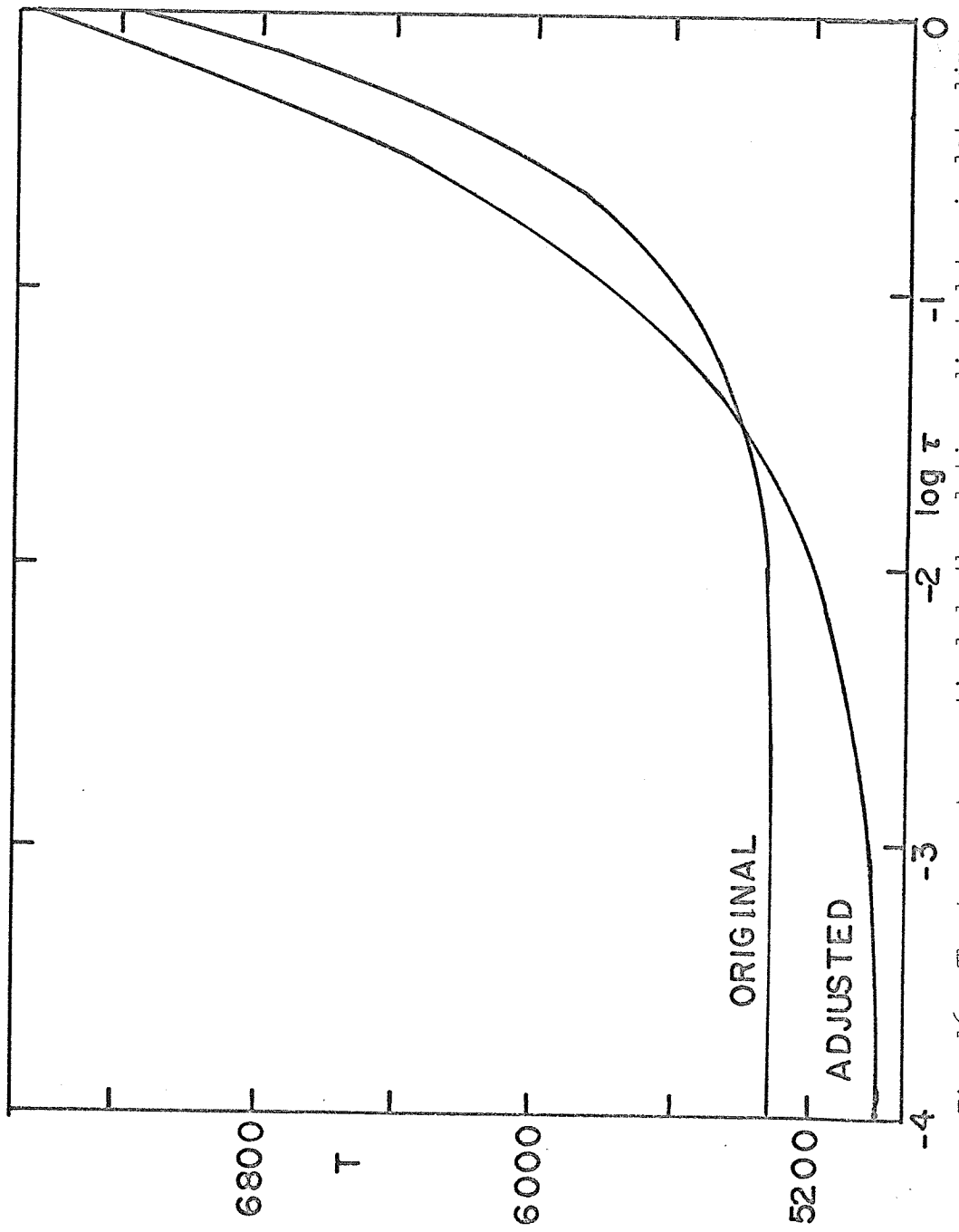

Fig. 16. The temperature-optical depth relation adjusted to simulate line blanketing in the 6500° log g = 1.5 model.

Table 18. Line strength calculations with the original and adjusted temperature distributions.

$T_e = 6500°$ log g = 0.1
$V_t = 3.5 \times 10^{-5} \rho^{-\frac{1}{2}}$

	log W(A)	
Line	Orig.	Adj.
Fe I 5371	2.64	2.67
Fe II 5197	2.78	2.78
Fe II 5234	2.84	2.84

$T_e = 6500°$ log g = 1.5
$V_t = 6.5 \times 10^{-5} \rho^{-\frac{1}{2}}$

	log W(A)	
Line	Orig.	Adj.
Fe I 5371	2.55	2.58
Fe II 5197	2.50	2.52
Fe II 5234	2.56	2.58

C. Investigation of the non-LTE Effects

We have demonstrated that the relative behavior of the Fe I, Fe II, and O I 7774 lines with spectral type and luminosity can be understood in terms of a turbulent velocity which increases with height in the atmosphere. In this section we show that non-LTE effects do not account for the increase in line strength with luminosity. They do affect the comparison of the derived abundances for iron and oxygen with the solar values and the actual (not relative) size of the turbulent velocities.

In recent years a large number of people have been working on the solution of line transfer problems without the simplifying assumption of LTE. We will follow the formulation of the problem developed by Thomas and Jefferies as described in Jefferies' (1968) text to show how the non-LTE effects can be estimated for the lines we have observed.

We recall that in the simple case of LTE and lines formed by pure absorption the emergent intensity at the center of the disk at a particular frequency is

$$I_\nu(0) = \int_0^\infty S_\nu(\tau_\nu)\, e^{-\tau_\nu}\, d\tau_\nu \qquad \text{(V-11)}$$

where

$$S_\nu = B_\nu \quad , \text{ the local Planck function} \qquad \text{(V-12)}$$

If the temperature of the atmosphere decreases toward the surface, the surface intensity at a frequency where the absorption coefficient

is higher than at a neighboring point will be lower because the radiation comes from the cooler surface layers. In the LTE case the intensity in the center of a strong absorption line is given approximately by the Planck function evaluated at the surface temperature while the intensity in the adjacent contiuum is roughly the value of the Planck function at optical depth unity.

Dropping the assumption of LTE means that we have to consider the microscopic processes which determine the source function in the atmosphere. Thomas (1957) has worked out an instructive form of the line center source function in terms of the population of the upper and lower levels of the line:

$$S_{12} = \frac{2h\nu_{12}^3}{c^2}\left[\frac{n_1/g_1}{n_2/g_2} - 1\right]^{-1} \qquad \text{(V-13)}$$

We see that if n_1 and n_2 follow the Boltzmann law, then the source function is given by the local Planck function as expected. However if the ratio n_2/n_1 is less than the equilibrium value, the source function will be smaller than the Planck function and the residual intensity in the line will be less than in the LTE case.

We can solve for the source function in the atmosphere by using the equation of transfer and the condition that the level populations be independent of time. For simplicity consider a two level atom in which the only transitions are caused by electron collisions and radiation. Following Peterson's (1969) summary of the problem we find that the condition of statistical equilibrium for the two levels

$$\frac{dn_1}{dt} = 0 = -(R_{12} + C_{12}) \qquad \text{(V-14)}$$

R_{12} = net rate of radiative transitions out of level 1

C_{12} = net rate of collisional transition out of level 1 (V-15)

implies that

$$S_{12} = (1-\varepsilon) J_{12} + \varepsilon B_{12}$$

$$J_{12} = \int I_{12} \, d\Omega \qquad (V\text{-}16)$$

$$\varepsilon = \frac{C_{21}(1-e^{-h\nu_{12}/kT})}{A_{21} + C_{21}(1-e^{-h\nu_{12}/kT})}$$

A_{21} = Einstein coefficient, C_{21} = corresponding collision rate

ε is a measure of the probability that an atom in the upper level is de-excited by collisions. As ε approaches one, the collisions dominate the problem and insure that the source function approaches the LTE value. For small ε, however, the probability is large that an atom will re-emit an absorbed photon before a collision occurs. In this case the radiation field determines the source function and the assumption of LTE is not valid. Then the source function is found by using the equation of trnasfer from the integral equation

$$S_{12}(\tau) = (1-\varepsilon) \int_0^\infty K(t,\tau) S_{12}(t) \, dt + \varepsilon B_{12}(\tau)$$

$$K(t,\tau) = \frac{1}{2} \int_{-\infty}^{\infty} \phi(\nu,) \phi(\nu, t) E_1(|t_\nu - \tau_\nu|) \, d\nu$$

$\phi(\nu,\tau)$ = normalized line profile (V-17)

In general S_{12} must be obtained from a numerical solution of the equation. However, useful general properties of the solution can be found directly. Rybicki (as quoted by Avrett and Loeser, 1966) has shown that the surface behavior of S_{12} is

$$S_{12} \to \sqrt{\varepsilon} \, B_{12} \quad \text{as} \quad \tau \to 0 \qquad (V\text{-}18)$$

Avrett and Hummer (1965) demonstrated that for an atmosphere in which the parameters are independent of depth:

$$S_{12} \to B_{12} \quad \text{as} \quad \tau \to \infty \qquad (V\text{-}19)$$

and furthermore that the depth at which

$$S_{12} \rightarrow B_{12} \tag{V-20}$$

is

$$\tau_{12} \sim 1/\varepsilon \tag{V-21}$$

We see that if collisions dominate,

$$C_{21} >> A_{21} \tag{V-22}$$

then

$$S_{12} \sim B_{12} \tag{V-23}$$

at all depths. Thus collisions tend to restore the case of LTE. However consideration of the atomic parameters indicates that

$$C_{21}/A_{21} \sim 10^{-16} N_e \tag{V-24}$$

and for the electron densities typically found in stellar atmospheres

$$\varepsilon < 0.01 \tag{V-25}$$

Accordingly

$$S_{12}(\tau=0) \leq 0.1 \; B_{12}(\tau=0) \tag{V-26}$$

and the situation is well out of the LTE case. We note that these values imply an absorption line with a depth of 0.9 relative to the continuum will occur in an atmosphere of constant temperature, for which the LTE assumption would yield no line at all. The line exists because the atmosphere has a boundary. As we approach the surface, there is less radiation available to excite the atom, the population of the upper level drops, and the line source function is decreased in turn.

A complete detailed analysis of a spectral line must include all processes which affect the line source function. Peterson (1969) has done such a solution for the lower levels of hydrogen and shown that it agrees with the line center observations of the Balmer lines much better than does the LTE model. Unfortunately atoms with more complicated spectra are very difficult to analyze in this manner, and we can only estimate possible non-LTE effects for them.

We will look at the O I 7774 line in some detail and then discuss the others in terms of it. Avrett and Kalkofen (1968) and Avrett and Loeser (1966) have described how to determine which microscopic process (collisions, bound-free transitions, etc.) will dominate the line transfer problem. Collisional transitions of any kind, bound-free radiative transitions, and interactions of the line with the continuum all work to maintain equilibrium populations of the levels and the source function in this approach while bound-bound radiative transitions work against the equilibrium processes. We should emphasize that only one equilibrium maintaining process has to dominate in order for the line source function to approach the LTE value.

In order to assess the importance of the different processes for the O I 7774 transition we have scaled the atomic parameters from Peterson's results for hydrogen. We will use the 6500° log g = 0.1 and 1.5 models to represent the range of conditions encountered in the F I stars. Let us consider the bound-bound collisions first.

The ratio of collisional to radiative de-excitations determines the surface behavior of the source function and is proportional to the electron density N_e. Since N_e decreases with height in the atmosphere and with decreasing gravity, N_e at $\tau_{5000} = 1$ in the 6500° log g = 1.5 model will be the maximum value of interest encountered in the F I stars. At this point

$$N_e = 1.95 \times 10^{13} \quad T = 7142 \tag{V-27}$$

Since

$$\varepsilon_{coll} \sim C_{21}/A_{21} \quad \text{for} \quad \varepsilon \ll 1 \tag{V-28}$$

$$\varepsilon_{coll} = 1.2 \times 10^{-16} N_e = 3 \times 10^{-3} \tag{V-29}$$

At $\tau = 0.01$, which is more appropriate for the line center,

$$\varepsilon_{coll} = 1.4 \times 10^{-5} \tag{V-30}$$

Therefore even in the region where the line wings are formed in the higher gravity model, the collisions do not maintain equilibrium.

Analogous to the collision case the ε for bound-free radiative transitions has the form

$$\varepsilon_{b\text{-}f} \sim \frac{R_{2k}}{R_{2k} + A_{21}} \tag{V-31}$$

where R_{2k} is the rate of transitions from the upper level to the continuum. If $\varepsilon_{b\text{-}f} \gg \varepsilon_{coll}$, then the bound-free transition, not collisions, dominate the problem. If $\varepsilon_{coll} \gg \varepsilon_{b\text{-}f}$, the reverse is true. For a 6500° radiation field

$$R_{2k}/A_{21} = 5 \times 10^{-3} \text{ and } \varepsilon_{b\text{-}f} \quad 5 \times 10^{-3} \tag{V-32}$$

At $\tau = 1$ $\varepsilon_{b\text{-}f} > \varepsilon_{coll}$ and at $\tau = 0.01$ $\varepsilon_{b\text{-}f} \gg \varepsilon_{coll}$. The bound-free processes are more important than the collisions throughout the region of line formation.

The above values of ε can be used to determine the scale and surface behavior of the problem as long as we are considering very strong lines. We have seen that the optical depth in the line at which

$$S_{12} \rightarrow B_{12} \tag{V-33}$$

is

$$\tau_{12} \sim 1/\varepsilon \tag{V-34}$$

If this occurs at continuum optical depths of one or less, then the above treatment gives the correct behavior. However, for weak lines it would predict that S_{12} is less than B_{12} at large optical depths in the continuum. This cannot occur because at these depths the effects of a boundary are small and the radiation field is nearly in equilibrium with its surroundings. The equation of transfer insures that equilibrium occurs in this case and Avrett (1965) has shown how the line-continuum interactions can be estimated. He defines a quantity δ, which has the same meaning as the above ε ,

$$\delta = 2r \int_0^\infty \frac{\phi(x)\,dx}{\phi(x)+r} \quad ; \quad r = k_{12}/l_{12} \tag{V-35}$$

The value of the integral can be approximated by x_o such that

$$\phi(x_o) = r \tag{V-36}$$

and then

$$\delta \sim 2r x_o \tag{V-37}$$

For example, if the line profile is a gaussian,

$$\phi(x) = \frac{1}{\sqrt{\pi}}\, e^{-x^2} \tag{V-38}$$

then for $r = 10^{-3}$

$$\delta \sim 5 \times 10^{-3} \tag{V-39}$$

If δ is much greater than the ε'_0 for a particular line but still is considerably smaller than one, the surface behavior and relaxation length are given by

$$S_{12}(\tau=0) \approx \sqrt{\delta}\, B_{12}(\tau=0)$$
$$S_{12} \rightarrow B_{12} \text{ at } \tau_{12} \sim 1/\delta \qquad \text{(V-40)}$$

If we assume a normal oxygen abundance for the F supergiants and a turbulent velocity of 5 km/sec for the log g = 1.5 model, then

$$\delta = 4 \times 10^{-2} \qquad \text{(V-41)}$$

For the log g = 0.1 model the ratio of continuous to line absorption is 0.69 as large as in the log g = 1.5 model if the turbulent velocity is the same. If the velocity is roughly 10 km/sec, as seems likely, the factor is 1.38. Thus for log g = 0.1

$$\delta = 2.8 \times 10^{-2} \text{ or } 5.5 \times 10^{-2} \qquad \text{(V-42)}$$

and in either case is within 40% of the value for log g = 1.5. For the F I stars

$$\delta \gg \varepsilon_{b\text{-}f} \qquad \text{(V-43)}$$

and the oxygen line is controlled by the line continuum interactions, which are not very luminosity dependent. Since the surface value of the source function is proportional to $\sqrt{\delta}$ for $\delta \ll 1$, it varies by 20% or less with luminosity. In the LTE case the models predict that saturated lines at 7774A should have residual intensities at their centers of approximately 0.50. If

$$\delta = 4 \times 10^{-2} \qquad \text{(V-44)}$$

the line centers in the non-LTE case would have residual intensities of 0.10. A 40% change in this value produces a range of

0.08 to 0.12 for the F I stars and hardly affects the equivalent width of the line. Evidently the observed luminosity effect in the O I lines, in which their strength doubles in going from log g = 1.5 to 0.1, is not caused by non-LTE effects. However, the effects are present and are important in determining the abundance and the size of the turbulent velocities.

The above calculations imply that for the 7774 line

$$S_{12}(\tau=0) \ll B_{12}(\tau=0)$$
$$n_2/n_1 \ll \frac{g_2}{g_1} e^{-h\nu_{12}/kT} \qquad \text{(V-45)}$$

Accordingly an absorption line such as 6158, which arises from level 2, ought to behave differently than 7774 if non-LTE effects cause the latter to increase in strength with luminosity. However we have seen in table 6 that 6158 seems to vary in the same way as 7774. Bearing in mind that abundances derived from saturated lines are very uncertain because the abundance goes as the fourth power of the line strength, we have used the data and the models to find the oxygen to hydrogen ratio from the two lines. Table 19 indicates that within the errors both transitions yield

$$N(O)/N(H) = 10^{-2.1 \pm 0.4} \qquad \text{(V-46)}$$

for the log g = 0.1 and 1.5 models. Since the calculations assume LTE holds, the absolute values of the abundance may be incorrect, but the fact that the abundances obtained from level 2 and level 1 are roughly the same in the Ib and Ia star implies that non-LTE effects do not cause the increase in strength with luminosity.

The fact that the Fe II, O I 8446, Mg II, and N I lines also

Table 19. Abundances derived from individual lines. Tabulated values are relative to hydrogen and are on a logarithmic scale.

Line	α Per	HD 10494
O I 6156	-2.07	-1.96
O I 6158	-1.75	-1.76
O I 7771	-2.38	-2.15
Fe I 5321	-4.47	-4.57

increase in strength with luminosity is additional evidence against the non-LTE case. These lines represent quite different transitional schemes, and it is unlikely that departures from LTE could cause all of them to behave the same way. Since Fe I is similar to the O I, Mg II, and N I lines in that the upper levels of the observed lines of each ion are within $4\frac{1}{2}$ eV of the continuum, its failure to show the luminosity effect at F5 is not caused by differences in its term scheme with respect to the others. In any case all our observed lines ought to be dominated by the line-continuum interactions if their atomic parameters are similar to hydrogen, and we have shown that these interactions are insensitive to gravity.

In our discussion of the oxygen abundances we have used values of the turbulent velocity that duplicated the observed iron line strengths in the F5 stars for the abundance $N(Fe)/N(H) = 10^{-4.10}$, which is a factor of 10 greater than the solar value. The derived oxygen abundance $N(O)/N(H) = 10^{-2.10}$ is also ten times larger than in the sun. As the two stars used in the analysis are typical of the supergiants, the oxygen to hydrogen ratio in their atmospheres is normal within the observational errors, which are approximately a factor of 3.

We investigated the iron abundance in more detail because the large number of Fe I lines measured gave a better determination of the mean curve of growth. The strength of a weak Fe I line was corrected so that it fell on the mean curve and then used with the same turbulent velocity that was used for the other oxygen and iron

lines to obtain the abundance. Table 19 indicates that this line yields a lower iron to hydrogen ratio, $10^{-4.50}$, than the strong lines, but the discrepancy is less than our estimated error. Since it is possible that non-LTE effects, which are not included in the models, account for this overabundance, we cannot be sure it is real. We note, however, that the observed line strengths require both a high turbulent velosity and an overabundance with respect to the sun. Even if the non-LTE effects are strong enough to make the lines have nearly zero residual intensities in their centers, they will not reduce both the turbulence and the abundance to normal, i.e., main sequence, values. We conclude that the effects by themselves do not account for the strong lines in the F supergiants.

D. Summary and Prospects for Future Work

The results of the present study of the F supergiants are the following:

(1) The relation between the strength of O I 7774 and luminosity was established by using stars in clusters and associations. The line can be used to determine the absolute magnitude of F stars brighter than $M_V = -4$ with an accuracy of $\pm 0^m.5$. It also separates Ia stars (and the Ib's) of different luminosity from one another.

(2) The hypothesis that the luminosity effect was caused by an increase in the microturbulence was checked by measuring curves of growth for Fe I and Fe II lines beyond 5000A. We found that the oxygen line strength and Fe II microturbulent velocity were correlated, but that the Fe I velocities were insensitive to luminosity at F5. The difference between the behavior of Fe I and Fe II decreased in the stars of later spectral type.

(3) Other lines of O I and the infrared Mg II lines and N I lines also increase with luminosity. The common feature of all these lines is that they are not sensitive to ionization effects at the temperatures and pressures found in the F supergiants. For example, oxygen is mostly neutral and iron is mostly ionized. The strengths of the Fe I lines, however, are very dependent on the degree of ionization.

(4) Observations of the continuum fluxes and hydrogen line widths of supergiants in clusters can be used with the predictions of model atmospheres to obtain reasonable effective temperatures. The gravities derived for the Ia supergiants are appreciably lower than are expected from stellar interiors calculations although they are not as low as previous work indicated. This discrepancy was present in the Ib stars but was not as large.

(5) It was shown that low gravities were a result of the electron pressure being smaller than predicted by a factor of two approximately. Pulsational effects of the type which have been observed in the F supergiants produce a negligible change in the electron pressure. If we insert a pressure term to allow for turbulent motions in the hydrostatic equation, we find that the velocity required to produce the observed reduction in electron pressure is of the same order as the observed values.

(6) Using the physical parameters indicated by the models we found that the observed turbulent velocities and oxygen line strengths were mutually consistent. A decrease in the continuous opacity with increasing luminosity contributed to the strengthening of the oxygen line.

(7) It was also shown that non-LTE effects, while they should be present, do not account for the luminosity effect. They could change the derived abundance or turbulent velocity but are not sensitive to luminosity.

(8) The models indicate that for F stars with $\log g < 2$ there

is a zone beneath the photosphere in which the acceleration due to radiation pressure exceeds the surface gravity. The resulting gas pressure inversion could cause the large turbulent motions in supergiants. It was shown how the presence of the zone depends on temperature and gravity. Although g_{rad} goes as the fourth power of the temperature, it also depends on the opacity, which decreases rapidly with increasing temperature. Accordingly the zone exists on the main sequence only in the hottest stars.

(9) It was noted that the oxygen line begins to increase in strength with luminosity at the gravity where the inversion zone first appears, i.e., in the F Ib stars. This indicates that the presence of the zone is related to the turbulence in the F supergiants.

(10) Calculations using the models showed that a turbulent velocity increasing with height in the atmosphere accounts for the observed behavior of the Fe I and Fe II lines. The two ions give roughly the same velocity in the F5 Ib stars, because they are formed at the same depth. In the F5 Ia stars the increased ionization of iron causes the Fe II lines to be formed at a greater height in the atmosphere than the Fe I lines, and this is why the Fe II velocity is higher. Ionization effects also explain the dependence of the stratification on temperature in the Ia stars.

The results suggest that future theoretical work should

concentrate on understanding: (1) the mechanism that produces the turbulence in supergiants, (2) how the motions should vary with height in the atmosphere, and (3) what their effect on the structure of the atmosphere will be. In particular we would like to know why the turbulence increases as it does with luminosity in the F stars and if it will explain the narrowing of the hydrogen lines in the Ia stars.

We believe that further observations of the oxygen line made with a photoelectric technique similar to the one described here should be directed toward: (1) improving the calibration of the luminosity effect in the F stars, (2) investigating the behavior of the line in A stars with a wider range of absolute magnitudes than we observed and (3) determining the relation between absolute magnitude and line strength in the Magellanic Cloud supergiants. In addition the luminosity effect makes it possible to study the distribution of F supergiants in the galaxy.

Observations of the line profiles made with high resolution photoelectric equipment should yield a more detailed picture of the velocity field in supergiant atmospheres. Analysis of the profiles by the Goldberg method or by a similar technique which allows for variations in the turbulence with height would provide a more accurate determination of the density dependence of the motions than we obtained from the equivalent width data. The high resolution measures should enable a detailed study of the line formation mechanisms and the temperature structure of the

atmosphere to be made. Consequently, accurate values of the chemical abundances could be determined.

References

Abt, H.A. 1957, Ap.J., 126, 138.

_____ 1960, Ap.J., 131, 99.

Abt, H.A., Osmer, P.S., and Kraft, R.P. 1966, Ap.J., 145, 479.

Aller, L.H. 1963, The Atmospheres of the Sun and Stars (New York: Ronald Press), p. 251.

Avrett, E.H. 1965, Smithsonian Special Report, No. 174.

Avrett, E.H., and Hummer, D.G. 1965, M.N.R.A.S., 130, 295.

Avrett, E.H., and Kalkofen, W. 1968, J.Q.S.R.T., 8, 219.

Avrett, E.H., and Loeser, R. 1966, Smithsonian Special Report, No. 201.

Beardsley, W.A. 1961, Ap.J.Supp., 5, 381.

Bell, R.A., and Rodgers, A.W. 1965, M.N.R.A.S., 129, 127.

Bidelman, W.P. 1951, Ap.J., 113, 304.

_____ 1957, Pub.A.S.P., 69, 147.

Bidelman, W.P., and McKellar, A. 1957, Pub.A.S.P., 69, 31.

Bohm-Vitense, E. 1956, Pub.A.S.P., 68, 57.

Chaffee, F.H. 1968, Thesis, University of Arizona.

Cohen, J. 1969, private communication.

Corliss, C.H., and Warner, B. 1964, Ap.J.Supp., 8, 395.

Danziger, I.J. 1965, M.N.R.A.S., 130, 99.

Feinstein, A. 1967, Ap.J., 149, 107.

Goldberg, L. 1958, Ap.J., 127, 308.

Hardie, R.H., Seyfert, C.K., and Gulledge, I.S. 1960, Ap.J., 132, 361.

Helfer, H.L., and Wallerstein, G. 1964, Ap.J.Supp., 9, 81.

Hiltner, W.A. 1956, Ap.J.Supp., 2, 389.

Iben, I. 1966, Ap.J., 143, 505.

Jefferies, J.T. 1968, Spectral Line Formation (Waltham, Mass.: Blaisdell).

Keenan, P.C., and Hynek, J.A. 1950, Ap.J., 111, 1.

Kurucz, R.L. 1969, Ap.J., 156, 235.

Merrill, P. 1925, Pub.A.S.P., 37, 272.

_____ 1934, Ap.J., 79, 183.

Mihalas, D. 1965 Ap.J.Supp., 9, 321.

_____ 1969, Ap.J., 156, L155.

Mitchell, R.I. 1960, Ap.J., 132, 68.

Moore, C.E., Minnaert, M.G.J., and Houtgast, J. 1966, The Solar Spectrum 2935A to 8770A, Second Revision of Rowland's Preliminary Table of Solar Spectrum Wavelengths, N.B.S. Monograph 61.

Morton, D.C. 1967, Ap.J., 147, 1017.

Oke, J.B. 1964, Ap.J., 140, 689.

Parsons, S.B. 1964, Ap.J., 140, 853.

_____ 1967, Ap.J., 150, 263.

_____ 1969a, Ap.J.Supp., 18, 127.

_____ 1969b, private communication.

Payne-Gaposchkin, C., and Mayall, N.U. 1946, Harvard Bull., No. 918, p. 11.

Pesch, P. 1959, Ap.J., 130, 764.

_____ 1960a, Ap.J., 132, 689.

_____ 1960b, Ap.J., 132, 696.

Peterson, D.M. 1969, Smithsonian Special Report, No. 293.

Rosendhal, J.D. 1968, Thesis, Yale University.

Rybicki, G.B. 1966, quoted by Avrett, E.H, and Loeser, R. 1966, Smithsonian Special Report, No. 201, p. 23.

Sargent, W.L.W. 1961, Ap.J., 134, 142.

_____ 1965, Obs., 85, 33.

Sargent, W.L.W., and Osmer, P.S. 1968, Mass Loss from Stars, ed. M. Hack (New York: Springer-Verlag).

Searle, L., Sargent, W.L.W., and Jugaku, J. 1963, Ap.J., 137, 268.

Stothers, R. 1966, Ap.J., 143, 91.

Strom, S.E., and Avrett, E.H. 1965, Ap.J.Supp., 12, 1.

Strom, S.E., and Peterson, D.M. 1968, Ap.J., 152, 859.

Struve, O., and Elvey, C.T. 1934, Ap.J., 79, 409

Thomas, R.N. 1957, Ap.J., 125, 260.

Underhill, A.B. 1949, M.N.R.A.S., 109, 562.

Unno, W. 1959a, Ap.J., 129, 375.

_____ 1959b, Ap.J., 129, 388.

Whitford, A.E. 1958, A.J., 63, 201.

Wiese, W.L., Smith, M.W., and Glennon, B.M. 1966, Atomic Transition Probabilities, N.S.R.D.S.-N.B.S. 4, 1.

Wildey, R.L. 1964, Ap.J.Supp., 8, 439.

Wright, K.O. 1946, J.R.A.S.Canada, 40, 183.

_____ 1947, J.R.A.S.Canada, 41, 49.

_____ 1955, I.A.U.Trans., 9, 739.

_____ 1966, Abundance Determinations in Stellar Spectra (I.A.U. Symposium, No. 5), p. 15.

Wrubel, M.H. 1949, Ap.J., 109, 66.